Assessment of heavy metals, their dispersion characteristics and composite-based remediation approaches in the Brahmaputra River System

Submitted in partial fulfilment of requirement for the degree of

DOCTOR OF PHILOSOPHY

by

VIJAY MEENA

(Roll No. – 196104117)

Under the guidance of

Prof. ARUP KUMAR SARMA

&

(Late) Prof. CHANDAN MAHANTA

DEPARTMENT OF CIVIL ENGINEERING

INDIAN INSTITUTE OF TECHNOLOGY GUWAHATI

May-2026

DECLARATION

I, **Vijay Meena**, author of the Ph.D thesis **"Assessment of heavy metals, their dispersion characteristics and composite-based remediation approaches in the Brahmaputra River System"** would like to certify that

- The work presented in this thesis is original research work carried out by me.
- The research work has not been submitted for any degree or diploma or any other qualification either in this institute or in any other university.
- Whenever I have used resources [theory, concepts, texts, data, graphs, figures or any other things of similar nature] from other sources, a due credit by citing in the text of the thesis is clearly made.
- The work presented here is free from plagiarism to the best of my knowledge, and I take the responsibility for any issues.
- I also affirm that thesis supervisor is not responsible for any possible instance of plagiarism within this submitted work.

[Vijay Meena]

(196104117)

Department of Civil Engineering
Indian Institute of Technology Guwahati
Guwahati – 781039, Assam India

CERTIFICATE

This is to certify that the work describes in this thesis entitled **"Assessment of heavy metals, their dispersion characteristics and composite-based remediation approaches in the Brahmaputra River System"** submitted by **Vijay Meena (Roll No. 196104117)** in partial fulfilment of the requirements for the award of the degree of Doctor of Philosophy is an authentic record of the results obtained from the research work carried out under my supervision in the Department of Civil Engineering, Indian Institute of Technology Guwahati, India and this work has not been submitted elsewhere for a degree.

Dr. Arup Kumar Sarma
Professor
Department of Civil Engineering
Indian Institute of Technology Guwahati
Guwahati - 781039

ACKNOWLEDGMENT

First and foremost, I want to express my sincere gratitude towards my supervisor Prof. Arup Kumar Sarma and (Late) Prof. Chandan Mahanta for providing me an opportunity to work under their supervision. The defining role in shaping my academic career is felt in every page of this work. I am grateful to my supervisors for their consistent guidance, motivation, patience, kindness and support as well, over these years. They have always made available themselves for discussions besides their busy schedules. Their enthusiasm, sublime work ethics, analytical abilities, and never-say-die attitude toward research and life as well, have natured my scientific skills and also inspired me immensely to work hard. I am proud to have them as my Ph.D. supervisor. Thank you, Sirs for all your help, advice, and support.

I want to thank my doctoral committee member, Prof. Rajib Kumar Bhattacharjya, Dr. Sreeja Pekkat, and Prof. Subashisa Dutta, for their encouragement, insightful comments, and suggestions which have helped me to refine and widen my research from various perspectives. My sincere gratitude also goes to the various Heads of Department of Civil Engineering, Prof. Chandan Mahanta, Prof. Sharad Gokhale and Prof. Rajib Kumar Bhattacharjya, for providing all the resources needed for my research. I also thankful to all faculty and staff members of the Civil Engineering department who help me whenever I needed. Without their help, it would not have been possible to conduct my research. It is an honour for me to thank the Indian Institute of Technology Guwahati for giving me such an excellent opportunity for undergoing my research.

I gratefully acknowledge the NEHARI (North Eastern Hydraulic and Allied Research Institute), Water Resources Engineering Laboratory, Environmental Laboratory, NECBH centre (BT/NER/143/SP44675/2023) and Central Instrument Facility for providing me the various facilities to carry out my laboratory and experimental work to support this research during my Ph.D. at IIT Guwahati.

I want to thank my seniors, Dr. Anupal Baruah, Dr. Dipshikha devi, Dr. Gaurav Talukdar, Shakti Kalyani, Arghya Ghosh, Anurag Handique and Bhaswatee Baishya for their mentorship related to make things done and hand holding whenever I got stuck during the research. I should also mention about Satheesh, Shaivi and Jusmita for their timely help, suggestions, and encouragements. It was fun to work with the PG students whose contributions showed new dimension to this research. I am indebted to my colleagues and

friends Abir Saha, Bharat Rattan, Ibansiewlin Rymbai, Maina Rajbongshi, Sujata Paul, Sanjeev Bora, Rockey Kumar, Siddharth and Sahil who made this journey along with me, creating a memorable campus life.

My special gratitude goes to my family for their role in my life. I offer my regards to my loving parents, Mr. Shiv Charan Meena and Mrs. Kamleshi Devi, whose love, teachings, sacrifices, and blessings brought me this far. I am thankful to my elderly brother Mr. Dharm Singh Meena and sister Ms. Hukam Bai, Sureshi and Anju Meena for instances taking my share of responsibilities. My parents, brother and sister are the backbone of my happiness, and I dedicate my thesis to them.

Finally, I thank God for always being with me.

[VIJAY MEENA]

Abstract

The Brahmaputra River is a major transboundary river system, which originates in the Tibetan Plateau and traverses China, India, and Bangladesh before merging with the Ganga-Meghna River system. The Brahmaputra River is a key factor in economic development and environmental sustainability in the assam region, especially Guwahati and thus it is a subject of intense research due to increased anthropogenic impacts, fast-paced industrialization, and expansion of river navigation, which pose threats to water quality and sediment quality. Sustainable management of freshwater river basins requires an understanding of the levels of contaminants in river systems, how they are dispersed, and how they can be reduced. Heavy metals, which are elements with high density and atomic weight that naturally occur, are particularly hazardous to human beings and ecosystems when their concentrations exceed certain levels, particularly as a result of anthropogenic activity.

This research is focused on the eight heavy metals: copper (Cu), zinc (Zn), iron (Fe), manganese (Mn), nickel (Ni), cobalt (Co), chromium (Cr), lead (Pb), and cadmium (Cd) due to their relevance to the environment and the danger they present to human health. These metals are present in both dissolved and particulate form, and easily retained on and bind to sediments. They can be remobilized from sediments when the physicochemical conditions change, thereby having the potential to affect aquatic system health and human health. Existing removal techniques such as chemical precipitation, ion exchange, membrane filtration, and electrochemical methods are effective but often limited by high cost, sludge generation, and secondary pollution. Hence, the development of bio-based composite materials is essential as they are cost-effective, environmentally friendly, and sustainable. Bio-composites such as nanocellulose bentonite adsorbents offer high surface area, strong metal binding capacity, reusability, and the ability to utilize agricultural waste, making them particularly suitable for heavy metal remediation in large river systems like the Brahmaputra.

The initial investigations of this study focus on evaluating the feasibility of dredging operations for inland navigation by assessing heavy metal contamination in mid-sand bars of the Brahmaputra River. However, dredging contaminated sediments can pose significant ecological and health hazards. To address this concern, sediment samples were collected from 42 locations along an approximately 600 km stretch of the river, divided into Reach 1

and Reach 2. Vertical sampling was carried out at depths of 0, 50 and 100 cm within mid-sand bars. The concentrations of pernicious metals, namely Cu, Zn, Fe, Mn, Ni, Co, Cr, Pb, and Cd, were analyzed, and several contamination indices were employed to evaluate pollution levels. The Enrichment Factor (EF) revealed pronounced spatial variability in metal enrichment. Reach 2 was found to be highly enriched with toxic metals, significantly constraining dredging activities, whereas Reach 1 exhibited low enrichment and was considered suitable for dredging operations. The elevated contamination in Reach 2 was attributed to anthropogenic inputs such as effluents from pharmaceutical industries, oil refineries, and industrial and domestic runoff. Multivariate statistical analyses further confirmed that the heavy metals shared similar anthropogenic origins. The findings suggest that dredging is feasible in Reach 1 and in selected localized zones of Reach 2, provided that appropriate mitigation measures and sediment management strategies are adopted for contaminated dredged materials.

In the first phase of this study, we evaluated the level of sediment contamination. The second phase involves a study of the changes in the levels of heavy metals found in river waters over time and their potential risk to human health. The COVID-19 lockdown period provided a unique natural experiment to evaluate the influence of anthropogenic activities on river water quality. Comparative analysis of water samples collected during and after the lockdown revealed a marked contrast in heavy metal concentrations. During the lockdown, concentrations of heavy metals were below detection limits, indicating a significant improvement in water quality due to reduced industrial and human activities. In contrast, post-lockdown samples showed elevated concentrations of Ni, Cd, Pb, and Cr, exceeding permissible limits. The Heavy Metal Pollution Index (HMPI) classified the water as “low to medium polluted” during the lockdown and “critically polluted” in the post-lockdown period. Human health risk assessment indicated no significant non-carcinogenic risk during the lockdown; however, in the post-lockdown period, approximately 33% of children, 33% of teenagers, and 11% of adults were found to be at potential risk. These results highlight the strong dependence of river water quality on anthropogenic activities and reinforce the need for sustainable pollution control measures to protect both ecological integrity and public health.

In the next part of the study, to link the transport of pollution, it is necessary to understand the transport and dispersion of contaminants. Therefore, the third component of the research work is to estimate the longitudinal dispersion coefficients in the Brahmaputra River. Tracer experiments were conducted using a physical hydraulic model of the river

developed at the North Eastern Hydraulic and Allied Research Institute (NEHARI), scaled at 1:500 horizontally and 1:67 vertically. A conservative tracer, methylene blue dye, was introduced in a selected 30 km stretch of the river, and solute concentrations were measured using UV Visible spectrophotometry. Dimensional analysis and least-squares regression techniques were employed to develop new empirical relationships for longitudinal dispersion coefficients based on hydraulic parameters such as channel width, flow depth, discharge, and velocity. The proposed equations showed close agreement with existing theoretical and experimental formulations and demonstrated improved applicability for braided river morphology. These findings provide critical insights into pollutant transport dynamics in large alluvial rivers and support the development of reliable hydrodynamic and water quality models for the Brahmaputra River basin.

Recognizing the need for sustainable remediation strategies to address heavy metal pollution, the final component of the study explores the development of a novel composite based adsorbent for heavy metal removal. A nanocellulose bentonite (RNC-BENT) composite was synthesized using rice husk waste from the Bao dhan variety, promoting the valorization of agricultural residues. The composite was characterized using Fourier transform infrared spectroscopy (FTIR), X-ray diffraction (XRD), scanning electron microscopy (SEM), and energy dispersive X-ray analysis (EDAX). Batch adsorption experiments demonstrated high removal efficiency for Ni(II) and Cr(VI), with adsorption kinetics following a pseudo second order model and equilibrium behaviour best described by the Freundlich isotherm. The maximum adsorption capacities were found to be 22.46 mmol/g for Ni(II) and 19.71 mmol/g for Cr(VI). Regeneration studies using dilute nitric acid showed minimal reduction in adsorption efficiency over multiple cycles, indicating good reusability and practical applicability. This eco-friendly composite material offers a promising solution for treating heavy metal contaminated water and managing leachates from dredged sediments.

Overall, this thesis presents an integrated framework for assessing heavy metal contamination, understanding dispersion characteristics, and developing sustainable remediation strategies in the Brahmaputra River system. The findings provide valuable scientific insights to support navigation planning, environmental risk assessment, and river basin management, and contribute to the sustainable utilization and protection of large braided river systems in India and similar fluvial environments worldwide.

Table of Contents

List of Figures

List of Tables

List of Abbreviations

Terms	Abbreviations
AAS	Atomic Absorption Spectroscopy
AE	Absolute Error
APHA	American Public Health Association
BDL	Below Detection Limit
BOD	Biochemical Oxygen Demand
CA	Cluster Analysis
CD	Contamination degree
CEC	Cation Exchange Capacity
CF	Contamination factor
CI	Crystallinity Index
COD	Chemical Oxygen Demand
Dx	Dispersion coefficient
EDAX	Energy dispersive X-ray analysis
EF	Enrichment Factor
EPA	Environmental Protection Agency
FESEM	Field Emission Scanning Electron Microscope
FTIR	Fourier transform infrared spectroscopy
HPI	Heavy Metal Pollution Index.
Igeo	Geo-accumulation index
MB	Methylene Blue
MI	Metal Index
NaOH	Sodium Hydroxide
NEHARI	North Eastern Hydraulic and Allied Research Institute
PCA	Principal Component Analysis
PCM	Principal Correlation Matrix
PERI	Potential ecological risk index
Pfo	Pseudo first order
PLI	Pollution Load Index
Pso	Pseudo second order

PLI	Pollution Load Index
Pso	Pseudo second order
RE	Relative Error
RNC	Rice Nanocellulose-
RNC-BENT	Rice Nanocellulose-Bentonite
SSA	Specific Surface Area
USEPA	United States Environmental Protection Agency
WHO	World Health Organization
XRD	X-ray diffraction

List of Machines Used for Different Testing

Atomic Absorption Spectroscopy (AAS) (Varian, SpectrAA-55, HG-AAS)

Fourier Transform Infra-red spectroscopy (FTIR) (IRAffinity-1 from Japan)

Hot oven-(IKON, Model: IK-109, India)

Muffle furnace-(YOMO, Model: MF - 5510 D, India)

Rotary Shaker (Bio Technics from India)

Sigma field emission microscopy- (Make: Zeiss, Germany)

Surface Area Analyzer (Quantachrome Instruments, Model: Autosorb-IQ MP)

Weighing balance- (Sartorius, Model: Cubis®, Germany)

X-Ray diffraction system (Make: Rigaku technologies, JAPAN, Model: Smartlab)

Chapter 1

INTRODUCTION

1.1 PREFACE

Freshwater river systems constitute a vital component of natural and socio-economic infrastructure, supporting ecological processes, human settlements, and regional development [1]. The Brahmaputra River represents one of the most significant freshwater systems in South Asia and a critical transboundary river originating from the Tibetan Plateau [2]. Flowing through China, India, and Bangladesh before merging with the Ganga–Meghna River system, it ranks among the largest rivers in the world in terms of discharge and sediment transport [3]. In India, particularly within the state of Assam, the Brahmaputra plays a central role in sustaining agriculture, fisheries, navigation, water supply, and regional livelihoods [4]. The city of Guwahati, located along the southern bank of the river, has experienced rapid urban and industrial growth in recent decades, resulting in intensified anthropogenic pressure on the river system [5]. Increasing municipal discharges, industrial effluents, and unregulated waste disposal have contributed to the deterioration of both water and sediment quality, making the Brahmaputra a subject of sustained scientific investigation and environmental concern [6].

Heavy metals introduced into river systems through anthropogenic activities present sustained risks to both ecosystem integrity and human health [7]. Industrial operations such as oil refining, pharmaceutical production, metal processing, paper and pulp manufacturing, and hazardous waste recycling contribute significantly to the release of metals into surface waters. Once discharged, heavy metals exist in both dissolved and particulate forms and exhibit a strong affinity for sediments, particularly fine-grained and organic-rich deposits [8]. River sediments therefore function as long-term repositories of contamination, while also acting as potential secondary sources under changing hydrodynamic and physicochemical conditions [9]. Processes such as flooding, dredging, and redox fluctuations can remobilize sediment-bound metals, increasing their bioavailability. Chronic exposure to elevated metal concentrations [10], has been associated with carcinogenic effects, organ toxicity, neurological impairment, and bioaccumulation through aquatic food chains [11], thereby highlighting the need for systematic investigation of their distribution, transport behaviour, and mitigation. Effective and sustainable management of large river

basins requires a comprehensive understanding of contaminant levels, their spatial and temporal variability, transport mechanisms, and potential control measures [12]. Among various pollutants, heavy metals—characterized by high density and atomic weight—are of particular concern when their concentrations exceed natural background levels due to anthropogenic inputs. Metals such as copper (Cu), zinc (Zn), iron (Fe), manganese (Mn), nickel (Ni), cobalt (Co), chromium (Cr), lead (Pb), and cadmium (Cd) are environmentally significant owing to their toxicity, persistence, and tendency to accumulate in sediments [13]. In braided river systems like the Brahmaputra, mid-channel sand bars play an important role in sediment storage and pollutant retention, thereby influencing long-term river health and management decisions [14, 15].

In this context, the present thesis aims to examine the occurrence, distribution, dispersion, and remediation of heavy metals in the Brahmaputra River system through an integrated experimental and analytical approach [16]. The first component of the research focuses on evaluating sediment quality and the feasibility of dredging operations for inland navigation by assessing heavy metal contamination in mid-sand bars [17]. While dredging offers potential benefits for navigation and flood management, it also poses environmental and health risks when contaminated sediments are disturbed [18]. To address this issue, sediment samples were collected from forty-two locations along an approximately 600 km stretch of the river, divided into two reaches. Vertical sampling was carried out at depths of 0, 50, and 100 cm within mid-sand bars, and concentrations of selected heavy metals were analysed using standard analytical techniques. Several contamination indices were applied to assess enrichment levels and ecological risk. The results indicated pronounced spatial variability in heavy metal enrichment along the river corridor. The downstream stretch influenced by urban–industrial activities exhibited elevated contamination levels, constraining dredging feasibility, whereas the upstream reach displayed relatively low enrichment and was found to be suitable for dredging. Multivariate statistical analyses further demonstrated that the heavy metals shared common anthropogenic origins, primarily linked to industrial effluents and urban runoff [19]. These findings emphasize the importance of sediment quality assessment as a prerequisite for sustainable navigation planning and sediment management in large river systems. The second component of the thesis examines temporal variations in river water quality and associated human health risks. The COVID-19 lockdown period provided a unique opportunity to evaluate the influence of reduced anthropogenic activity on river pollution [20]. Comparative analysis of water samples collected during and after the lockdown revealed substantial differences in heavy

metal concentrations [21]. During the lockdown, reduced industrial activity resulted in improved water quality, whereas post-lockdown conditions showed elevated concentrations of several toxic metals, exceeding permissible limits [22]. Health risk assessment indicated potential non-carcinogenic risks for vulnerable population groups in the post-lockdown period, underscoring the strong dependence of river water quality on human activities.

To further understand pollutant fate and transport, the third component of the research investigates longitudinal dispersion characteristics of the Brahmaputra River. Tracer experiments were conducted using a scaled physical hydraulic model [23], and empirical relationships for dispersion coefficients were developed through dimensional analysis and regression techniques. These results contribute to improved understanding of pollutant transport dynamics in braided river systems and support the development of reliable hydrodynamic and water quality models [24]. Recognizing that assessment and modelling must be complemented by effective remediation strategies, the final component of the thesis focuses on the development of a sustainable adsorbent material for heavy metal removal [25]. Recognizing the necessity for eco-friendly cleaning-up practices, the paper introduced the innovative combined adsorbent created out of the nanocellulose (extracted from the Bao Dhan rice husk) and bentonite clay. The composite showed excellent adsorption capabilities for Ni(II) and Cr(VI) metals, accompanied by good kinetics, isotherm properties, and regeneration ability [26]. As a result, the composite is a cheap and environmentally friendly way to treat polluted water, which not only solves water pollution but also utilizes the waste from the agricultural sector and clay minerals effectively. In short, this dissertation connects the assessment through the transport aspect to the clean-up part and aims at solving the heavy-metal pollution issue concerning large river systems. The combination of on-site sampling, modelling, source identification, and material innovation that is applied in the study is a powerful tool for policymakers, environmental engineers, and river management authorities to develop sustainable strategies that would keep the Brahmaputra River's health intact.

Overall, this thesis presents an integrated framework that combines contamination assessment, source identification, transport analysis, and remediation development to address heavy metal pollution in the Brahmaputra River system. The findings contribute scientific insights relevant to navigation planning, environmental risk assessment, and sustainable river basin management, and are intended to support informed decision-making for large braided river systems in India and similar fluvial environments worldwide.

1.2 RIVER SYSTEMS AND SEDIMENT DYNAMICS

Rivers are dynamic geomorphic systems that continuously adjust their channel geometry, sediment transport capacity, and flow characteristics in response to climatic, hydrological, and anthropogenic influences [27]. The interaction between flowing water and sediment governs river morphology, channel stability, and habitat diversity. In alluvial rivers, where the bed and banks consist of unconsolidated materials, sediment dynamics play a dominant role in shaping the river course [28]. Sediments transported by rivers originate from weathering and erosion processes in the upstream catchment. These sediments vary widely in size, composition, and mineralogy, ranging from clay and silt to sand and gravel [29]. Once deposited within the river channel, sediments influence hydraulic resistance, bed roughness, and flow distribution. Fine-grained sediments, in particular, possess high surface area and strong adsorption capacity, making them effective carriers of heavy metals and other contaminants [30]. In large river systems, sediment transport occurs through a combination of bed load and suspended load mechanisms. Seasonal variations in discharge, especially in monsoon-dominated regions, lead to significant fluctuations in sediment erosion, transport, and deposition [31]. During high-flow conditions, sediments may be eroded and transported over long distances, whereas during low-flow periods, deposition dominates, resulting in the formation of bars, islands, and shoals [32].

The Brahmaputra River is globally recognized for its exceptionally high sediment load, derived primarily from the young and tectonically active Himalayan region. The river exhibits a braided channel pattern characterized by multiple shifting channels separated by mid-channel bars and islands [33]. These geomorphic features are highly dynamic, undergoing frequent formation, migration, and erosion in response to seasonal hydrological variability. Mid-channel sand bars, while being natural components of braided rivers, pose serious challenges for navigation and river management [34]. From an environmental perspective, these sand bars often act as repositories of fine sediments and associated contaminants. Over time, pollutants introduced into the river through industrial effluents, urban runoff, and agricultural inputs tend to accumulate within these depositional environments. Consequently, sand bars can serve as long-term sinks of heavy metals, which may be remobilized under disturbed conditions. Understanding sediment texture, grain size distribution, organic matter content, and mineralogical composition is therefore essential for assessing sediment quality. Such information provides insights into sediment transport history, depositional environment, and contamination potential. In the context of dredging, sediment dynamics assume even greater

significance, as excavation directly alters the natural equilibrium of erosion and deposition within the river system.

1.3 RIVER POLLUTION DUE TO HEAVY METALS

River pollution is a complex phenomenon resulting from the interaction of natural processes and anthropogenic activities. Broadly, river pollution can be classified into physical, chemical, biological, and thermal pollution [35]. Physical pollution involves increased turbidity, sediment load, and changes in flow regime. Biological pollution arises from pathogenic microorganisms introduced through sewage discharge [36]. Chemical pollution includes nutrients, organic compounds, and toxic elements, among which heavy metals represent one of the most critical categories [37]. Heavy metal pollution is of particular concern due to the non-biodegradable nature of metals, their tendency to accumulate in sediments, and their potential to enter the food chain [38]. In riverine environments, heavy metals originate from both natural sources, such as weathering of rocks and soils, and anthropogenic sources, including industrial effluents, mining activities, agricultural runoff, urban wastewater, and atmospheric deposition [39]. Once introduced into a river system, heavy metals partition between the dissolved phase and the particulate phase. Fine-grained sediments, organic matter, and clay minerals play a dominant role in controlling metal distribution through adsorption, ion exchange, and complexation processes. Over time, contaminated sediments act as secondary sources of pollution, releasing metals under changing physicochemical conditions or physical disturbances such as dredging [40].

The following subsections discuss the occurrence, distribution, and environmental impact of individual heavy metals of concern in riverine sediments and water, with particular relevance to large alluvial rivers such as the Brahmaputra.

1.4 OCCURRENCE, DISTRIBUTION, AND IMPACT OF INDIVIDUAL HEAVY METALS

1.4.1 Copper (Cu)

Copper is an essential trace element required for biological processes; however, elevated concentrations can be toxic to aquatic organisms and humans [41,44]. In river systems, copper occurs naturally through weathering of copper-bearing minerals but is predominantly introduced through anthropogenic activities such as industrial effluents, metal processing, electrical industries, antifouling paints, and domestic sewage [42]. In sediments, copper

exhibits a strong affinity for organic matter and fine particles, leading to its accumulation in depositional zones such as mid-channel sand bars and floodplains [43,52]. Elevated copper concentrations can impair enzymatic activity in aquatic organisms, disrupt photosynthesis in algae, and cause gastrointestinal and liver disorders in humans upon prolonged exposure.

1.4.2 Zinc (Zn)

Zinc is another essential metal involved in metabolic functions; however, excessive zinc concentrations are harmful to aquatic life [41,45]. Major anthropogenic sources of zinc include galvanization industries, batteries, fertilizers, pesticides, and urban runoff [42]. In riverine environments, zinc is commonly associated with fine sediments and iron–manganese oxides. High zinc concentrations can cause growth inhibition and mortality in fish and benthic organisms [43,52]. In humans, excessive zinc intake may result in nausea, immune system dysfunction, and interference with the absorption of other essential elements.

1.4.3 Iron (Fe)

Iron is one of the most abundant elements in river sediments and occurs primarily from natural sources such as rock weathering and soil erosion. Anthropogenic contributions arise from industrial discharge, mining activities, and corrosion of iron structures [49,50]. Although iron is not highly toxic, excessive concentrations can adversely affect water quality by increasing turbidity, altering taste and color, and promoting the growth of iron bacteria [51]. In sediments, [52,43] iron oxides play a crucial role in binding other heavy metals, thereby influencing their mobility and bioavailability.

1.4.4 Manganese (Mn)

Manganese occurs naturally in river systems through geological sources but is also introduced through industrial effluents, mining, and agricultural activities [42,53]. Its distribution in sediments is strongly controlled by redox conditions, with higher concentrations often observed under reducing environments [54,52]. While manganese is an essential micronutrient, elevated exposure can cause neurological disorders in humans and physiological stress in aquatic organisms [55]. Its association with iron oxides makes it an important indicator of sediment geochemistry.

1.4.5 Nickel (Ni)

Nickel contamination in rivers primarily originates from industrial discharge, oil refineries, electroplating units, and fossil fuel combustion [42,57]. In sediments, nickel is often associated with clay minerals and organic matter [43,41]. Nickel is known for its carcinogenic potential

and can cause skin allergies, respiratory disorders, and kidney damage in humans [59,60]. In aquatic ecosystems, elevated nickel levels adversely affect fish reproduction and benthic organisms.

1.4.6 Cobalt (Co)

Cobalt occurs naturally in trace amounts in river systems but is increasingly introduced through industrial activities, metal processing, and waste disposal [42,53]. It is commonly associated with iron and manganese oxides in sediments. Although cobalt is required in small quantities for biological functions, excessive exposure can lead to cardiovascular and neurological effects in humans [63]. Its accumulation in sediments reflects both geogenic and anthropogenic influences [52,43].

1.4.7 Chromium (Cr)

Chromium exists in multiple oxidation states, with Cr(III) and Cr(VI) being the most environmentally relevant. Industrial activities such as leather tanning, electroplating, dye manufacturing, and metal finishing are major sources of chromium pollution [42]. Cr(VI) is highly toxic and carcinogenic [64,44], whereas Cr(III) is relatively less harmful. Chromium strongly binds to sediments, particularly under reducing conditions. Elevated chromium concentrations pose serious risks to aquatic life and human health, including cancer and organ damage [43,52].

1.4.8 Lead (Pb)

Lead is a non-essential and highly toxic heavy metal introduced into river systems through industrial discharge, battery manufacturing, paints, fuel combustion, and urban runoff [42,44]. In sediments, lead exhibits strong binding with organic matter and fine particles [43]. Lead exposure causes severe neurological damage, particularly in children, and affects the hematopoietic and renal systems. Its persistence in sediments makes it a critical pollutant of concern in dredging studies [41,52].

1.4.9 Cadmium (Cd)

Cadmium is among the most toxic heavy metals and is introduced primarily through industrial effluents, phosphate fertilizers, battery production, and waste disposal [42,44]. It readily accumulates in sediments and biota. Cadmium exposure leads to kidney dysfunction, bone damage, and carcinogenic effects in humans [43,52]. Even at low concentrations, cadmium poses significant ecological and health risks [41], making its assessment essential in sediment quality evaluation.

1.5 EXISTING REMOVAL TECHNIQUES OF HEAVY METALS

The increasing incidence of heavy metal contamination in aquatic environments has led to the development and application of a wide range of treatment and remediation techniques. Heavy metals, owing to their non-biodegradable nature, persistence, and tendency to bioaccumulate, pose long-term risks to ecosystems and human health [65,66]. Consequently, their removal from contaminated water and sediments has become a critical aspect of environmental engineering and water resource management. Existing heavy metal removal techniques can be broadly classified into physical, chemical, biological, and hybrid methods, each having distinct advantages and limitations.

1.5.1 Physical Treatment Techniques

Physical methods primarily involve separation processes that remove heavy metals without altering their chemical form. Common physical techniques include sedimentation, filtration, membrane separation, and dredging. Sedimentation and filtration are widely employed for the removal of particulate-bound metals, particularly in water treatment facilities [67]. However, these methods are generally ineffective for dissolved metal species.

Membrane-based techniques such as reverse osmosis, nanofiltration, and ultrafiltration have been extensively used for heavy metal removal due to their high efficiency and ability to treat a wide range of contaminants [68]. Reverse osmosis is capable of removing most dissolved metal ions; however, its application is limited by high capital and operational costs, membrane fouling, and energy requirements. Nanofiltration offers relatively lower operating pressure and cost but is selective toward multivalent ions, making it less effective for certain metals.

In riverine and sediment-contaminated environments, dredging is often adopted as a physical removal method. While dredging effectively removes contaminated sediments from the riverbed, it does not constitute a complete remediation strategy unless combined with safe disposal or treatment of dredged material [69]. Moreover, dredging can result in sediment resuspension and secondary pollution if not properly managed.

1.5.2 Chemical Treatment Techniques

Chemical methods involve the transformation of dissolved heavy metals into less mobile or insoluble forms. Precipitation is one of the most commonly used chemical techniques, where metals are converted into insoluble hydroxides, sulfides, or carbonates through the addition of reagents such as lime or sulfide compounds [67, 70]. Although precipitation is relatively simple

and cost-effective, it generates large volumes of metal-laden sludge that require further treatment or disposal.

Chemical coagulation and flocculation are often used in conjunction with precipitation to enhance metal removal efficiency. Coagulants such as alum, ferric chloride, and polyaluminum chloride destabilize suspended particles and facilitate the aggregation of metal-bearing solids[71]. However, chemical consumption and sludge management remain major challenges associated with these techniques.

Ion exchange is another widely applied chemical method for heavy metal removal. Synthetic resins selectively exchange metal ions with benign ions such as sodium or hydrogen [72]. Ion exchange exhibits high removal efficiency even at low metal concentrations, but its application is constrained by high material costs, sensitivity to competing ions, and the need for periodic regeneration using chemical reagents.

Electrochemical techniques, including electrocoagulation and electrochemical oxidation, have also gained attention for heavy metal removal [72]. These methods rely on electric current to induce coagulation or redox reactions that immobilize metals. While effective, electrochemical processes require careful control of operational parameters and may involve high energy consumption.

1.5.3 Biological Treatment Techniques

Biological methods utilize living organisms or biological materials to remove heavy metals from contaminated environments. Biosorption, bioaccumulation, and phytoremediation are among the most extensively studied biological approaches [73]. Microorganisms such as bacteria, fungi, and algae possess functional groups on their cell walls that can bind heavy metal ions through adsorption and complexation. Phytoremediation involves the use of plants to uptake, stabilize, or transform heavy metals in contaminated soils and sediments. Although environmentally friendly and cost-effective, phytoremediation is generally slow and limited to shallow contamination zones [73,74]. Moreover, disposal of metal-enriched biomass presents additional challenges. Biological methods are particularly attractive due to their sustainability and low environmental impact; however, their application in large river systems is constrained by variable environmental conditions, long remediation timeframes, and limited control over removal efficiency.

1.5.4 Adsorption-Based Techniques

Among the existing treatment methods, adsorption has emerged as one of the most promising and versatile techniques for heavy metal removal. Adsorption involves the

accumulation of metal ions onto the surface of solid materials through physical or chemical interactions [75]. A wide variety of adsorbents have been investigated, including activated carbon, natural clays, agricultural wastes, industrial by-products, and engineered nanomaterials. Activated carbon is highly effective due to its large surface area and porous structure, but its high cost limits large-scale application [75,76]. Natural adsorbents such as bentonite, zeolite, and laterite offer cost-effective alternatives with reasonable adsorption capacity. Agricultural waste-derived materials, including rice husk, sawdust, and biochar, have gained increasing attention due to their low cost, renewability, and environmental compatibility [76,77]. Recent advances in material science have led to the development of nanomaterial-based and composite adsorbents, which exhibit enhanced surface area, functional group availability, and adsorption efficiency. Hybrid materials combining organic and inorganic components have demonstrated superior performance compared to conventional adsorbents, particularly for multi-metal systems.

1.5.5 Integrated and Hybrid Approaches

Given the limitations of individual techniques, integrated treatment approaches are increasingly being adopted. Hybrid systems combining physical separation, chemical stabilization, and adsorption offer improved efficiency and sustainability. For example, dredging followed by adsorption-based treatment of contaminated sediments represents a viable strategy for river management, particularly in navigation-oriented dredging projects.

In the context of large braided rivers such as the Brahmaputra, the selection of an appropriate heavy metal removal technique must consider site-specific factors including sediment characteristics, contamination level, hydrodynamic conditions, and economic feasibility. Sustainable remediation strategies require not only effective metal removal but also minimal ecological disturbance and long-term environmental protection.

1.6 GENERAL OBJECTIVE OF THE PRESENT WORK

The general objective of the present research is to comprehensively evaluate the feasibility of dredging operations in the Brahmaputra River by integrating sediment quality assessment, heavy metal contamination analysis, pollutant transport behaviour, and associated environmental and human health risks. The study primarily focuses on the mid-channel sand bars of the Brahmaputra River, particularly in the Guwahati region, where intense anthropogenic activities have significantly influenced the riverine environment. A major objective of this work is to understand the spatial and vertical distribution, enrichment characteristics, and contamination intensity of heavy metals in river sediments, and to

distinguish between natural and anthropogenic sources using geochemical indicators and multivariate statistical approaches. In parallel, the research aims to evaluate the implications of heavy metal and microbiological contamination on human health by conducting comparative health-risk assessments of river water during and after the COVID-19 lockdown period, considering different exposure pathways and age groups. The present study also seeks to enhance understanding of pollutant transport processes in a large braided river system by investigating longitudinal dispersion characteristics of the Brahmaputra River through scaled physical modelling and tracer experiments. Such analysis is essential for predicting the downstream fate of contaminants released due to sediment disturbance during dredging operations. Furthermore, the research aims to identify and map potential anthropogenic sources of heavy metal pollution in the Brahmaputra basin by integrating industrial categorization, toxicological reference values, and statistical source apportionment techniques. By synthesizing sediment contamination assessment, health-risk evaluation, hydrodynamic dispersion analysis, and remediation strategies, including the development of nanocellulose bentonite composite adsorbents for heavy metal removal, the present work aims to establish a scientific framework for environmentally responsible dredging and sustainable inland navigation. Ultimately, this research aspires to support informed decision-making, sustainable river management practices, and long-term ecological protection of the Brahmaputra River system.

1.7 ORGANISATION OF THE THESIS

The thesis is split into eight chapters, with each chapter dealing with a particular aspect of the research framework. The organization of the chapters is as follows:

Chapter 1 introduces in general river pollution, heavy metals, pollutant dispersion, and composite-based remediation materials. It describes the motivation, research gaps, objectives, and overall scope of the study.

Chapter 2 aggregates the literature review regarding heavy-metal contamination through river systems, water quality changes, pollution-source identification, large river dispersion modelling, and eco-friendly remediation technologies.

Chapter 3 Provides an information on spatial and vertical distribution of heavy metals in mid-sand bars of the Brahmaputra River. Analytical methods, contamination indices, and geochemical interpretations are the aspects that are illustrated.

Chapter 4 illustrated the comparative evaluation of the water quality during and post-COVID-19 lockdown along with the heavy-metal concentrations, microbial contamination, pollution indices, and human health-risk evaluation.

Chapter 5 is concerned with the use of industrial category data, TRVs, and multivariate statistical methods for source apportionment in mapping the potential sources of sand-bar heavy-metal pollution.

Chapter 6. describes the longitudinal dispersion features that were obtained from the physical tracer-model studies. The chapter also explains empirical models for dispersion coefficients and discusses their environmental implications.

Chapter 7 presents composite-based remediation strategies with an emphasis on the nanocellulose–bentonite composite synthesis, characterization, and adsorption performance for the removal of Ni(II), Cr(VI), and other heavy metals.

Chapter 8 recaps the primary findings of the research and offers the management recommendations to the river-management authorities. Also, it suggests the next steps of research that combine the field assessment, hydrodynamic modelling, and green remediation solutions.

1.8 SUMMARY

This chapter presents an overview of the Brahmaputra River system with emphasis on its hydrological, geomorphological, and environmental significance, particularly in the Guwahati region. The importance of the river for inland navigation, socio-economic development, and ecological sustainability is discussed. A detailed background on river pollution is provided, highlighting various types of pollution with specific focus on heavy metal contamination in water and sediments. The occurrence, distribution, and environmental impacts of major heavy metals are briefly introduced to establish the context of sediment quality assessment. Existing techniques for heavy metal removal and remediation are also outlined to emphasize current mitigation approaches and their limitations. Furthermore, the chapter introduces the challenges associated with dredging operations in large braided rivers and the necessity of integrating sediment quality and environmental risk assessment into navigation planning. The organization of the thesis is also presented in this chapter. A comprehensive review of literature related to sediment contamination, heavy metal assessment, pollutant transport, dredging impacts, and remediation strategies, and identifies the research gaps and objectives of the present study in Chapter 2.

Chapter 2

Literature Review

2.1 Introduction

This chapter provides a comprehensive review of the existing literature relevant to the present research, focusing on riverine sediment contamination by heavy metal, pollutant transport processes, dredging impacts, health risk assessment, and remediation strategies in large river systems. Particular emphasis is placed on studies related to braided alluvial rivers such as the Brahmaputra River, where complex hydrodynamics, high sediment load, and intense anthropogenic pressures govern sediment quality and contaminant behaviour. Further, a systematic review of previous investigations addressing the occurrence, distribution, and enrichment of heavy metals in river water and sediments, along with their ecological and human health implications. It also examines the influence of industrialization, urbanization, and land-use practices on heavy metal contamination in river basins. In addition, studies related to microbiological contamination and integrated water quality assessment are reviewed to provide a holistic understanding of river pollution dynamics.For a structured and coherent analysis, the literature review has been organized into multiple sections, each addressing specific themes relevant to the objectives of the present research. Figure 2.1 illustrates the overall structure and thematic organization of the literature review.

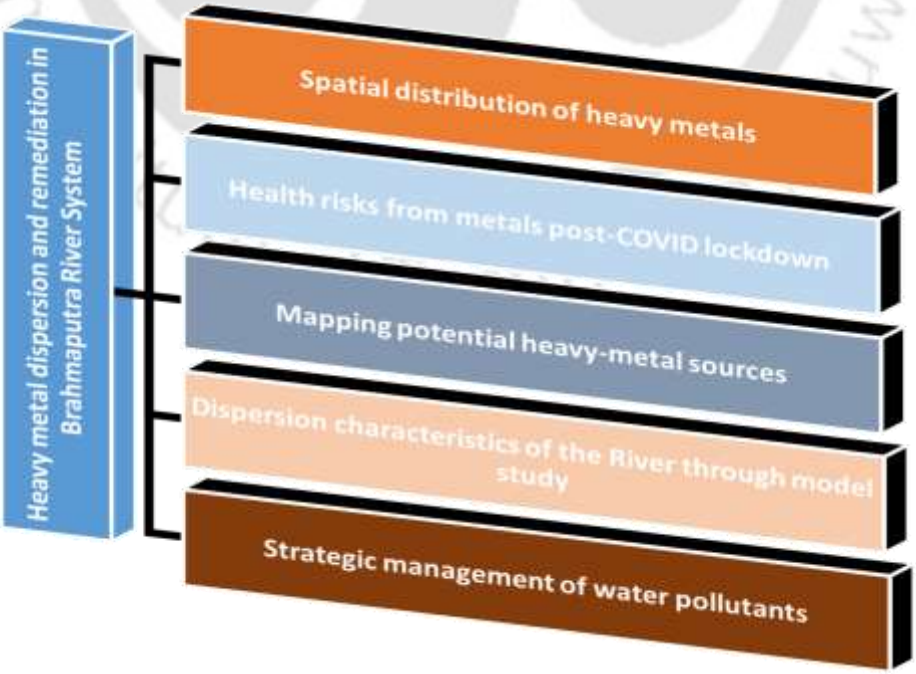

Fig 2.1 Overall structure a thematic organization of the literature review

In this chapter, a detailed review of river pollution and sediment contamination studies is presented in Section 2.2. it discusses the sources, geochemical behaviour, and toxicity of heavy metals in aquatic environments. An extensive review of pollution indices, geochemical assessment tools, and multivariate statistical techniques used for sediment quality evaluation is also provided. Studies related to the impact of dredging on sediment disturbance, contaminant resuspension, and environmental risk are critically examined based on past literature. Section 2.3 presents previous work on health risk assessment of heavy metals and microbiological indicators in river water, with special reference to exposure pathways and age-specific risk evaluation considering COVID-19 global impacts. The literature on pollutant transport and longitudinal dispersion in rivers, including tracer studies and physical modelling approaches, is reviewed in Section 2.4. Remediation and management strategies for heavy metal-contaminated water and sediments, including adsorption-based and composite material approaches, are discussed in Section 2.5. Furthermore, Section 2.6 summarizes literature specifically related to the Brahmaputra River basin, identifying regional research trends and knowledge gaps. The critical research gaps identified from the reviewed literature are outlined in Section 2.7, followed by the scientific motivation of the present study in Section 2.8. Section 2.9 formulates the research questions addressed in this thesis, while Section 2.10 outlines the specific objectives of the present work. Finally, Section 2.11 highlights the novelty and originality of the research and the chapter concludes with a conclusion section discussed in section 2.12.

2.2 LITERATURE REVIEW ON HEAVY METALS IN RIVERINE SEDIMENTS

Riverine sediments play a fundamental role in governing the transport, accumulation, and long-term fate of heavy metals in aquatic environments. Unlike surface water, which reflects short-term pollution dynamics, sediments integrate contamination over extended periods and therefore serve as reliable indicators of environmental quality. Consequently, sediment-based assessments have been widely adopted to evaluate heavy metal pollution, ecological risk, and anthropogenic impacts in river systems [78,79]. Heavy metals such as copper (Cu), zinc (Zn), iron (Fe), manganese (Mn), nickel (Ni), cobalt (Co), chromium (Cr), lead (Pb), cadmium (Cd), and arsenic (As) are among the most persistent and toxic pollutants reported in riverine sediments worldwide. These metals originate from both natural sources, including weathering of parent rocks and soil erosion, and anthropogenic sources such as industrial effluents, mining activities, urban runoff, agricultural inputs, pharmaceutical waste, and municipal discharge

[80,81]. Their non-biodegradable nature, ability to bioaccumulate, and long environmental residence times make them major contaminants of concern in aquatic systems. Numerous studies have demonstrated that fine-grained sediments, owing to their higher surface area, clay mineral content, and organic matter, exhibit a greater capacity for heavy metal adsorption compared to coarse sediments [82]. As a result, sediments act not only as sinks but also as secondary sources of heavy metals, releasing contaminants back into the overlying water column under changing physicochemical conditions such as variations in pH, redox potential, hydrodynamic energy, and sediment disturbance [83].

Investigations conducted on major river systems across the globe—including the Ganga, Yamuna, Yangtze, Mekong, Nile, and Mississippi—have consistently reported elevated heavy metal concentrations in sediments within urban and industrial stretches [84,85]. Spatial variability in sediment contamination is a common observation, with higher metal concentrations typically recorded downstream of industrial zones, densely populated regions, and polluted tributary confluences. Vertical profiling of sediment cores has further revealed historical accumulation trends, reflecting temporal changes in industrialization, land-use patterns, and pollution control measures [86]. In large alluvial and braided rivers, sediment dynamics exert strong control on heavy metal distribution. Depositional environments such as mid-channel sand bars (chars), point bars, and floodplains act as preferential sinks for heavy metals due to reduced flow velocity and enhanced deposition of fine particles [87]. Braided river systems such as the Brahmaputra are characterized by complex sedimentation patterns, making mid-channel sand bars particularly susceptible to pollutant accumulation. Studies conducted along the Brahmaputra River have revealed pronounced spatial and vertical variability in heavy metal concentrations within surface, middle, and deeper sediment layers, with several mid-channel sand bars exhibiting enrichment factors indicating moderate to extremely high contamination levels. Industrial effluents, agricultural runoff, pharmaceutical waste, and municipal discharge have been identified as dominant contributors to sediment contamination in the region [88,89].

To assess sediment contamination levels, several geochemical indices have been widely employed, including contamination factor (CF), enrichment factor (EF), geo-accumulation index (I_geo), pollution load index (PLI), and ecological risk index (ERI) [84,90]. These indices provide quantitative measures of contamination intensity and facilitate discrimination between natural and anthropogenic metal inputs. Enrichment factor analysis, commonly using iron or aluminium as reference elements, has been particularly effective in identifying anthropogenic metal enrichment in river sediments [91]. Multivariate statistical techniques

such as Pearson's correlation analysis, principal component analysis (PCA), factor analysis (FA), and hierarchical cluster analysis (HCA) are frequently applied to interpret complex sediment datasets [92]. These techniques aid in identifying metal associations, dominant controlling factors, and potential pollution sources. Literature indicates that combining geochemical indices with multivariate statistical approaches enhances the robustness of source apportionment and reduces uncertainty in sediment contamination assessment [93].

The environmental significance of heavy metals in sediments has been widely emphasized. Under stable hydrodynamic conditions, metals may remain immobilized within sediments; however, physical disturbances such as dredging can resuspend contaminated sediments, increase metal bioavailability, and enhance downstream transport [94]. This issue is particularly critical in large rivers where dredging is undertaken for navigation purposes. Recent studies have highlighted the importance of integrating sediment contamination assessment with hydrodynamic and pollutant transport analyses, especially in large river systems [95]. Nevertheless, most existing dispersion and transport models have been developed for small or single-thread rivers, limiting their applicability to large braided rivers such as the Brahmaputra.

Overall, the reviewed literature underscores the importance of sediment-based heavy metal assessment for river management and environmental protection. Despite extensive research, significant gaps remain in understanding the spatial and vertical distribution of heavy metals in mid-channel sand bars, source identification in complex river basins, and the coupling of sediment quality with pollutant transport processes—particularly in large rivers such as the Brahmaputra.

2.3 LITERATURE REVIEW ON WATER QUALITY AND TEMPORAL VARIATION OF HEAVY METALS

River water quality is a dynamic characteristic governed by a complex interplay of natural processes and anthropogenic activities. Unlike sediments, which integrate contamination over longer time scales, water quality reflects more immediate changes in pollution sources, hydrological conditions, and seasonal variability. Consequently, monitoring river water quality is essential for understanding short-term fluctuations in contaminant levels and assessing potential risks to aquatic ecosystems and human health.

The temporal variation of heavy metals in river water is strongly influenced by seasonal discharge, hydrological regime, and land-use practices. Several studies have reported that heavy metal concentrations in river water vary significantly between high-flow (monsoon) and

low-flow (dry) seasons due to dilution, resuspension of contaminated sediments, sediment–water exchange processes, and variations in pollutant loading [96,97,98] During high-flow periods, increased discharge generally results in dilution of dissolved metals, whereas low-flow conditions often promote concentration buildup due to reduced dilution and continuous pollutant input. In urban and industrial river stretches, temporal variation is further exacerbated by fluctuations in industrial discharge, municipal wastewater input, and stormwater runoff. Numerous studies conducted worldwide have demonstrated that heavy metal concentrations in river water tend to increase downstream of urban centers and industrial clusters, particularly during dry seasons when dilution capacity is limited [99,100]. Such variations underline the importance of time-specific water quality assessment rather than relying solely on annual averages. The global COVID-19 lockdown presented a rare and unprecedented natural experiment to evaluate the impact of reduced anthropogenic activity on river water quality. During the lockdown period, industrial operations, transportation, and commercial activities were significantly curtailed, leading to observable improvements in water quality across several river systems worldwide. Multiple studies reported substantial reductions in heavy metal concentrations during periods of industrial inactivity, highlighting the dominant role of anthropogenic inputs in river pollution [101,102].

The presence of heavy metals in river water poses significant health risks, as prolonged exposure can adversely affect vital organs such as the kidneys, liver, bones, and nervous system. Health risk assessment studies have demonstrated that toxic metals such as Cr, Ni, Pb, and Cd contribute substantially to non-carcinogenic risk through ingestion and dermal exposure pathways. Application of hazard quotient and hazard index models to Brahmaputra River water has indicated that children and adolescents represent the most vulnerable population groups due to their higher exposure rates and physiological sensitivity [103]. The observed temporal variability in water quality and associated health risks emphasizes the necessity of continuous and systematic monitoring of river water, particularly in rapidly urbanizing regions. Periodic assessment capturing seasonal and anthropogenic variability is essential for effective pollution control, public health protection, and sustainable river management. The reviewed literature clearly indicates that integrating temporal water quality analysis with sediment contamination studies provides a more comprehensive understanding of riverine pollution dynamics, but the impact of COVID-19 halting industrial activities caused an impact on water bodies especially in large rivers such as the Brahmaputra, is also need to be explored.

2.4 LITERATURE REVIEW ON DISPERSION CHARACTERISTICS, IDENTIFICATION AND MAPPING OF POLLUTION SOURCES

Understanding pollutant dispersion characteristics and identifying pollution sources are essential components of river water quality assessment and management, particularly in large and hydrodynamically complex river systems. Dispersion governs the downstream transport and spatial spread of contaminants, while accurate source identification enables targeted mitigation and regulatory control. In riverine environments, dispersion processes are influenced by flow velocity, channel geometry, turbulence, sediment transport, and morphological features of the river.

Longitudinal dispersion plays a dominant role in controlling the downstream movement of dissolved and particulate pollutants. Numerous classical and empirical studies have demonstrated that dispersion coefficients are strongly dependent on hydraulic parameters such as channel width, flow depth, discharge, mean velocity, and shear velocity [104,105,106]. However, most of the existing dispersion models and empirical relationships were developed for straight or mildly meandering rivers, limiting their applicability to large braided rivers where flow bifurcation, channel shifting, and complex mixing processes prevail. Tracer experiments and physical hydraulic modelling have been widely adopted to quantify dispersion characteristics in rivers. Conservative tracers, such as dyes or salts, are commonly used to evaluate solute transport and mixing behaviour under controlled conditions [104, 107]. In recent years, scaled physical models have gained prominence as effective tools for investigating dispersion processes in large rivers where field-based tracer studies are logistically challenging. Such models enable controlled experimentation under varying hydraulic conditions and facilitate the derivation of improved empirical relationships for dispersion coefficients.

To effectively evaluate river pollution, it is necessary to determine both the sources and transport pathways of contaminants. Human-induced pollutant inputs are commonly identified using multivariate statistical techniques such as correlation analysis, hierarchical cluster analysis, and principal component analysis (PCA), which help differentiate between geogenic contributions and anthropogenic sources [108, 109]. These techniques have been extensively applied in river basins worldwide to interpret complex datasets and establish relationships among heavy metals.

Source-identification studies conducted in river systems across the globe have consistently revealed that industrial corridors, mining belts, tanneries, and chemical processing

zones are major contributors to heavy metal loads in adjacent rivers [110,111,112]. In the context of the Brahmaputra River basin, industrial clusters located along Tinsukia, Dibrugarh, Jorhat, Kamrup, and Dhubri districts have been identified as significant pollution hotspots due to concentrated industrial activity and inadequate wastewater treatment infrastructure [113]. Studies conducted specifically on the Brahmaputra River have shown strong inter-element correlations among metals such as Cu, Zn, Ni, Pb, and Cr, indicating common anthropogenic origins [114]. Detailed industrial-unit surveys further revealed that red-category industries—including pharmaceutical units, oil refineries, paper and pulp industries, metal processing units, and cement plants—are major contributors of heavy-metal effluents to the river system [113].

In recent years, the integration of toxicological reference values (TRVs) with geochemical and statistical analyses has emerged as an effective approach for identifying pollution hotspots and prioritizing management interventions. TRV-based assessment helps link contaminant concentrations with potential ecological and human health risks, thereby supporting decision-making related to dredging feasibility and pollution abatement strategies [103]. The coupling of dispersion analysis with source identification is particularly critical in the context of dredging operations. Physical disturbance of contaminated sediments can enhance downstream dispersion of pollutants, extending the influence of localized pollution sources. Therefore, integrating hydrodynamic dispersion studies with multivariate statistical source apportionment, industrial categorization, and TRV-based risk assessment provides a comprehensive framework for understanding pollution dynamics in large braided rivers. Recent literature emphasizes the necessity of adopting integrated approaches that combine tracer-based dispersion analysis, physical modelling, multivariate statistics, and spatial mapping for effective river pollution management [112,115]. Such approaches are especially relevant for complex braided river systems like the Brahmaputra, where conventional single-method analyses may not adequately capture the interactions between flow dynamics, sediment transport, and contaminant distribution.

Overall, the reviewed literature highlights that accurate characterization of dispersion behaviour, along with robust identification and spatial mapping of pollution sources, is essential for informed river management. Despite substantial progress, gaps remain in developing dispersion relationships tailored to braided rivers and in integrating source identification with hydrodynamic transport analysis. Addressing these gaps is crucial for environmentally responsible dredging, pollution mitigation, and sustainable management of large river systems such as the Brahmaputra.

2.5 LITERATURE REVIEW ON COMPOSITE-BASED REMEDIATION APPROACHES FOR HEAVY METAL REMOVAL

The remediation of heavy metal–contaminated water has been a major focus of environmental engineering research due to the persistent, toxic, and non-biodegradable nature of metals such as chromium, lead, cadmium, and nickel. Conventional heavy metal removal technologies, including reverse osmosis, chemical precipitation, ion exchange, and electrodialysis, have been widely applied for wastewater treatment. However, these techniques are often associated with high capital and operational costs, significant energy requirements, membrane fouling, and the generation of secondary waste streams that require further handling and disposal [116, 117]. As a result, their application for large-scale river water remediation remains limited. Among the various treatment methods, adsorption has emerged as an effective, economical, and environmentally friendly approach for heavy metal removal from aqueous systems. The process offers advantages such as operational simplicity, high removal efficiency, flexibility in design, and the possibility of adsorbent regeneration [118, 119]. Consequently, adsorption-based techniques have attracted considerable attention for the treatment of metal-contaminated river water. Recent advances in adsorption technology indicate a gradual transition from purely bio-based or purely mineral adsorbents toward hybrid composite materials that combine organic and inorganic components to achieve superior performance. These composite materials benefit from synergistic effects, where the limitations of individual components are overcome through material integration [120]. Such innovations have significantly improved adsorption capacity, mechanical stability, and reusability of adsorbents. Bentonite has been extensively studied as an inorganic adsorbent for heavy metal removal due to its high cation-exchange capacity, large specific surface area, swelling ability, and layered aluminosilicate structure. Numerous studies have reported the effective removal of metal ions such as Cr(VI), Ni(II), Pb(II), and Cd(II) using bentonite and bentonite-based materials [121,122]. However, the application of bentonite alone is often limited by poor mechanical strength and difficulties in post-treatment separation.

In parallel, nanocellulose derived from agricultural waste has gained increasing attention as a sustainable bio-adsorbent. Nanocellulose is characterized by high surface functionality, large surface area, excellent mechanical properties, and biodegradability. The presence of abundant hydroxyl groups enables strong interaction with metal ions through complexation and hydrogen bonding [123,124]. Utilization of agricultural residues such as rice husk for nanocellulose production further enhances the environmental and economic sustainability of

this approach. Globally, hybrid composite adsorbents have become a focal point of research due to their synergistic adsorption properties, tunable surface chemistry, structural stability, and cost-effectiveness [125,126,127].

Overall, the reviewed literature demonstrates that composite-based adsorption approaches offer a sustainable and efficient alternative to conventional heavy metal removal technologies. Despite notable progress, further research is required to synthesis a bio composite material as an adsorbent for effectively removal of heavy metals from the aqueous solution and is of reusable in nature with long-term performance for real-field applications.

2.6 LITERATURE REVIEW ON INTEGRATED APPROACHES LINKING ASSESSMENT, DISPERSION, AND REMEDIATION

Recent environmental studies point to the integration of pollutant measurement, source identification, dispersion modelling, and remediation in a single framework. Such combined methods are the basis for sustainable implementation of the water-resources management, the conservation of the ecosystem and the formulation of pollution-control policies. In the Brahmaputra basin, integrating sediment analysis, water-quality assessment, temporal variation examination, anthropogenic source mapping, and dispersion modelling provides a thorough understanding of heavy-metal dynamics [128,129,130,131]. Pollutant transport forecasting facilitates the setting up of rapid-response systems for contamination incidents and also helps in the surveillance networks' optimization. At the same time, the invention of high-performance adsorbent composites like nanocellulose-bentonite materials is very promising for immediate practical use in on-site remediation, industrial effluent treatment, and localized pollution control [132]. Several river basins have also implemented similar integrated strategies, where assessment serves as a guide for management and remediation decisions [133,134,135].

Therefore, the body of research points out that a comprehensive approach is needed—where assessment locates the problem, dispersion modelling forecasts its spread, and remediation offers eco-friendly solutions. This research takes a similar framework to deal with heavy-metal contamination in the Brahmaputra River system.

2.7 RESEARCH GAPS

On the basis of the literature reviewed and the analysis given in detail in Section 1.2, the first set of research gaps regarding heavy-metal pollution, dispersion behaviour, and remediation strategies in the Brahmaputra River system has been identified as follows:

- Limited research has been conducted on sediment from mid-sand bars (chars) of the Brahmaputra River. The majority of heavy-metal studies in the Brahmaputra that we came across concentrate on sediment from the riverbank or water samples. There is a lack of investigation of the spatial and vertical distributions of heavy metals in riverbed sand bars for that matter, although they play a significant role as pollutant sinks in braided river systems. Consequently, the manner in which toxic metals are distributed amongst the various sediment layers (surface, mid-depth, and deeper strata) has not been sufficiently elucidated.
- There is an absence of temporal water-quality evaluation that is connected with major anthropogenic disturbances. While several worldwide studies have examined the changes in river water quality during the shutdown of human activities, the impact of large-scale events like the COVID-19 lockdown on heavy-metal concentrations and microbiological indicators in the Brahmaputra remains poorly understood. The lack of comparison between pre-and post-disturbance periods impedes the determination of the river's capacity to bounce back and its susceptibility.
- There are insufficient mapping and classification of heavy-metal sources. Though numerous studies have pointed out the industrial and municipal discharges as the main contributors, there is scant systematic integration of industrial categorization, toxicity reference values (TRVs), and multivariate statistics for locating and mapping the potential heavy-metal-contributor industries along the Brahmaputra basin. A well-organized connection between sediment contamination hotspots and specific anthropogenic origins is mostly absent.
- There is a lack of fundamental studies on dispersion characteristics in braided river systems. The majority of dispersion studies are based on rivers that are either straight or meandering. On the other hand, the Brahmaputra, being a braided river, has complicated morphologies, variable flow depths, and it is constantly shifting channels. Very few studies have conducted physical tracer experiments or developed empirical dispersion models that are specific to its unique hydrodynamics. The unavailability of model-based dispersion coefficients limits robust pollutant-transport predictions.
- The under exploration of sustainable remediation materials for region-specific heavy-metal removal. Heavy-metal remediation strategies, as practiced in India, mainly depend on traditional physico-chemical methods. Composite materials, such as nanocellulose–bentonite hybrids, for the adsorptive removal of Ni, Cr, and other dominant metals in the Brahmaputra, have not been sufficiently researched. The region-specific agricultural waste

(e.g., Bao Dhan rice husk) is still largely untapped despite its high potential for value-added environmental applications.

- The major part of the research works focus only on one of the aspects: either assessment, or modelling, or remediation. There is a significant gap in the creation of a comprehensive framework that integrates these elements: spatial/vertical assessment, temporal health-risk evaluation, source mapping, hydrodynamic dispersion modelling, and sustainable pollutant-removal materials. Such an integrated approach is essential for the efficient management of a river basin in the long run.

2.8 MOTIVATION

The present research is primarily concerned with the necessity of saving the Brahmaputra River which provides water to Northeast India and is severely contaminated by heavy metals. Essentially, the river ecosystem's health and the communities that depend on it are the ones to be jeopardized due to pollutant loads resulting from rapid industrialization, urban growth, and agricultural expansion. The study's impetus stems from these key issues: firstly, heavy metals such as Ni, Cr, Pb, and Zn are particularly problematic because they remain in sediment and water for a very long time, and even after decades, they continue to threaten the environment and people's health. Locating their spatial distribution, vertical mobility, and temporal variability is crucial for precisely monitoring and taking early actions. Secondly, the COVID-19 lockdown was quite different from any other time because it was a natural experiment that showed how the reduction of human activities would affect water quality. Comparisons made in time help to figure out how much human activities influence the river system. Thirdly, the Brahmaputra River changes its channel repeatedly and has a large discharge which makes it very difficult hydrodynamically; however, there are hardly any studies on dispersion conducted specifically for this river. Without the improvements in dispersion models, it would be difficult to forecast where pollutants travel during situations such as industrial accidents, waste discharges, or flood-induced contamination. Fourthly, the increased popularity of eco-friendly and less costly solutions to pollution is a major factor behind the move toward composite-based adsorbents. Besides, using abundant local biomass (like Bao Dhan rice husk) makes it possible for the introduction of new materials that have high adsorption capacity for metal pollution. Last but not least, the present study was propelled by the imperative to conceive an overarching, unified environmental management plan linking pollutant assessment, source identification,

predictive modelling, as well as remediation measures. Such a system can be used as a compass to set policy, protect human health, and enable sustainable river management in the long run.

2.9 RESEARCH QUESTIONS

1. How do the spatial and vertical distributions of heavy metals in the sediment of the Brahmaputra River reflect contaminations?
2. Will knowing the dispersion characteristics of heavy metals can help in spatially mapping the anthropogenic sources of heavy metals in the Brahmaputra River basin?
3. Can sustainable nanocellulose–bentonite composite adsorbents be synthesized and optimized to effectively remove dominant heavy metals from aqueous environments, thereby supporting strategic remediation and environmentally responsible river management?

2.10 OBJECTIVES OF THE PRESENT WORK

Based on the above research gaps and scientific motivations, the following key objectives are formulated for the present thesis:

1. To investigate the spatial and vertical distribution of heavy metals in the mid-sand bars of the Brahmaputra River and assess contamination intensities using geochemical indicators.
2. To perform a comparative health-risk assessment of heavy metals and microbiological indicators by analysing river water during and after the COVID-19 lockdown and evaluating pollution indices for different age groups.
3. To evaluate the longitudinal dispersion characteristics of the heavy metals through scaled physical modelling and tracer studies, and mapping of possible anthropogenic sources of heavy metals in the Brahmaputra River basin.
4. To develop and assess strategic management and remediation approaches, including the synthesis and characterization of composite adsorbent materials (nanocellulose–bentonite) for effective removal of dominant heavy metals from aqueous environments.

2.11 RESEARCH NOVELTY

1. Firstly, to exhaustively examines the mid sand bar quality through vertical sample profiling, risk assessment indexes, and morphological study to understand the feasibility of dredging activity for navigation purposes.

2. Secondly, to assess the COVID-19 lockdown impact considering the heavy metal and microbiological quality of Brahmaputra River water and how do the resulting variations influence non-carcinogenic health risks.
3. Thirdly, tracer studies for identifying the dispersion characteristics of heavy metals for mapping the possible anthropogenic sources in the Brahmaputra River basin.
4. Finally, effectively removal of heavy metals from aqueous solution through synthesis of bio based composite material (nanocellulose-bentonite).

2.12 CONCLUSION

The literature review has played a crucial role in establishing the scientific basis for integrating sediment geochemistry, health risk assessment, hydrodynamic dispersion studies, and material-based remediation approaches within a single research framework. This chapter has presented a comprehensive review of the existing literature related to sediment quality assessment, pollutant transport processes, health risk evaluation, dredging impacts, and remediation strategies in riverine environments. Special emphasis has been placed on studies concerning large alluvial and braided river systems, with particular reference to the Brahmaputra River basin. The review has highlighted the occurrence, distribution, and enrichment behaviour of heavy metals in river water and sediments, along with their ecological and human health implications. The literature review has also demonstrated that conventional approaches to source identification, health risk assessment, and pollutant dispersion analysis often lack integration, particularly in the context of complex braided rivers. Furthermore, limitations in existing empirical dispersion models and remediation strategies for large river systems have been identified.

The chapter concludes with an overview of the organization of the thesis. The subsequent chapter describes the study area, materials, data sources, and methodological approaches adopted for sediment sampling, water quality analysis, physical modelling, tracer experiments, and synthesis of composite adsorbent materials, forming the foundation for the detailed analyses presented in later chapters.

भारतीय प्रौद्योगिकी संस्थान गुवाहाटी
Indian Institute of Technology Guwahati

Chapter 3

Sediment Quality Assessment and Dredging Feasibility for Navigation

3.1 INTRODUCTION

Over the past few decades, researchers have explored the Brahmaputra River extensively in Assam, India, but there are also no studies focused on understanding whether it would be possible to conduct dredging activities in mid-sand bars (fluvial islands) for navigation purposes. This will be the first study of its kind done in northeastern India. This research provides an idea of dredging feasibility of mid-sand bars by utilizing vertical sampling, risk assessment indices, and morphological study techniques. The sediment sampling sites with Geographical coordinates, considered in this study are presented in sec. 3.2.1. Several Pollution indices were used to measure the degree of pollution in mid-sand bars due to heavy metal deposits found within their sediment levels are presented in sec. 3.2.6. Measuring possible sources of contamination through CM, CA, and PCA are explained in sec. 3.2.7. Furthermore, corelation matrix depicted a strong relationship among the heavy metals demonstrates the same level of contamination and common sources of pollution in sediment layers. sec 3.5. presented the tabulated case studies which illustrate the examples of dredging operations and their impact on water bodies, aquatic organisms and drinking water systems through the creation of sediment suspensions.

3.2 MATERIAL AND METHODS

3.2.1 Study Area

The Brahmaputra River originates from the chemayungdung glacier of the Kailash range situated in the Tibet region (altitude 5300 m). It passes through China (1625 km), India (918 km), and Bangladesh (337 km) before it is on its way to join the Bay of Bengal [136]. The state of Assam in India occupies a total length of 750 km out of 2900 km. Sadiya, in Tinsukia District, is the river's first entry point in Assam [137]. The length of the polluted stretch of the Brahmaputra River is 373 km out of 750 km of the total length in Assam. The river length identified as polluted is from Bogibeel to Sualkuchi [138]. A total of 42 sediment sampling sites, starting from Jorhat, Guwahati to Dhubri, as shown in Fig. 3.1, were collected through various mid sand bars of the Brahmaputra River from upstream to the

downstream direction in Assam, India. The first and last sampling sites bear the Geographical coordinates as (26° 54' 27.648" N, 94° 9' 29.412" E) and (26° 1' 14.88" N, 90° 0' 51.12" E). A sampling of the mid-sandbars is not feasible during the monsoon season because of the river's high flow and turbulence. Hence, sampling was carried out during the winter season as the sand bars were exposed during the winter time.

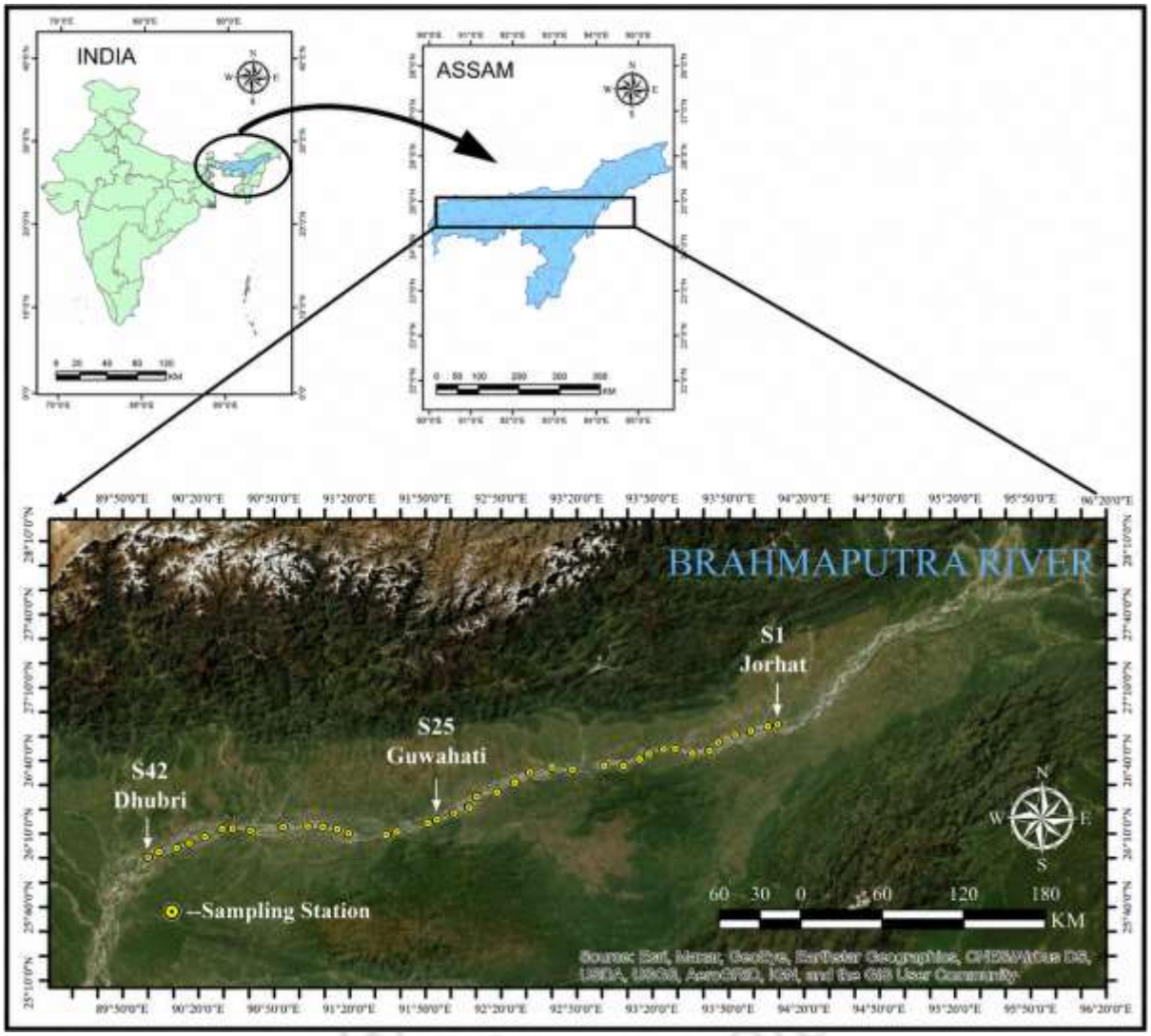

Fig. 3.1 Study area with sampling stations

3.2.2 Sampling Stations

A total of 126 sediment samples were collected through various mid sand bars following the centerline of the Brahmaputra River from the upstream region to the downstream region; with the help of Auger, sediment sampler, and measuring tape, 42 sampling sites were sampled. Three sediment samples were taken from each sampling site as bed surface sediment, 50 cm depth, and 100 cm depth below the bed surface sediment. Distance between two consecutive sampling stations was selected as 10-15 km; however, this distance increases to 20 km at some sampling sites as mid sand bars were not found at the chosen distance. Therefore, all 42

sampling sites were representative of around 600 km of reach length of the river. Precleaned plastic bags were used for collecting the sample from the river and were air-dried in the laboratory at room temperature (25-30° C).

3.2.3 Standard Preparation

Analytical grade chemicals and deionized water were used to prepare all standard samples for the Atomic Absorption Spectroscopy (AAS) calibration. A stock solution of 1000 ppm has been made by adding Zn, Fe, Mn, and Ni, metals of 1g each, in 10 ml HNO_3, while Cu, Co, and Cd have been added in 5, 20, 20 ml HNO_3, respectively. For Pb, 1.599 g of Pb $(NO_3)_2$ (= 1g of Lead) was added in 10 ml HNO_3, whereas Chromium stock was made using 1.923g of CrO_3 (= 1g of Chromium), acidified with distilled water. All stock has been diluted to make a volume of 1 L [139]. This way, stock solutions of Zn, Ni, Cu, Fe, Mn, and Cr in 1000 mg/l were prepared. Micropipettes were used to prepare 100 ml each of 0.1, 0.5, 1.0, 5, and 10 mg/l of standard solutions of particular metal from a stock solution in 5 ml of 2 N Nitric acid. The same method was used to prepare blank reagents as samples to avoid contamination of the samples with reagents [140].

3.2.4 Sample Preparation and Analysis

An accurately weighed sample (20 to 25 g) was placed into a silica crucible, then seared in a laboratory oven at 120 °C. A mortar and pestle were used to grind the sediment until no more gritty residue was seen. The < 63 µ fraction has been chosen for studying heavy metal concentrations in sediments. Such smaller size Reduces grain-size dependency on concentration rates. It has a prolonged residence time in the river reach, which accumulates the highest amounts of metals, is identical to the material flowing through suspension, and allows better comparisons [141]. The sediment was digested entirely by adding aqua regia (1 : 3 ratio of HCL + HNO_3) with 5 ml HF in 0.1 g of sediment. The mixture was kept inside a Teflon beaker covered by a Watch glass, kept on the Hotplate at 100° C for 90 minutes [142,143]. Once digested, the samples were filtered with filter paper, and distilled water was used to make the volume up to 25 ml before proceeding to analyze the total heavy metals present in the sediment.

The metal concentration in digested samples was determined using a standard analytical method using Atomic Absorption Spectroscopy (AAS) (Varian, SpectrAA-55, HG-AAS). An absorbance and instrumentation limit for measuring a particular metal concentration are shown in Table 3.1. Flame condition and absorbance were optimized, and AAS was set up to perform atomic absorption measurements [144]. The flame was aspirated initially for the distilled water, standards for particular metal concentration, Blank standard sample, and then digested samples

[145]. During the calibration process, concentration versus absorbance was determined, and then data were analyzed by the method of least square. A blank reading was taken to calculate the concentrations of various elements, and corrective measures were taken [146].

Table 3.1. Lower Limits of Quantitation and Wavelength of AAS

Element	Instrumental detection limit (mg/l)	Wavelength (nm)
Cu	0.02	324.7
Zn	0.005	213.9
Fe	0.03	248.3
Mn	0.01	279.5
Ni	0.04	232.0
Cr	0.05	357.9
Co	0.05	240.7
Cd	0.005	228.8
Pb	0.1	283.3

3.2.5 Organic Matter Content, Texture, and Mineralogy

All sediment samples collected from mid-sand bars were dried at 105° C and 550° C to find the organic matter content [147]. Sieve analysis was carried out to obtain an idea about the texture of the sediment. Mineralogical studies on ten selected representative samples from each layer have been carried out to identify the presence of minerals. The sample was grinded using agate and mortar and sieved through 53 µm mesh size. X-ray diffractogram was recorded using a 9 KW powder X-Ray diffraction system (Make: Rigaku technologies, JAPAN, Model: Smartlab). It consists of a curved graphite crystal diffracted monochromator with a source of CuKα radiation and a NaI (Tl) scintillation counter detector. Diffraction patterns were recorded for the 2θ value ranges from 10°- 90° [148,149]. surface morphology of the sediment was observed using FESEM (Gemini 500) of the above-selected samples.

3.2.6 Evaluation of sediment enrichment with heavy metals

The amount of contamination level in sediment layers through heavy metals was found using several indices such as contamination factor (CF), enrichment factor (EF), Contamination degree (CD), Geo-accumulation index (I_{geo}) and Pollution load index (PLI). However, the ecological risk was calculated through the potential ecological risk index (PERI & E_r^i) value. The methods used for evaluating the index and their classification have been summarized with their references in **Table 3.2**

Table 3.2. Various indices for classifying sediment quality

Index	Equation	Classification of Contamination level	References
EF	$EF = \frac{\left[\frac{C_M}{C_{Fe}}\right]_{Sample}}{\left[\frac{C_M}{C_{Fe}}\right]_{Shale}}$	EF: 2 - 5 low to moderate EF: 5 – 10 moderate to severe EF: 10 - 25 severe EF: 25 – 50 high EF: ≥ 50 extremely high	[150,151,152,153]
CF	$CF = \frac{C_n}{B_n}$	CF < 1 low 1 ≤ CF < 3 moderately 3 ≤ CF < 6 considerably CF ≥ 6 highly	[154,155]
CD	$\sum_{i=1}^{n} CF_i$	CD < 6, Class 1; low 6 ≤ CD <12, Class 2; moderate 12 ≤ CD < 24, Class3; considerable CD ≥ 24 Class 4; very high	[156]
PLI	$PLI = \sqrt[n]{(CF_1)\ X\ (CF_2)\ X\ (CF_3)\ X \ldots\ldots (CF_n)}$	PLI = 0, excellent state for pollution; PLI = 1 represent minimum level of pollutants; PLI > 1 indicates an increment in site deterioration	[157,158]
I_{geo}	$I_{Geo} = Log_2 \frac{C_n}{1.5\ B_n}$	$I_{geo} \leq 0$, Class 0; practically uncontaminated; $0 < I_{geo} \leq 1$, Class 1; uncontaminated to low contaminated; $1 < I_{geo} \leq 2$, Class 2; low contaminated to moderately contaminated; $2 < I_{geo} \leq 3$, Class 3; moderately contaminated to heavily contaminated; $3 < I_{geo} \leq 4$, Class 4; Heavily contaminated; $4 < I_{geo} \leq 5$, Class 5; Heavily contaminated to extremely contaminated; ($I_{geo} > 5$, Class 6; extremely contaminated.	[154,159,160,161]
E_r^i	$E_r^i = T_r^i \frac{C_{sample}}{C_{background}}$	E_r^i : < 40 (low risk) E_r^i : 40 - 80 (moderate risk) E_r^i : 80 - 160 (considerable risk) E_r^i : 160 - 320 (high risk) E_r^i : ≥ 320 (significantly high risk)	[155]
PERI	$PERI = \sum E_r^i$	PERI: < 150 (low risk) PERI: 150 - 300 (moderate risk) PERI: 300 - 600 (high risk) PERI: 600 – 1200 (significantly high risk) PERI: ≥ 1200	[155]

3.2.7 Statistical Analysis

Minitab software (version 17) was used to perform the statistical analysis to examine the properties of the heavy metals in core sediments; Pearson's correlation matrix (CM), cluster analysis (CA), and principal component analysis (PCA) were carried out [162]. An assessment of possible contamination sources (natural or anthropogenic) was conducted using CM, CA, and PCA.

CA is used to explore and visualize relationships in categorical data. It examines the associations between categorical variables, such as survey responses, preferences, or any data that uses categories rather than numerical values [163]. CM is used to identify groups (clusters) of similar objects or cases within a dataset [164]. This technique aims to group data points into clusters based on similarity or distance metrics, whereas PCA reduces dimensionality and visualizes data. It transforms many potentially correlated variables into a smaller number of uncorrelated variables called principal components [165]. Because of fundamental exploratory data analysis, they are used across various disciplines to gain insights from data sets of different types and sizes.

3.3 RESULTS AND DISCUSSION

3.3.1 Texture and Mineralogy

The sieve analysis of 126 sediment samples collected from different sandbars of the river Brahmaputra resulted in graphs, as shown in **Fig. 3.2,** which depicts that sediment characteristic varies from silty to fine sand. Organic matter content and texture characteristics of the sediment, along with the coordinate location of the sampling station, can be found in **Table 3.3**. The soil types in the three layers were similar though they varied based on sampling locations. Moreover, the d_{50} was also different in each case, as represented by **Fig. 3.3**. Interestingly S3, S5, S6, S10, S20, and S23 were newly formed locations and showed higher average $d_{50,}$

Table 3.3. Texture and organic matter content of sediments corresponding to station coordinate

Sampling Station	Latitude	Longitude	Texture	Organic Matter Content (%)
S1	26°54'27.648"N	94°9'29.412"E	Fine sand	0.82
S2	26°52'45.552"N	94°5'23.712"E	Silty-Fine sand	0.6
S3	26°52'17.724"N	93°58'7.68"E	Fine sand	0.56
S4	26°50'42.252"N	93°52'47.532"E	Silty-Fine sand	0.5
S5	26°48'6.48"N	93°45'36"E	Fine sand	0.52
S6	26°44'0.024"N	93°42'37.512"E	Fine sand	0.18
S7	26°43'45.732"N	93°36'7.308"E	Fine sand	0.2
S8	26°45'6.3"N	93°28'44.904"E	Fine sand	0.22
S9	26°44'56.076"N	93°24'45.252"E	Fine sand	0.18
S10	26°43'10.524"N	93°18'28.908"E	Fine sand	0.2
S11	26°40'8.148"N	93°12'59.112"E	Fine sand	0.06
S12	26°37'35.76"N	93°8'6.936"E	Fine sand	0.7
S13	26°38'13.416"N	93°0'30.06"E	Fine sand	0.48
S14	26°36'22.608"N	92°48'10.548"E	Fine sand-Silty	0.52
S15	26°36'43.128"N	92°39'45.396"E	Fine sand	0.64
S16	26°35'48.228"N	92°32'30.696"E	Silty-Fine sand	0.44
S17	26°33'9"N	92°27'21.816"E	Fine sand-Silty	0.16
S18	26°29'59.712"N	92°23'23.064"E	Fine sand	0.6
S19	26°25'43.5"N	92°17'25.224"E	Silty-Fine sand	0.56
S20	26°25'44.544"N	92°10'34.032"E	Fine sand	0.7
S21	26°24'37.548"N	92°9'31.356"E	Fine sand-Silty	0.28
S22	26°19'52.788"N	92°5'41.1"E	Fine sand	0.72
S23	26°18'24.372"N	92°1'41.124"E	Fine sand	1.06
S24	26°16'21.432"N	91°55'2.208"E	Fine sand	0.94
S25	26°14'22.56"N	91°51'41.904"E	Fine sand-Silty	0.74
S26	26°10'0.624"N	91°38'5.388"E	Fine sand	0.28
S27	26°9'5.6952"N	91°34'36.624"E	Fine sand	0.52
S28	26°10'30"N	91°18'14.4"E	Fine sand-Silty	0.54
S29	26°11'57.372"N	91°14'7.836"E	Silty-Fine sand	1.14
S30	26°12'43.38"N	91°10'17.688"E	Fine sand	0.58
S31	26°13'3.648"N	91°2'38.328"E	Fine sand-Silty	0.46
S32	26°12'33.984"N	90°53'11.076"E	Fine sand	0.50
S33	26°11'6.828"N	90°39'35.028"E	Fine sand	0.43
S34	26°11'58.272"N	90°34'30.216"E	Silty-Fine sand	0.30
S35	26°12'6.84"N	90°29'49.92"E	Fine sand	0.27
S36	26°9'19.044"N	90°21'36.684"E	Fine sand	0.68
S37	26°6'7.2"N	90°18'9.36"E	Fine sand	0.45
S38	26°4'22.872"N	90°13'25.752"E	Fine sand-Silty	0.56
S39	26°4'47.28"N	90°12'37.44"E	Fine sand	0.74
S40	26°2'20.4"N	90°4'36.84"E	Fine sand-Silty	0.72
S41	26°1'26.94"N	90°1'13.656"E	Fine sand	0.30
S42	26°1'14.88"N	90°0'51.12"E	Fine sand	0.18

whereas the sampling stations marked as vegetative were S14, S16, S17, S21, and S25, found to have lower average d_{50}.

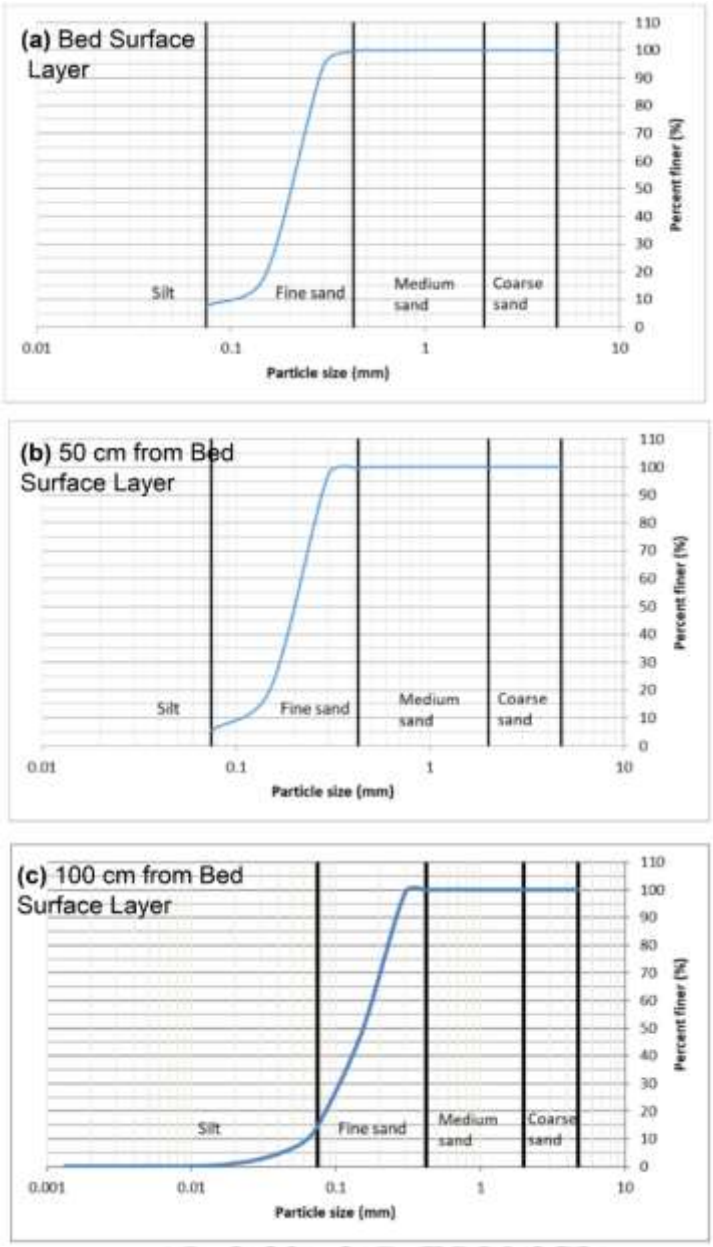

Fig.3.2 Grain size distribution curve for (a) bed surface layer; (b) 50cm from bed surface layer; (c) 100cm from bed surface layer

As shown in Fig. 3.4, XRD analysis reported the minerals present were Quartz, feldspar, kaolinite, illite, Augite, hematite, albite, gypsum, calcite, and plagioclase. Quartz and feldspar were mainly present in all samples, probably due to the weathering and erosion action of water on the silico-clastic and sedimentary rocks. Feldspar mineral is primarily from the disintegration of parent rocks (like Basaltic rocks) and transportation of sediment load from tributaries associated with the river Brahmaputra. Transport of the presence of calcite is likely

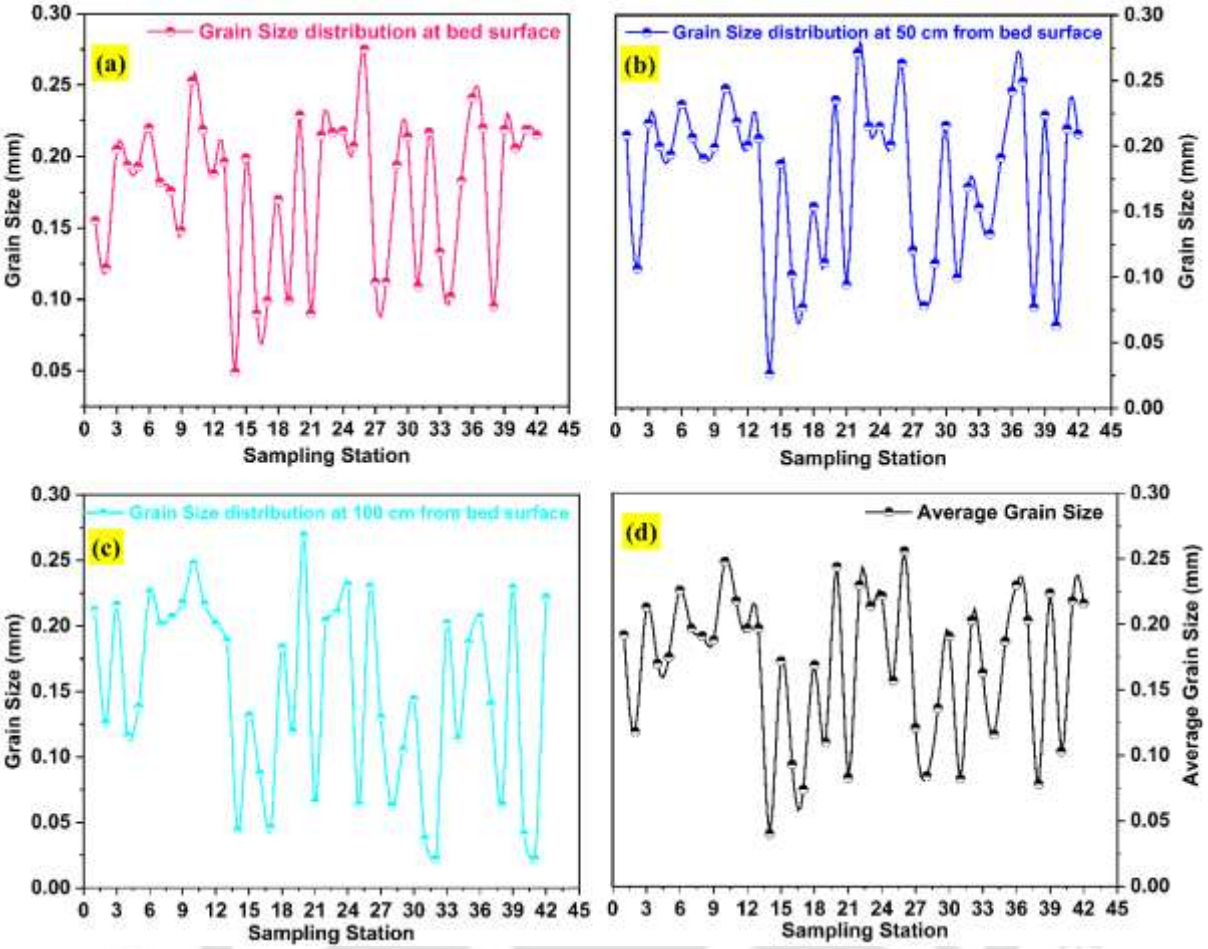

Fig.3.3 Grain size distribution (d50) at (a) bed surface layer; (b) 50cm from bed surface layer; (c) 100cm from bed surface layer and (d) average grain size

to be from the geologic formations near the river. It could be related to the erosion and weathering of the geologic actions as it can be precipitated due to a decrease in water flow and the evaporation process. The gypsum in a few sediment samples suggests its contribution from nearby agricultural soil. It could be the other sources of gypsum, whereas kaolinite production is due to the weathering of older sediments with clay proportions. Sources of hematite may be from the erosion of agricultural alluvial soils near the river's south bank.

3.3.2 Total Metal Concentration

Table 3.4. summarizes the heavy metals concentration in the sediment of River Brahmaputra. Based on average concentration, the total content of heavy metals was found in bed surface layer is in order of: Fe (4781.79 µg/g) > Mn (142.46 µg/g) > Zn (53.85 µg/g) > Ni (29.99 µg/g) > Cr (19.75 µg/g) > Cu (6.22 µg/g). The concentration of trace elements in 50 cm depth and 100 cm depth from the surface sediment follows the same increasing order as the bed surface sediment layer.

Table 3.4. Summary of Heavy Metal Concentration (μg/g) in the Brahmaputra River Sediment

Elements	Cu	Zn	Mn	Ni	Cr	Fe
Min. [a]	0.35	0.6	15	0.25	7.45	368
Min. [b]	0.25	0.25	39.5	0.75	6.425	438.5
Min. [c]	0.25	1.675	2.5	0.25	4.975	324.5
Max. [a]	24.95	677.25	283.25	150.5	286.65	12387.5
Max. [b]	38.48	125.40	1672.50	76.50	175.03	61271.75
Max. [c]	22.38	61.93	344.00	84.25	59.13	12240.00
Average [a]	6.22	53.85	142.46	29.99	19.75	4781.79
Average [b]	7.99	29.76	186.52	23.53	19.00	6742.42
Average [c]	7.03	26.84	140.34	26.71	11.09	5840.99
Median [a]	2.29	29.30	152.25	19.88	11.98	4411.38
Median [b]	3.26	24.01	142.75	19.75	10.93	5854.00
Median [c]	2.38	31.04	136.50	17.63	11.50	5866.13
SD [a]	6.93	125.69	64.76	32.24	48.24	3526.28
SD [b]	9.46	25.23	245.39	23.15	33.72	9270.98
SD [c]	7.45	15.46	66.83	26.91	15.89	4097.68
Cv (%) [a]	111.38	233.43	45.46	107.48	198.15	73.74
Cv (%) [b]	118.41	84.77	131.56	98.38	142.24	137.50
Cv (%) [c]	105.97	57.60	47.62	100.74	88.71	70.15

Note: [a] Bed Surface Sediment, [b] Sediment at 50 cm depth from Bed Surface, [c] Sediment at 100 cm depth from Bed Surface, Cv = coefficient of variation, Cv = (SD/average) x 100, SD = Standard Deviation.

The average concentration of Cu in all three layers is 6.22 ± 6.93, 7.99 ± 9.46, and 7.03 ± 7.45, respectively. Minimum Cu concentration in the bed surface layer was found at sampling station S30 while the maximum was at station S38 as shown in **Fig. 3.5**. Cu concentration was BDL at some locations, which have been excluded while computing the average value. It has been observed from the graph that there is a sudden increment in Cu concentration from stations S13 - S25 and S34 - S42. Concentrations of copper increased suddenly, mainly due to industrialization and other human activities. Polluted stretches of the river starting from

sampling station S13 are due to waste disposal from nearly located industries and towns in Tezpur at Dhenukhana stretch to Panbazar, Fancy Bazar till Kacharighat stretch located nearby the sampling station S25.

The maximum rise in the concentration level of other metals such as Zn, Mn, Ni, Cr, and Fe has been observed at sampling stations S33, S32, S28, S34, and S32, respectively. Sualkuchi location at sampling station S26 and Jogighopa at S34 contribute to the river from industrial discharges, runoff from residential areas, disposal of household effluent, and various non-point

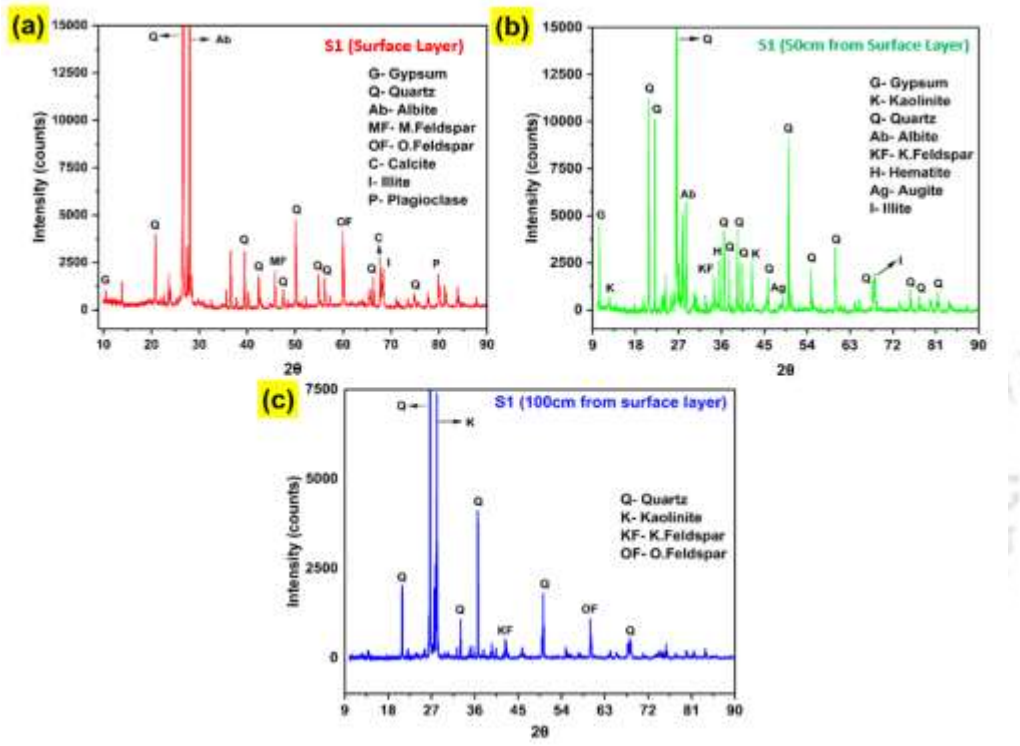

Fig.3.4 XRD pattern for sediment form (a) bed surface layer; (b) 50cm from bed surface layer; (c) 100cm from bed surface layer

sources (Action Plan Brahmaputra report, 2019). Therefore, natural and human factors are likely responsible for the induction of different metals in sediment. However, the concentration of heavy metals in this study has been compared with the various parameters presented in **Table 3.5**. The present study reveals that only Zn concentration in sediment (36.81 µg/g) exceeds the Indian River System. The concentration of all metals was within the Toxicity reference value and USEPA standards, except Ni. The primary reason for toxic sediment enriched in the context of Ni was a large polluted stretch upstream, having a peek at sampling station S26. It is important to note that certain metals, particularly Zn, exhibit high coefficients of variation, indicating substantial spatial heterogeneity and the presence of localized contamination hotspots. In such cases, mean values may be influenced by extreme observations; therefore,

median values can provide a more robust representation of central tendency. This variability highlights the non-uniform distribution of heavy metals across the study area.

Table 3.5. Mean concentration value of the heavy metal in Brahmaputra River sediment (BRS) in comparison with Average Shale Values, Toxicity Reference Values, Indian River System, and World River System.

Heavy Metal	ASV [a]	TRV [b]	IRS [c]	WRS [d]	USEPA standards [e]	Present study (µg/g)
Cu	45	16	24	100	31.6	7.08
Zn	95	110	15	350	121	36.81
Mn	850		605	1050		156.44
Ni	68	16	-	90	22.7	26.75
Cr	90	26	-	100	43.4	16.61
Fe	47200		29000	48000		5788.40

[a] [154], [b,e] [103], [c] [166], [d] [167]

The average Concentration of Ni for all sampling stations ranged from 0.25 to 150.5 µg/g in the surface layer, 0.75 to 76.50 µg/g at 50 cm depth, and 0.25 to 84.25 µg/g at 100 cm depth from the bed surface of the river. Maximum Ni was observed at stations S8, S10, S14, and S26 indicating the direct influence of anthropogenic activities on abrupt changes in Ni concentration. The level of Ni in the mid sand bar is 26.75 µg/g while TRV is 16 µg/g [103], as shown in **Table 3.5**. Ni concentration was observed above the permissible limit from station S1 to station S26. However, Ni was found within the permissible limit after station S26. A comparative analysis of the present study with other rivers has been presented in **Table 3.6**.

Table 3.6. Heavy metal concentration in the sediment of the Brahmaputra River and other rivers

Location	Cu	Zn	Mn	Ni	Cr	Fe	References
Brahmaputra, India (Bed Surface Layer)	7.1	36.8	156.4	26.7	16.6	5788.4	Present Study
Bharali Tributary, Brahmaputra, India	39.00	39.00	255.00	-	-	23651.00	[168]
Cauvery, India	35.00	26.00	319.00	-	-	17600.00	[166]
Yamuna, India	22.20	59.20	-	-	-	-	[169]

Cont.							
Chilika Lagoon, India	88.20 – 141.80	52.70 – 103.60	185.30 – 432.60	29.70 – 145.80	-	25562.40 –30041.50	[170]
Ganga, India	56.00	103.00	-	51.00	158.00	-	[171]
Buriganga, Bangladesh	184.40	502.30	-	-	101.20	-	[172]
Meghna Bangladesh	-	79.02	442.60	76.10	31.74	-	[173]
Eupharates, Iraq	18.91	48.00	228.18	67.08	58.4	2249.47	[174]
Yarlung Tsangbo	30.15	84.83	693.68	50.55	97.51	33748.00	[175]
Yangtze, China	60.03	230.40	-	41.90	108.00	-	[176]

3.3.3 Assessment of Heavy Metals in the Vertical Profile

The soil sample beneath the surface must be collected to quantify the accumulation of heavy metals in the soil layer (Linde et al., 2001). The vertical profile of six heavy metals, i.e., Cu, Zn, Mn, Fe, Cr, and Ni, have been presented in **Fig. 3.5 (a-f)**. Heavy metal concentration in sediments varies very little with depth or is relatively uniform, as illustrated in **Table 3.4**. The concentration of Cu remains similar in all three layers from stations S1 to S13 and S26 to S33. Cu shows enrichment in concentration from station S14 to S25 before attaining a peak at station S38 in the Surface layer and S35 in the middle (50 cm depth) and lower (100 cm depth) layer. Industrial effluents and anthropogenic inputs were mainly responsible for the enrichment of Cu concentration for the above-cited stations. Zn shows its similar concentration throughout the river stretch except for its peak at sampling stations S8 and S33 in the surface layer. The middle and lower layer of sediment indicates the abrupt change in concentration of Zn. It has been found that the concentration of Mn and Fe was enriched in the middle layer showing a peak at station S32, while the surface and lower layer vary within a narrow range over the entire stretch of the river. The surface layer of sediment has a uniform concentration of Cr except for stations S9 and S34, where Cr indicated the maximum concentration. The enrichment of Ni was found from station S1 to S26 in the surface layer and till S24 in the middle and lower layer before attaining a uniform curve towards the downstream. The different peaks for various heavy metals are due to the kind of effluents discharging in the river. Agricultural runoff, industrial effluents, and residential discharges may have a different proportion of heavy metals. Depending on the disposal station location, a heavy metal may accumulate at a particular station at different rates. The sediments where effluent was discharged will have a high level

of heavy metals. In contrast, sediments located far out from the disposal station will have a lower concentration due to dilution.

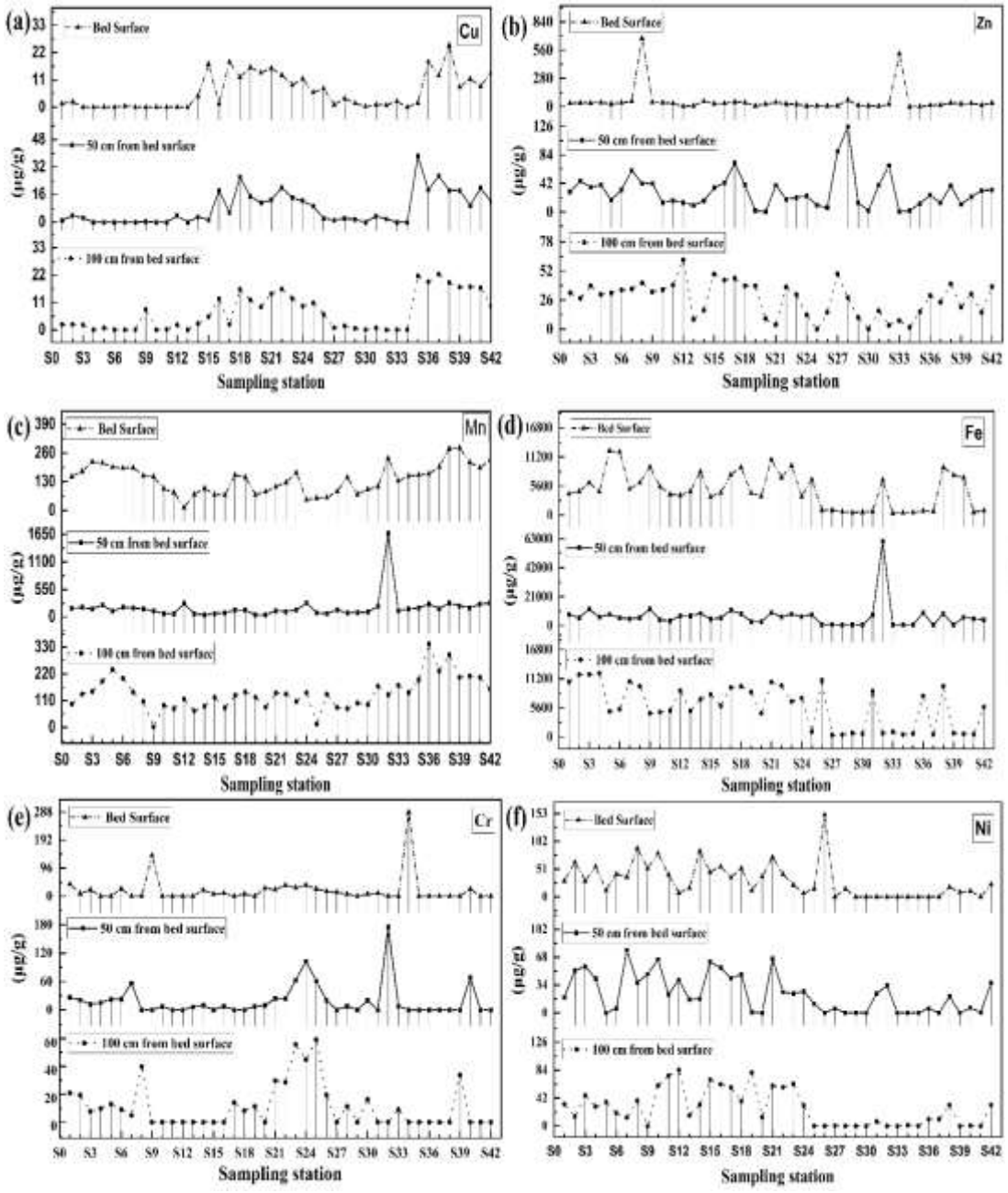

Fig. 3.5 Vertical distribution of heavy metals in the Brahmaputra River sediment

3.3.4 Assessment of Sediment Contamination

Reach 1 and Reach 2 zones have been created by dividing all 42 stations into upstream and downstream segments. Upstream region contains sampling station S1 (Jorhat) to S25 (Guwahati) and S26 (Sualkuchi) to S42 (Dhubri). It was done to examine the river stretch

before and after the Guwahati, where many effluents have been discharged. Anthropogenic influence on sediment quality was assessed by examining six indices, namely, Enrichment factor (EF), Contamination factor (CF), Geo-accumulation index (Igeo), Potential ecological risk index (PERI), Contamination degree (CD), and Pollution load index (PLI) as summarized in **Table 3.7**.

EF is widely used as an indicator of contamination level and distinguishes between natural and anthropogenic sources. The metal concentrations in the samples are normalized concerning conservation elements such as Fe and Al to account for mineral variation induced by heterogeneous sediments. This study selected Iron (Fe) as the normalizing element as the sediments of The Brahmaputra River is rich in iron content. EF value for Cr in the lower layer for Zn and Ni in all three layers indicate low to moderate enrichment in the upstream region, as shown in **Table 3.7**. In contrast, moderate to severe enrichment was found in Ni for the upper layer, Cu and Mn in the downstream region's upper and middle layer. Severe enrichment has been identified further in the downstream region in Cu for the lower layer, Zn for the middle and lower layer, and Cr in the upper layer. Zn in the upper layer towards the downstream region was the only element that showed high enrichment, indicating the anthropogenic influence load on the Zn element. Unpolluted sediment is measured by a contamination factor (CF). It is computed by comparing the measured concentration of heavy metal with the typical shale value of a conferred metal. Contamination factors for all sampling stations suggest low contamination in sediment, as tabulated in **Table 3.7**.

The evaluated Geo-accumulation index for river sediment belonging to class 0 (Igeo ≤ 0) represents the uncontaminated sediment in all three layers throughout the river stretch. Potential ecological risk factor (E_r^i), which has been accounted for all the layers at all sampling stations, outlined the low ecological risk to the aquatic environment. Integral indices are determined individually and then added to represent the sediment's overall performance. Contamination degree (CD), Pollution load index (PLI), and Potential ecological risk index (PERI) were three integrated indices used in this study. CD is the sum of all CF values for a particular sample. PLI is a method for determining the pollution load index for each sediment site. Sample quality and toxicity are assessed through PLI. The nth root of n number multiplying with the CF values together gives the PLI for a single site. The potential ecological risk index (PERI) is used here to evaluate the ecological risks posed by heavy metals. An

overall evaluation of heavy metal pollution risks is based on the Environmental Risk Index, which assesses both ecological and environmental toxicity. The evaluated CD indicated the low contamination degree, PLI represents an excellent state of pollution to occur, whereas PERI suggested low risk to aquatic living and the environment.

Table 3.7. Summary of sediment quality based on various indices

Depth (cm)	Index	Stream Location	Cu	Zn	Mn	Ni	Cr	Fe
Bed Surface Layer	EF	Reach 1	1.11 ± 1.53	4.66 ± 10.38	1.16 ± 0.59	4.95 ± 3.09	1.52 ± 2.07	--
		Reach 2	6.44 ± 7.34	49.88 ± 169.13	10.03 ± 6.78	8.52 ± 26.45	22.63 ± 83.40	--
	CF	Reach 1	0.13 ± 0.15	0.60 ± 1.37	0.15 ± 0.07	0.61 ± 0.35	0.21 ± 0.32	0.14 ± 0.06
		Reach 2	0.15 ± 0.16	0.52 ± 1.29	0.20 ± 0.08	0.19 ± 0.53	0.24 ± 0.76	0.05 ± 0.07
	I_{geo}	Reach 1	-2.04 ± 2.10	-2.26 ± 1.37	-3.54 ± 0.08	-1.61 ± 1.05	-1.54 ± 1.53	-3.57 ± 0.59
		Reach 2	-3.84 ± 2.05	-2.82 ± 2.11	-3.07 ± 0.67	-1.32 ± 2.35	-1.15 ± 1.80	-5.94 ± 1.61
	E_r^i	Reach 1	0.64 ± 0.76	0.60 ± 1.37	0.15 ± 0.07	3.04 ± 1.76	0.41 ± 0.64	--
		Reach 2	0.77 ± 0.81	0.51 ± 1.29	0.20 ± 0.08	0.97 ± 2.66	0.48 ± 1.53	--
Middle Layer (50 cm)	EF	Reach 1	1.16 ± 1.58	2.10 ± 1.40	1.12 ± 0.59	3.68 ± 3.03	1.60 ± 2.00	-
		Reach 2	9.47 ± 17.22	14.79 ± 34.68	8.06 ± 6.66	0.89 ± 1.65	3.53 ± 6.23	--
	CF	Reach 1	0.14 ± 0.17	0.30 ± 0.19	0.16 ± 0.08	0.50 ± 0.33	0.22 ± 0.28	0.15 ± 0.05
		Reach 2	0.23 ± 0.24	0.33 ± 0.36	0.31 ± 0.43	0.11 ± 0.18	0.20 ± 0.49	0.14 ± 0.31
	I_{geo}	Reach 1	-2.43 ± 2.26	-2.46 ± 1.24	-3.47 ± 0.82	-1.72 ± 1.50	-2.02 ± 1.65	-3.45 ± 0.58
		Reach 2	-2.67 ± 2.03	-3.28 ± 2.30	-2.77 ± 1.02	-1.65 ± 2.29	-0.84 ± 1.53	-5.23 ± 2.12
	E_r^i	Reach 1	0.71±0.86	0.30±0.19	0.16±0.08	2.52±1.67	0.44±0.57	--
		Reach 2	1.14 ± 1.27	0.33 ± 0.36	0.31 ± 0.43	0.53 ± 0.92	0.39 ± 0.98	--
Lower Layer (100 cm)	EF	Reach 1	1.18 ± 2.27	2.08 ± 1.15	0.89 ± 0.51	3.82 ± 2.71	2.02 ± 6.12	-
		Reach 2	11.15 ± 16.38	13.19 ± 19.04	11.07 ± 8.00	1.45 ± 3.43	3.50 ± 7.30	--
	CF	Reach 1	0.13 ± 0.13	0.33 ± 0.16	0.14 ± 0.06	0.61 ± 0.37	0.17 ± 0.20	0.17 ± 0.06
		Reach 2	0.26 ± 0.20	0.22 ± 0.15	0.20 ± 0.09	0.08 ± 0.15	0.06 ± 0.11	0.06 ± 0.08
	I_{geo}	Reach 1	-2.92 ± 2.22	-2.25 ± 1.03	-3.75 ± 1.34	-1.30 ± 0.93	-1.86 ± 1.67	-3.33 ± 0.76
		Reach 2	-2.52 ± 2.33	-2.94 ± 1.48	-2.99 ± 0.62	-1.39 ± 0.93	-0.90 ± 1.49	-5.82 ± 1.87
	E_r^i	Reach 1	0.63 ± 0.65	0.33 ± 0.16	0.14 ± 0.06	3.03 ± 1.84	0.33 ± 0.40	--
		Reach 2	1.00 ± 1.02	0.21 ± 0.15	0.20 ± 0.09	0.40 ± 0.77	0.12 ± 0.22	--
-----	CD	Reach 1	0.40 ± 0.41	1.23 ± 1.46	0.44 ±0.16	1.72 ± 0.71	0.59 ± 0.58	0.45 ± 0.12
		Reach 2	0.58 ± 0.56	1.06 ± 1.29	0.71 ± 0.49	0.39 ± 0.60	0.49 ± 0.86	0.25 ± 0.35
	PLI	Reach 1	0.12 ± 0.13	0.32 ± 0.22	0.14 ± 0.06	0.47 ± 0.30	0.12 ± 0.19	0.14 ± 0.04
		Reach 2	0.17 ± 0.17	0.21 ± 0.17	0.21 ± 0.09	0.05 ± 0.13	0.03 ± 0.06	0.05 ± 0.05
	PERI	Reach 1	1.99 ± 1.96	1.25 ± 1.41	0.43 ± 0.16	8.47 ± 3.46	1.20 ± 1.12	--
		Reach 2	2.93 ± 2.63	1.10 ± 1.23	0.71 ± 0.46	2.07 ± 2.90	1.08 ± 1.67	--

3.3.5 Correlation Matrix

Heavy metal sources were figured out using the Pearson's correlation matrix [177], and there is a single controlling factor for the heavy metal concentrations [178]. The correlation among the various metals in the sediment core is summarized in **Table 3.8.** Assessment of correlation matrix of heavy metals was categorized into three layers Bed surface layer, 50 cm depth from the bed surface, and 100 cm depth from bed surface layer. The strongly correlated and moderately correlated correlation suggested that effluents have similar types of sources.

Table 3.8. Heavy metal correlation matrix for Brahmaputra sediment

Bed Surface layer						
	Cu	Zn	Fe	Cr	Mn	Ni
Cu	1.00					
Zn	-0.16	1.00				
Fe	0.11	-0.01	1.00			
Cr	-0.16	-0.11	-0.02	1.00		
Mn	0.14	0.07	0.28	-0.01	1.00	
Ni	-0.02	0.19	0.29	-0.04	-0.18	1.00
Middle layer (50 cm)						
	Cu	Zn	Fe	Cr	Mn	Ni
Cu	1.00					
Zn	-0.17	1.00				
Fe	-0.11	0.28	1.00			
Cr	-0.10	0.13	0.73**	1.00		
Mn	-0.03	0.27	0.91**	0.72**	1.00	
Ni	-0.17	0.31*	0.25	0.10	0.08	1.00
Lower layer (100 cm)						
	Cu	Zn	Fe	Cr	Mn	Ni
Cu	1.00					
Zn	-0.01	1.00				
Fe	-0.10	0.44**	1.00			
Cr	0.11	-0.19	0.16	1.00		
Mn	0.44**	0.07	0.08	-0.20	1.00	
Ni	-0.02	0.61**	0.55**	0.10	-0.13	1.00
* Significant at $p < 0.05$, ** Significant at $p < 0.01$						

Particularly industrial effluents, municipal inputs, and runoff from agricultural and residential areas, at $p < 0.05$ and $p < 0.01$, There was no positive or negative, strong correlation identified among the heavy metals in the bed surface layer. However, at 50 cm depth from the surface layer, a strong positive correlation exists between Cr vs. Fe (0.73), Mn vs. Fe (0.91), and Mn vs. Cr (0.72) at the significance level of 0.01. A moderately correlated relation was found between Ni vs. Zn (0.31), corresponding to the significance level of 0.05. Moreover, Fe vs. Zn (0.44), Mn vs. Cu (0.44), Ni vs. Zn (0.61), and Ni vs. Fe (0.55) depicted a strong relationship corresponding to a significance level of 0.01 in the sediment located at 100 cm depth from the surface layer. A strong relationship among the heavy metals demonstrates the same level of contamination and common sources of pollution in sediment layers [175,179].

3.3.6 Principle Component Analysis

An effective method to determine the origin of heavy metals is to utilize Principal components analysis [180]. The heavy metal load on a principal component may be similar, and the maximum load on PC1 typically indicates anthropogenic origin. In contrast, maximum loading values on PC2 suggest that heavy metals are naturally derived [181]. Results of the PCA are summarized in **Table 3.9,** along with the eigenvalues, proportion, and cumulative proportion for each factor. A total of four selected PCs accounted for the variation in data with eigenvalues greater than 1.

Table 3.9. Principle component analysis of sediment core of the Brahmaputra River

Variables	PC1	PC2	PC3	PC4
Cu	0.36	0.43	0.40	-0.29
Zn	0.14	-0.52	0.08	0.64
Fe	0.66	-0.06	-0.34	-0.21
Cr	-0.27	0.03	-0.79	-0.20
Mn	0.46	0.38	-0.32	0.51
Ni	0.33	-0.62	0.01	-0.41
Eigen value	1.41	1.31	1.08	1.04
Proportion	0.23	0.22	0.18	0.17
Cumulative	0.23	0.46	0.63	0.81

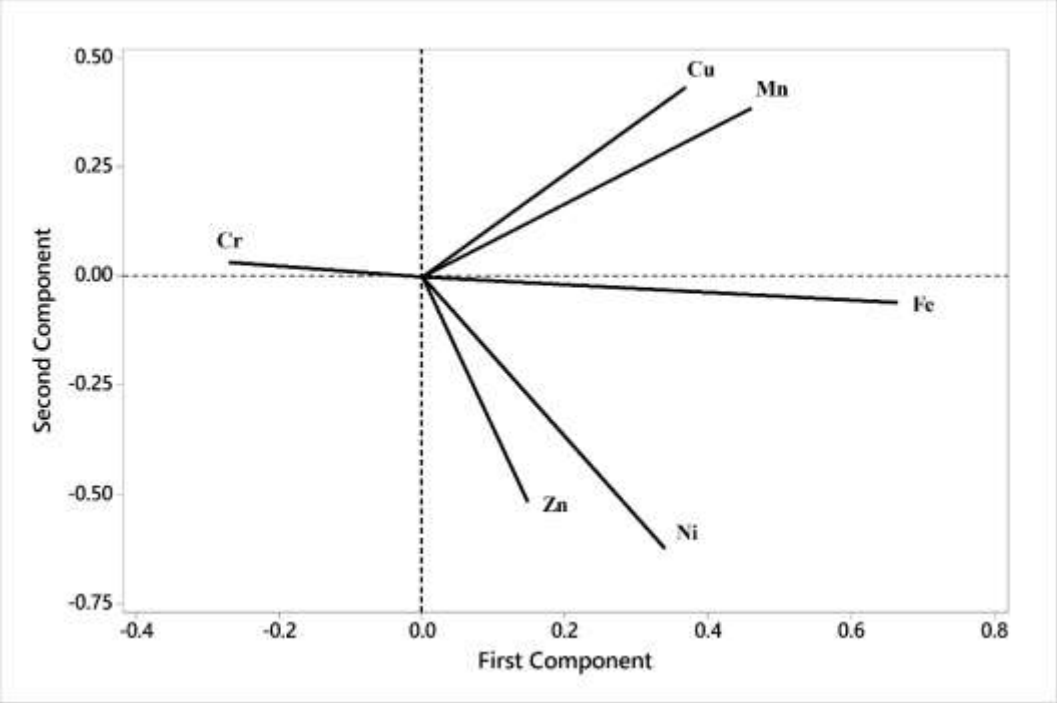

Fig.3.6 Principal component analysis of heavy metals at various different sediment sampling station

However, the loading plots for the first two components are represented in **Fig. 3.6**. These Components explain 80.80 % of the overall variance of metals and are expressed as four components. PC1 depicted the eigenvalue of 1.41 and exhibited the 23.5 % total variance magnitude having the highest loading of Cu, Fe, Mn, and Ni. These higher values indicated theirs accredited to human activities in copper, iron, manganese, and nickel. PC2 explained 21.9 % of total variance with the higher load on Cu and Mn, which shows an eigenvalue of 1.31. The higher load value of Copper and Manganese in sediment cores suggests they were formed naturally.

3.3.7 Cluster Analysis

A Hierarchical Cluster Analysis was run on all the parameters used in PCA to construct clusters with similar characteristics. The Euclidean distance method used by Ward has been implemented since it uses more cluster content information than the other available methods [182]. Applying cluster analysis to the analysis of sampling stations can also clarify the degree to which they are similar and dissimilar. Sampling stations with similar characteristics are displayed in one group while distinct traits in another, depending on their concentration.

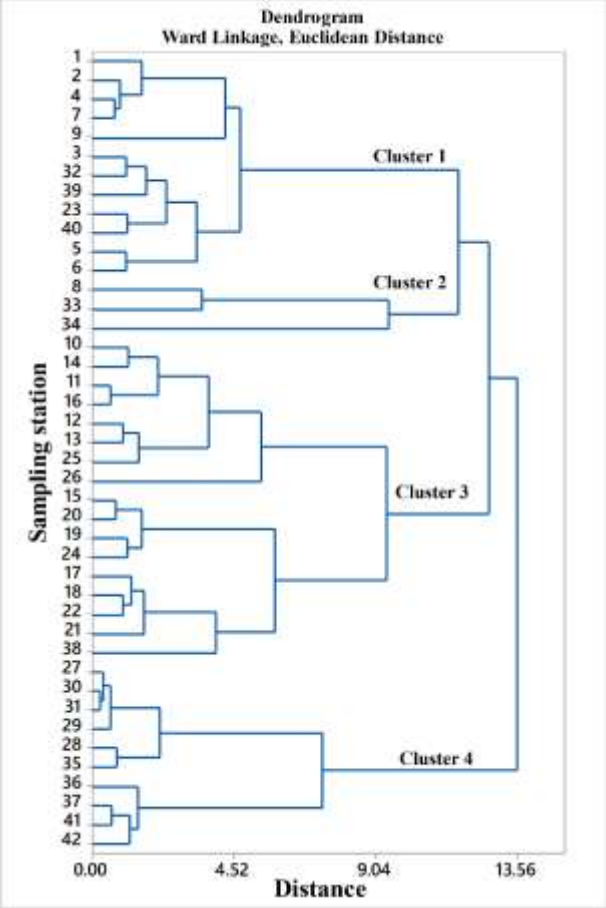

Fig.3.7 Cluster analysis of heavy metals

Two clusters were formed considering the similarity percentage of clusters. Cu and Mn indicate a similarity level of 56.95 % from cluster 1, whereas Zn, Fe, and Ni form cluster 2 with a similarity level of 51.21 %, as represented in **Fig. 3.7**. Out of six variables, Cr was the only element that didn't show any similarity with other variables. Based on another cluster analysis, the sampling stations were categorized into four major clusters, as shown in **Fig. 3.8**. Cluster 1 consists of 12 stations, cluster 2 has 3 stations, while cluster 3 and cluster 4 have 17 and 10 sampling stations, respectively.

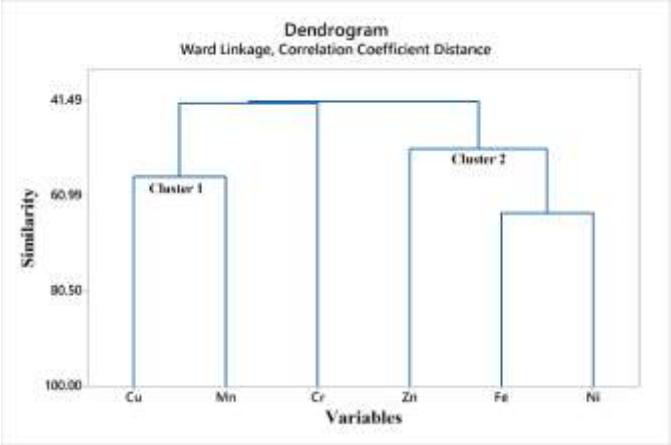

Fig.3.8 Cluster analysis of sediment sampling stations

3.3.8 Morphology Analysis of Sediment

Surface morphology of the sediment was observed for two numbers of samples from each layer (surface; 50 cm and 100 cm from surface layer) using FESEM (Gemini 500). It was observed that all the shape of the sediment was in an angular shape, as shown in **Fig. 3.9**. It represents that the sediment has been either weathered out recently.

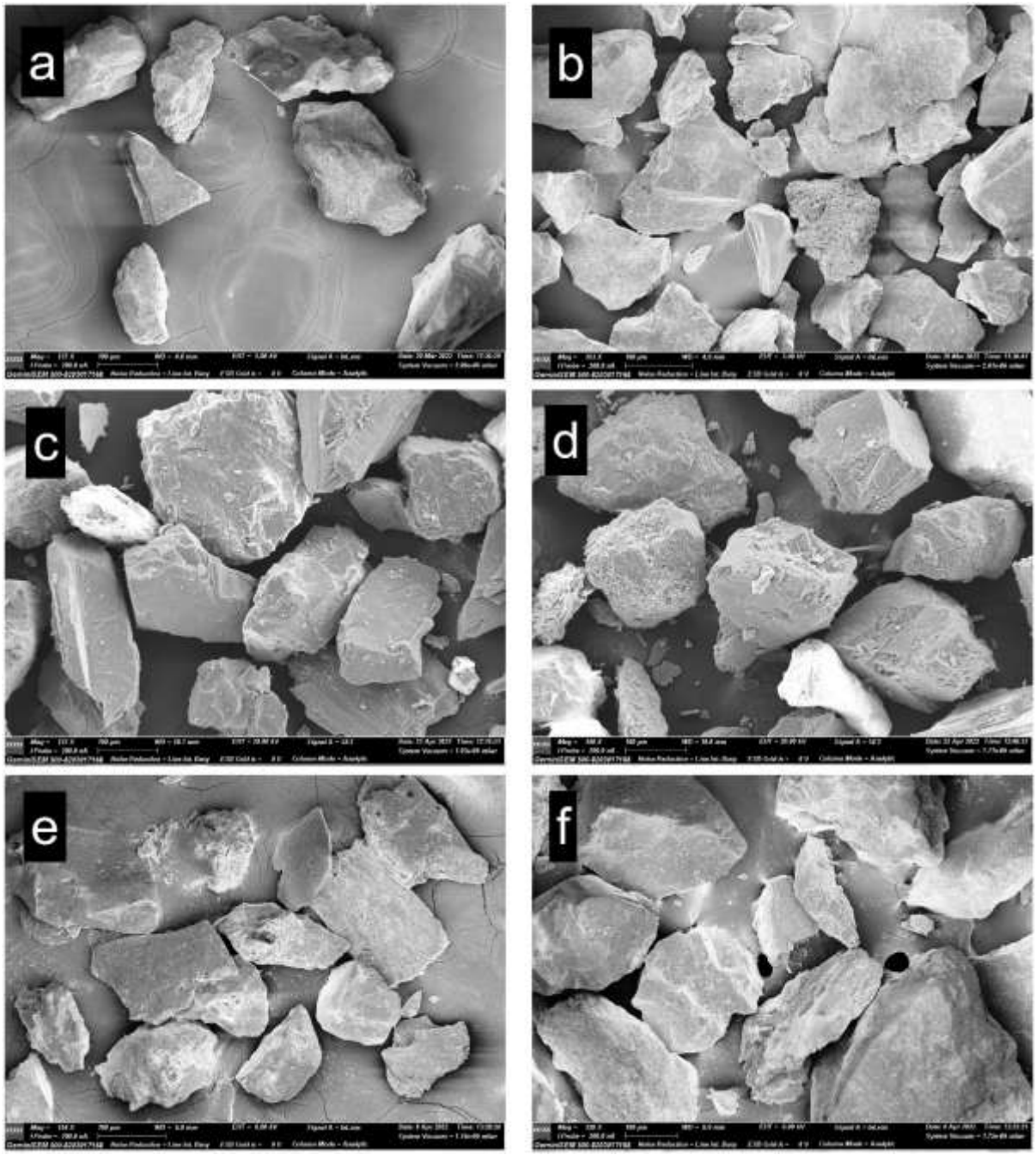

Fig.3.9 FESEM image of sediment samples for (a. b) from surface layer; (c, d) 50cm from surface layer; (e, f) 100cm from surface layer

The rounded shape of sediment depicts that sediment has travelled a lot, and its shape has been transformed from angular to subangular and further subrounded to rounded. It also suggests that it might be because of anthropogenic activity, which led to weathering and erosion.

3.4 NOVELTY AND ENVIRONMENTAL IMPLICATIONS

Over the past few decades, the Brahmaputra River (Assam, India) has been explored extensively. However, no research on the mid sandbars (fluvial islands) has been conducted to understand the feasibility of dredging activity for navigation purposes. The study is of its first kind in the Northeastern part of India. It exhaustively examines the mid sand bar quality through vertical sample profiling, risk assessment indexes, and morphological study.

The study selected 42 sampling stations covering around 600 km to explore dredging feasibility. Dredging can benefit society in numerous ways, such as creating navigable channels, reducing transportation time for freight and passengers, and increasing trade commerce (as depicted in **Fig. 3.10**). In areas of high flood where the narrow river width, dredging is a sustainable and simple solution. Also, the dredged materials can be efficiently used for various purposes, especially in Civil Engineering problems in Geotechnical, Transportation, and Construction Engineering. Other miscellaneous application includes beach nourishment, habitat enhancement, and land reclamation. Further, the presence of polluted sand bars forces policymakers to devise proper mitigation measures to minimize the adverse impact on the aquatic environment due to the leachability of contaminants present in the sand bar.

3.5 RISK ASSESSMENT

Risks associated with dredging activities may be related to environmental risks, operational risks and social and economic risks [183]. Environmental risks include habitat disruption, water quality degradation due to resuspension of sediments, potentially harming aquatic organisms and affecting drinking water supplies. Further sediments may contain contaminants (heavy metals, chemicals) that can be released into the water column [184]. Operational risks involve heavy machinery and high-risk activities, leading to potential injuries or fatalities. Malfunctions or breakdowns of dredging equipment can lead to project delays or accidents. Dredging vessels and equipment can pose risks to other river users and navigation. To minimize environmental risks during dredging, controlled dredging practices should be adopted to reduce sediment resuspension and contaminant spread. The installation of silt curtains around dredging zones can help contain suspended sediments and limit dispersion to surrounding waters. Proper handling, transportation, and disposal of contaminated dredged material must

be ensured following environmental guidelines. In addition, temporary containment and treatment of dredged sediments may be required before disposal. Continuous real-time monitoring of water quality parameters such as turbidity, dissolved oxygen, and contaminant levels should also be conducted throughout dredging operations to ensure environmental safety ***Table 10*** illustrates various case studies of dredging operations and their global impact.

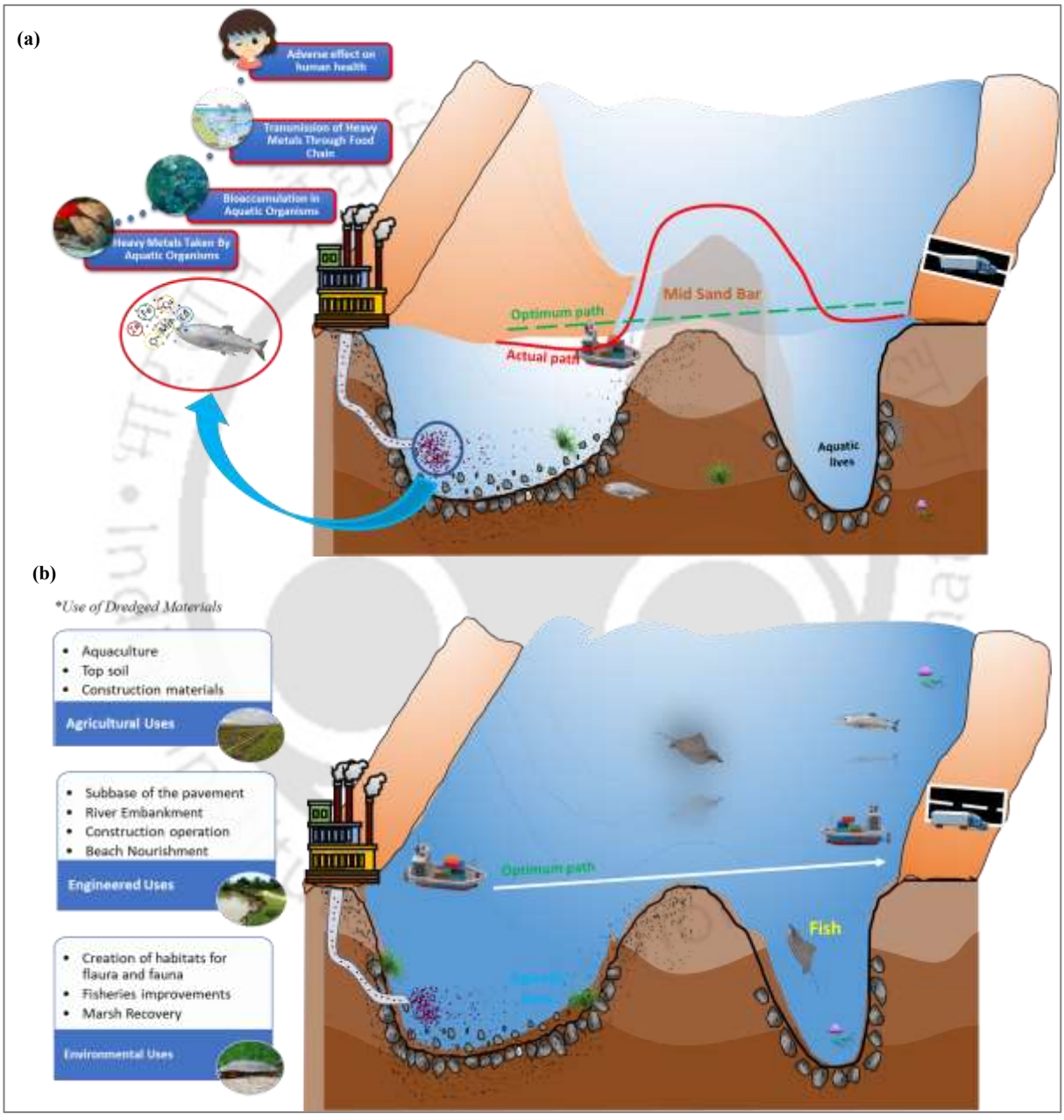

Fig.3.10 A conceptual representation of dredging operation in a river system: (a) Before Dredging (b) After dredging. It can be observed that dredging results in creating optimal navigable path, reduction in transportation time for freight and passengers

Table 3.10. Selected case studies of dredging operations and their impact

Country	Location	Year	Activity/Purpose	Scale of impact/damage	Mitigation measures	References
Australia	Nelly bay	2000-2004	Capital dredging of total volume 35000 m^3	No significant impacts were detected	None reported	[185]
Bahrain	Fasht Al-Adham (east coast)	1985-1992	Dredging for industrial development	Around 22 ha of coral reef were lost and additionally 8 ha lost further due to sedimentation and turbidity	None reported	[186]
Australia	Botany Bay, New South Wales	1942-1984	Widespread dredging, along with poor catchment management and uncontrolled effluent disposal	Loss of 257 ha of seagrass beds	None reported	[187,188]
Hong Kong (China)	Chek Lap Kok International airport	1994–1998	Dredging, construction and reclamation works were carried out for airport	*Zostera japonica* seagrass lost completely however recovery of Halophila ovata were observed	None reported	[189,190]
Australia	Cleveland Bay	1970	Capital and maintenance dredging at Ross River mouth and disposal at various dump sites	Extensive burial and loss of nearly all seagrass vegetation	None reported	[191]
Australia	Deception Bay, Queensland	1991-2002	Channel deepening and maintenance dredging of the access channel into Newport Waters Canal Estate	No significant impacts detected	Monitoring (3yrs.) and mapping	[192]

Cont.						
Australia	Port of Karumba, Queensland	1994-2004	Maintenance dredging of port entrance and river channel	No observable impacts on approx.1000 ha of seagrass within the Port area	Long-term monitoring	[193]
Brazil	Sepetiba Bay port, Rio de Janeiro State	1997	20.86 Mm3 sediments were dredged to increase the capacity of port	Heavy metals were settled on seagrass due to resuspension of contaminated sediment	None reported	[194]
Fiji	Suva, Fiji islands	1980	Sand was dredged for commercial purpose; cement production	Almost all seagrass beds were destructed however gradual recovery observed over time	Management plan	[195]
Italy	Gulf of Oristano, Sardinia	Early 1970s	Channel dredging and commercial port construction	Loss of benthic community of around 800 ha was estimated using map	None reported	[196]
Netherlands	Hond-Paap tidal flat, Ems estuary	2002-2003	Dredging and excavation of 0.25 Mm3 of sediment for the thickening of an existing gas conduit	No significant impacts on nearby eelgrass beds (Zostera marina)	EIA monitoring Programme, Restrictions to timing, turbidity plume modelling,	[197,198]

3.6 SUMMARY

There have been many ways we could assess the sediment quality of the Brahmaputra River and the feasibility of dredging because there are a number of contamination and ecological risk indices used to evaluate sediment quality. These findings show that sediment contamination is significantly different in space and suggest that an environmentally informed dredging strategy is needed. The findings provide a basis for evaluating the need to balance navigation improvements with environmentally protecting the river. Further assessment of the water quality, pollutant transport and remediation in the Brahmaputra River is possible based on this study. The following potential conclusion is drawn from the present experimental investigation.

1) The sediment layers were enriched with the heavy metals as observed in the order: Fe > Mn > Zn > Ni > Cr > Cu, whereas Co, Cd, and Pb were found below the detected limit (BDL).
2) The mean concentration of Ni in all three layers exceeds the toxic reference value of 16 μg/g and USEPA standards of 22.7 μg/g.
3) The different peaks for various heavy metals may be attributed to the various industrial effluents entering the river system.
4) Enrichment factor (EF) displayed the enrichment as - Cu, Ni moderately, Mn, Ni severe.
5) Zn was extremely high in the surface layer and almost identical trend was seen at 50 and 100 cm depth of reach 2, while the polluted sediment indices depicted no contamination and low enrichment for reach 1.
6) The primary reason for the abruptly elevated enrichment in reach 2 may be due to the uncontrol and non-judicial anthropogenic inputs from the Guwahati region, where pharmaceuticals manufacturing, oil refinery, and industrial and household effluents are uninterruptedly let out their effluents in the river.
7) Observing that the sediment of the mid-sand bar is enriched in reach 2, lots of care and strategic management needs to be taken care of while dredging the sand bar in this region.
8) CM, CA, and PCA methods were used to assess the potential sources of contamination and found that all heavy metals pose a similar origin. Based on the findings, the study concludes that the dredging activity is feasible in reach 1 and some selective spots in reach 2.
9) The finding from the study will help by providing an optimum path for navigation, reduction in floods, and deepening the channel, especially in the Guwahati region (reach 2), which is more affected by floods (during monsoon season: April to July), owing to its minimum width across Guwahati city.

भारतीय प्रौद्योगिकी संस्थान गुवाहाटी
Indian Institute of Technology Guwahati

Chapter 4

Impact of COVID-19 Lockdown on Water Quality and Human Health Risk

4.1 INTRODUCTION

Anthropogenic activities have been, among others, the main factors leading to the degradation of river water quality, mainly in densely populated and industrialized areas. The discharge of industrial effluents and urban wastewaters, as well as the activities related to transportation and tourism, are some of the ways through which the rivers are getting polluted. However, with the outbreak of the COVID, 19 pandemic and the subsequent complete lockdowns in many countries, these activities were drastically curtailed, leaving a very rare and incomparable situation for monitoring the changes in the river systems under reduced anthropogenic pressures. This chapter delves into the ramifications of the lockdown on the water quality of the Brahmaputra River emphasizing the heavy metal concentrations and microbiological levels. Besides, it looks into the potential health risks associated with the use of contaminated river water during and post, lockdown. The study presents a clear picture of the scale of human impact on the natural ecosystem and points out the impacts of COVID-19 Lockdown on Water Quality and Human Health Risk. The section 4.2 describes about the materials and methodology adopted in this study. The section 4.3.1 and 4.3.2 presents the determination of Heavy Metal Pollution Index (HPI) and Metal index (MI) to evaluate the quality of water. Further assessment of potential health risks was described in Section 4.3.3 depicting Chronic daily intake (CDI) considering the Heavy metal concentration, rate of ingestion, exposure frequency, bodyweight, average time and duration of exposure. Section 4.5 explains the result section in brief performing the statistical analysis of the data by cluster analysis (CA) in sec 4.5.3 and corelation matrix in sec 4.5.4 to establish the relationship for the lockdown and post-lockdown periods. There was no significant or weak relation between the heavy metals during the lockdown period, indicating low pollution. However, after the lockdown, a strong negative correlation was found among Cr, Cu, Ni, Zn, and Fe whereas a very strong positive correlation was found among Ni, As, and Cr. Section 4.5.5 highlights the possible risks to human health from different heavy metals hazard index (HI) based on hazard quotients (HQ). Control measure to be taken is summarised in section 4.7 before concluding the chapter in section 4.8.

4.2 MATERIALS AND METHODOLOGY

4.2.1 Study Area

The Brahmaputra River enters the Sadiya region and exits in the South Salmara-Mankachar region of Assam in India [199]. The present study comprises 11 sampling stations spanning a distance of approximately 600 km along the Brahmaputra River in the Assam region. When selecting the sample stations, two key criteria were considered. The first is the ease of access to all the places where the river flows in the Assam region; the second is the proximity of the sampling sites to the probable source(s) of pollutants. It includes the upstream, city area and downstream through which the river flows in the state. They are named as RB1: upstream Dibrugarh, RB2: Bogibeel Bridge, RB3: NimatiGhat, RB4: Biswanath Ghat, RB5: Chandrapur, RB6: Kachari Ghat (main Guwahati city), RB7: Dhenukapahar, RB8: Pandu, RB9: Sualkuchi, RB10: Dhubri and RB11: downstream Jogighopa (Fig.4.1).

4.2.2 Sample Collection and Analysis

The Pollution Control Board, Assam (PCBA) provided the data on 9 HMs such as Arsenic (As),

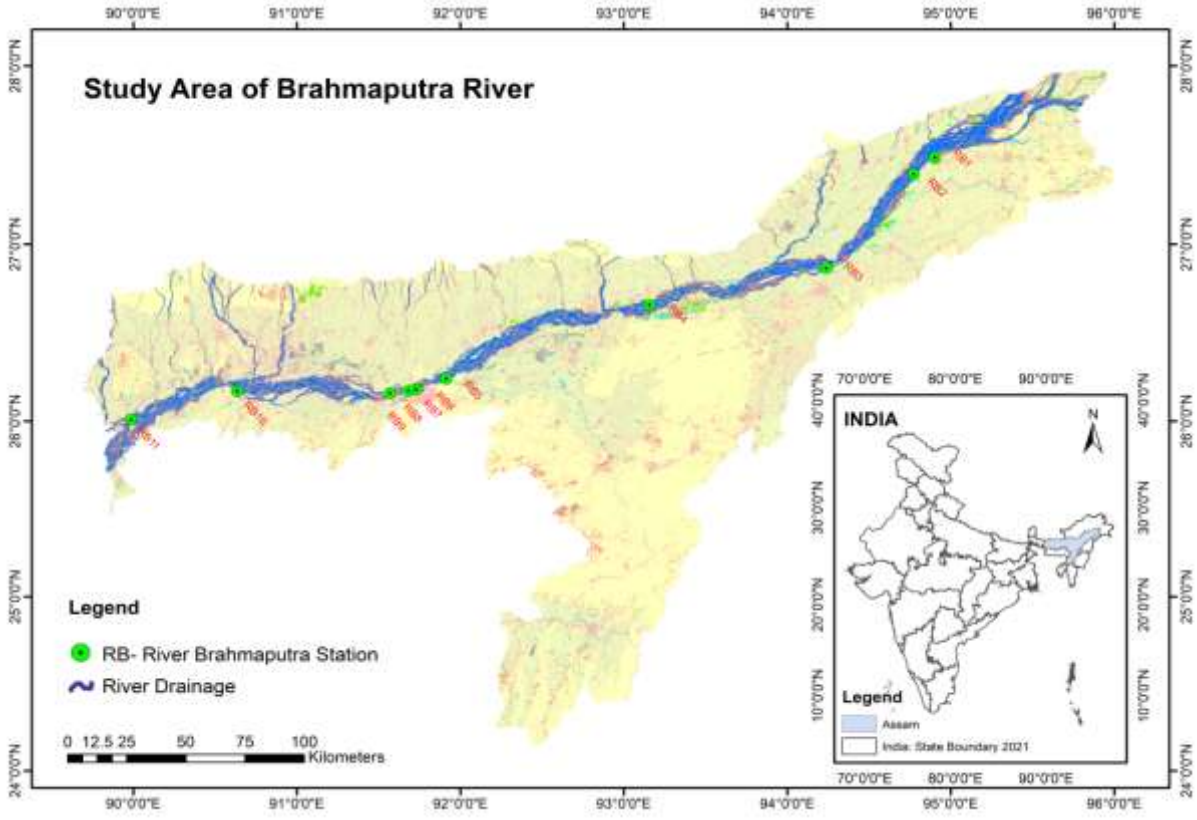

Fig.4.1. Study area map showing the various sampling stations of the Brahmaputra River in Assam, India

Cadmium (Cd), Mercury (Hg), Chromium (Cr), Iron (Fe), Nickel (Ni), Lead (Pb), Copper (Cu), Zinc (Zn) and microbiological indicators (Fecal Streptococci, Fecal coliform bacteria and Total coliform Bacteria). We used data from PCBA in our research because sampling in the

Brahmaputra River was not feasible due to the lockdown. They collected river water samples in June 2020 and April 2021, respectively, from the Brahmaputra River course, during and after the COVID-19 lockdowns. Following the standard procedures outlined by the American Public Health Association [200], water samples were collected and analyzed. Water samples were collected in pre-cleaned (1L) high-quality plastic bottles. The bottles were stored in iceboxes until they were transported to the lab for examination. A portion of the sample was acidified with concentrated nitric acid to a pH of 2.0. The samples were digested using nitric acid, and HMs were analyzed using an Atomic Absorption Spectrophotometer (AAS). The AAS is one of the essential methods for calculating the quantities of chemical elements in water samples by calculating the radiation that is absorbed while the chemical of interest is present. The preparation of each standard took place in a controlled setting. The values of standards obtained were consistently well within acceptable ranges, whereas those for the blanks were below the lowest detection limits. To make sure they were accurate and precise, the standards were retested after three samples. Additionally, faecal streptococci, faecal coliform bacteria, and total coliform bacteria were tested in the water samples using the Most Probable Number (MPN) method.

4.3 STATISTICAL ANALYSIS

The spatial variations of the Heavy Metal Pollution Index (HPI) were examined using the Inverse Distance Weightage (IDW) method in the software called ArcGIS 10.4.1. The interrelationship of the heavy metals was observed using Pearson's correlation matrix (PCM). Cluster analysis (CA) was used to classify sample stations with similar heavy metal concentrations into several clusters [201,202]. Pearson's correlation matrix and Cluster analysis were performed using Origin pro-2022 b (Learning edition).

4.3.1 Determination of HPI

Humans can get several diseases from water contaminated with heavy metals. The HPI is a reliable indicator of the heavy metal content of water generally [203]. We have calculated HPI using three steps [204,205,206,207].

The first step is to calculate the relative weight of each required parameter (W_j).

$$W_j \propto = \frac{1}{MAC} \rightarrow W_j = \frac{f}{MAC} \tag{4.1}$$

where, f = Constant of Proportionality; MAC = "Maximum Allowable Concentration"

The second step is to calculate the quality rating (Qj) of each required parameter.

$$Q_j = \sum_{j=1}^{n} \frac{|O_j - I_j|}{S_j - O_j} \times 100 \quad (4.2)$$

where, O_j = Observed value of the heavy metal of j^{th} sample; I_j = Ideal value of the j^{th} Sample; S_j = Standard value of the jth sample

The third step is to sum up all the sub-indices to calculate the total index.

$$HPI = \frac{\sum_{j=1}^{n} W_j Q_j}{\sum_{j=1}^{n} W_j} \quad (4.3)$$

where, Q_j = sub-index of the j^{th} parameter; W_j = unit weight for the j^{th} parameter; n = number of parameters

HPI values are listed in Table 4.1. An HPI rating of 100 or above is unacceptable for human consumption and can cause serious health problems [204,208].

Table 4.1. Quality of water based on Heavy Metal Pollution Index (HPI)

Heavy Metal Pollution Index Value (HPI)	Quality of Water
< 90	low polluted
90-150	medium polluted
> 150	highly polluted

4.3.2 Determination of MI

Metal index (MI) was utilized to evaluate the water quality for drinking. It can be computed by equation (4.4) [209,210].

$$\mathrm{MI} = \sum_{j=1}^{n} \frac{\mathrm{C_j}}{(\mathrm{MAC})_j} \quad (4.4)$$

C_j = measured amount of j^{th} water sample; MAC = maximum allowable limit of metals in j^{th} water sample. The MI values are listed in Table 4.2 [204,205,209].

Table 4.2. Water quality assessment based on Metal index (MI)

Metal Index Value (MI)	Quality of Water
<0.3	Extremely clean
0.3–1.0	Clean
1.0–2.0	Slightly affected
2.0–4.0	Moderately affected
4.0–6.0	Strongly affected
>6.0	Seriously affected

4.3.3 Assessment of potential health risks

Exposure to heavy metal-contaminated water can occur through various routes, including drinking, skin contact, and inhalation. The present study evaluated potential health risks by considering the drinking exposure pathway. Chronic daily intake (CDI) is measured to determine the amount of heavy metal pollutant a person consumes, expressed as the amount of pollutant per kilogram per day absorbed through the dietary pathway. (USEPA 2011). The equation for calculating CDI is given below in Equation (4.5) [209,211,212,213].

$$CDI = \frac{C_j \times IR \times EF \times ED}{B_j \times AT} \quad (4.5)$$

where, C_j = Heavy metal concentration (mg/L), IR= Rate of ingestion, EF = Exposure frequency, B_j = Bodyweight, AT= Average Time, ED = Duration of exposure.

Table 4.3. Input parameters to calculate CDI for children, teenagers and adults

Input parameters	Children	Teenagers	Adults
IR (L/day)	0.70	2	2
EF (days/year)	365	365	365
ED (years)	6	19	30
B_j (kg)	15	50	70
AT (days)	2190	6395	10,950

4.3.4 Hazard Quotient (HQ)

The HQ was evaluated using CDI and R_fD (Reference dose) as given in equation (4.6). R_fD is the daily dose at which a person can be exposed to heavy metals without experiencing any detrimental effects over a period of time. The unit of R_fD is typically expressed in milligrams per kilogram of bodyweight per day [209,213,214,215]. The values of R_fD for As, Cd, Cu, Pb, Cr, Ni, Zn, Hg and Fe were considered as 0.0003, 0.0005, 0.04, 0.0035, 0.003, 0.02, 0.3, 0.0003 and 0.7 respectively [216].

$$HQ = \frac{CDI}{R_fD} \tag{4.6}$$

HQ>1 denotes potentially dangerous non-carcinogenic effects, while HQ<1 suggests that a non-cancer hazard shouldn't be a problem.

4.3.5 Hazard Index (HI)

The HI is another key concept associated with HQ. It is considered that hazardous compounds present in the same medium will always present a cumulative toxic risk [209]. The HQs can be combined as shown in Equation (4.7) to provide the total hazardous risk, also known as the Hazard Index.

$$HI = \sum_{j=1}^{n} (HQ)_j \tag{4.7}$$

When HI is less than 1.0, it is assumed that the non-carcinogenic, unfavourable effect of the chemical compound is minimal.

Table 4.4. Statistical analysis of heavy metals and microbiological parameters in the Brahmaputra River water during and post-COVID-19 lockdown period (values represented as mean ± standard deviation)

Parameters	During Covid-19 Lockdown							Post Covid-19 Lockdown						Acceptable limit
	Units	Min	Max	Mean	EL	TSEL	% EL	Min	Max	Mean	EL	TSEL	% EL	
As	mg/L	BDL	BDL	BDL±	AS	0	0	0.01	0.01	0.01±	AS	0	0	0.01
Cd		BDL	BDL	BDL±	AS	0	0	0.02	0.02	0.02±	AE	11	100	0.005
Cu		0.001	0.006	0.003 ±0.002	AS	0	0	0.03	0.3	0.055 ±0.081	AS	0	0	1.5
Pb		BDL	BDL	BDL±	AS	0	0	0.1	0.1	0.1±	AE	11	100	0.01
Cr		BDL	BDL	BDL±	AS	0	0	0.06	0.061	0.060 ±	AE	11	100	0.05
Ni		BDL	BDL	BDL±	AS	0	0	0.1	0.1	0.1±	AE	11	100	0.07
Zn		0.01	0.06	0.02± 0.02	AS	0	0	0.01	0.31	0.06± 0.09	AS	0	0	15
Hg		BDL	BDL	BDL±	AS	0	0	0.001	0.003	0.0016 ±	RB3, RB5	2	18.18	0.002
Fe		0.014	0.16	0.117 ±0.038	AS	0	0	0.12	0.16	0.13± 0.01	AS	0	0	0.3
Total Coliform Bacteria	MPN/L	72	200	142.09 ±44	-	-	-	72	280	177.45 ±61	-	-	-	

Cont.														
Fecal Coliform Bacteria		30	91	66.63 ±19	-	-	-		30	140	72.2± 31	-	-	-	
Fecal Streptococci		BDL	BDL	BDL±	-	-	-		15	29.5	21.85 ±5.30	-	-	-	
Acceptable limit: Limit for all heavy metals were subjected to BIS 2012 standards except for Ni which was subjected to WHO 2011 standard and Cd and Hg were subjected to EPA standards; BDL- Below detection limit, AS- All safe, AE- All exceeded, EL- Samples exceed the limit, TSEL- Total number of samples exceed the limit														

4.4 RESULTS

4.4.1 Comparison of Heavy Metals and Microbiological Indicators Examined During and After the Lockdown

The statistical analysis of heavy metals and microbiological indicators of the Brahmaputra River water during and after the lockdown is summarized in Table 4.4. In this study, the acceptable limits for all heavy metals were based on the BIS 2012 standards, except for Ni, which was based on the WHO 2011 standards, and Cd and Hg, which were based on the EPA standards [213,217,218]. A total of 9 HMs, i.e., Cd, As, Cr, Cu, Fe, Hg, Ni, Zn and Pb, were analyzed in the current study. All the examined heavy metals were below the detection limit during the lockdown. The mean values of Cd, Ni, Cr and Pb, respectively, exceeded the acceptable limit post-lockdown. Arsenic was found below the detection limit (BDL) during the lockdown. It has a mean concentration of 0.01 mg/L during the post-lockdown period, which is equal to acceptable limit of 0.01 mg/L. Unlike most heavy metals that exist as cations in aqueous environments, arsenic predominantly occurs in the form of oxyanions**,** primarily as arsenite [As(III)] and arsenate [As(V)], depending on redox and pH conditions. These oxyanionic species exhibit distinct geochemical behavior, including higher mobility and different adsorption characteristics compared to cationic metals, which has important implications for their transport, bioavailability, and removal mechanisms. Cd was found BDL during the lockdown, but exceeded its permissible limit in the post-lockdown period. It was found to have a mean concentration of 0.02 mg/L during the post-lockdown period, i.e., exceeding the acceptable limit of 0.005 mg/L. During the lockdown, the mean value of Cu concentration was below the acceptable limit. For the post-lockdown period, the mean value of Cu was found to be 0.055 mg/L, which exceeds the acceptable limit of 1.5 mg/L. Pb, Hg, Cr and Ni were BDL during the lockdown period. After the lockdown, the mean concentration of Pb was 0.1 mg/L at all sampling stations, exceeding the acceptable limit of 0.01 mg/L. Similarly, the mean value of Ni was found to be 0.1 mg/L at all sampling stations, which exceeded the acceptable limit of 0.07 mg/L. The concentration of Cr ranged from 0.060 to 0.061 mg/L, exceeding the acceptable limit of 0.05 mg/L. The mean value of Hg was BDL during the lockdown; it exceeded the acceptable limit in the sampling station at RB3 and RB8. The Fe concentration was in the range of 0.014-0.16 mg/L during lockdown and ranged from 0.12 to 0.16 mg/L post-lockdown. Both of these ranges were below the acceptable limit.

The variation in bacteria and fecal streptococci during and after the lockdown period is shown in Fig. 4.2. The range of total coliform bacteria counts was 72-200 MPN/L and 72-280 MPN/L

during the lockdown and post-lockdown periods, respectively. The range for fecal coliform bacteria varied from 30-91 MPN/L and 30-140 MPN/L during and in the post-lockdown period, respectively. Another indicator of pollution is fecal streptococci, which were BDL during the lockdown and had an average value of 21.85 MPN/L post-lockdown periods. The decrease in

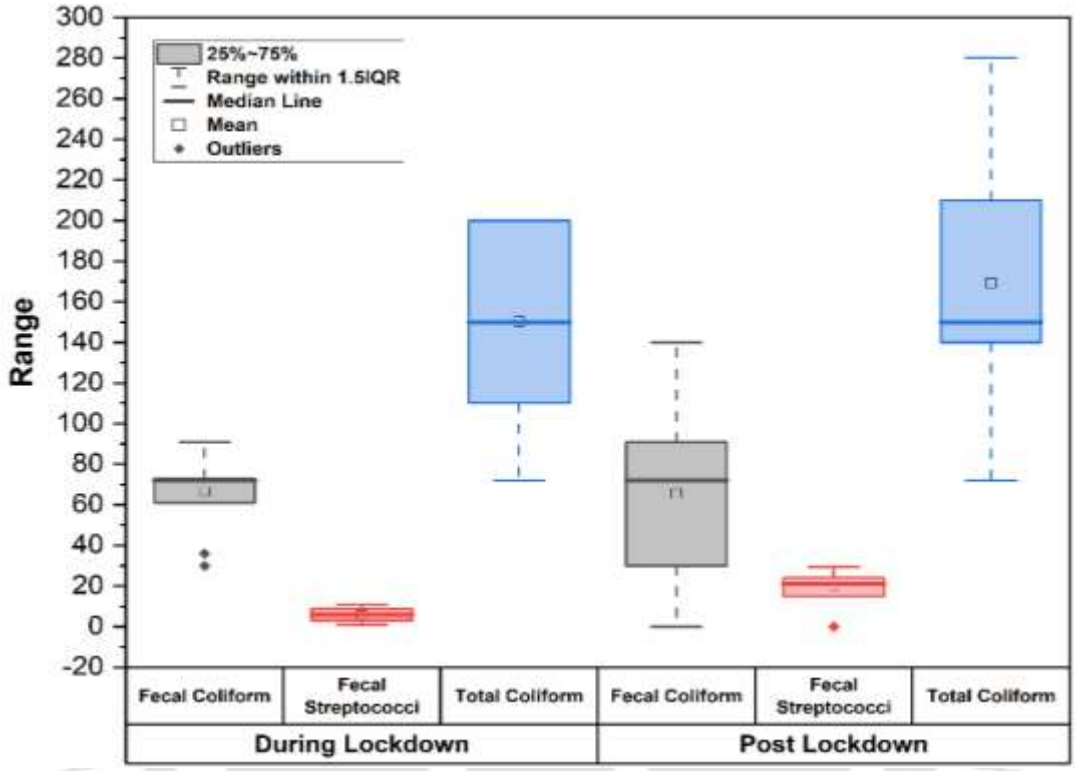

Fig. 4.2. Microbiological variation during and after the COVID-19 lockdown

bacteria and fecal streptococci during the lockdown may be attributed to the probable closure of industries, hotels, colleges, and hostels, as well as reduced waste disposal, limited bathing activities, and the use of sanitizers by people. However, after the lockdown, all restrictions were lifted, leading to an increase in pollution and its associated count.

4.4.1.1 HPI

The HPI values varied from 94.47 to 94.66 and from 320.17 to 439 during and after the lockdown period, respectively. These HPI values correspond to “medium polluted” during the lockdown, and “highly Polluted” after the lockdown ended (Table 4.1). RB5, Chandrapur, had the maximum value of HPI during the post-lockdown period (Table 4.5). Figure 4.3a and 4.3b show the spatial distribution of various HPI values during the lockdown and post-lockdown, respectively.

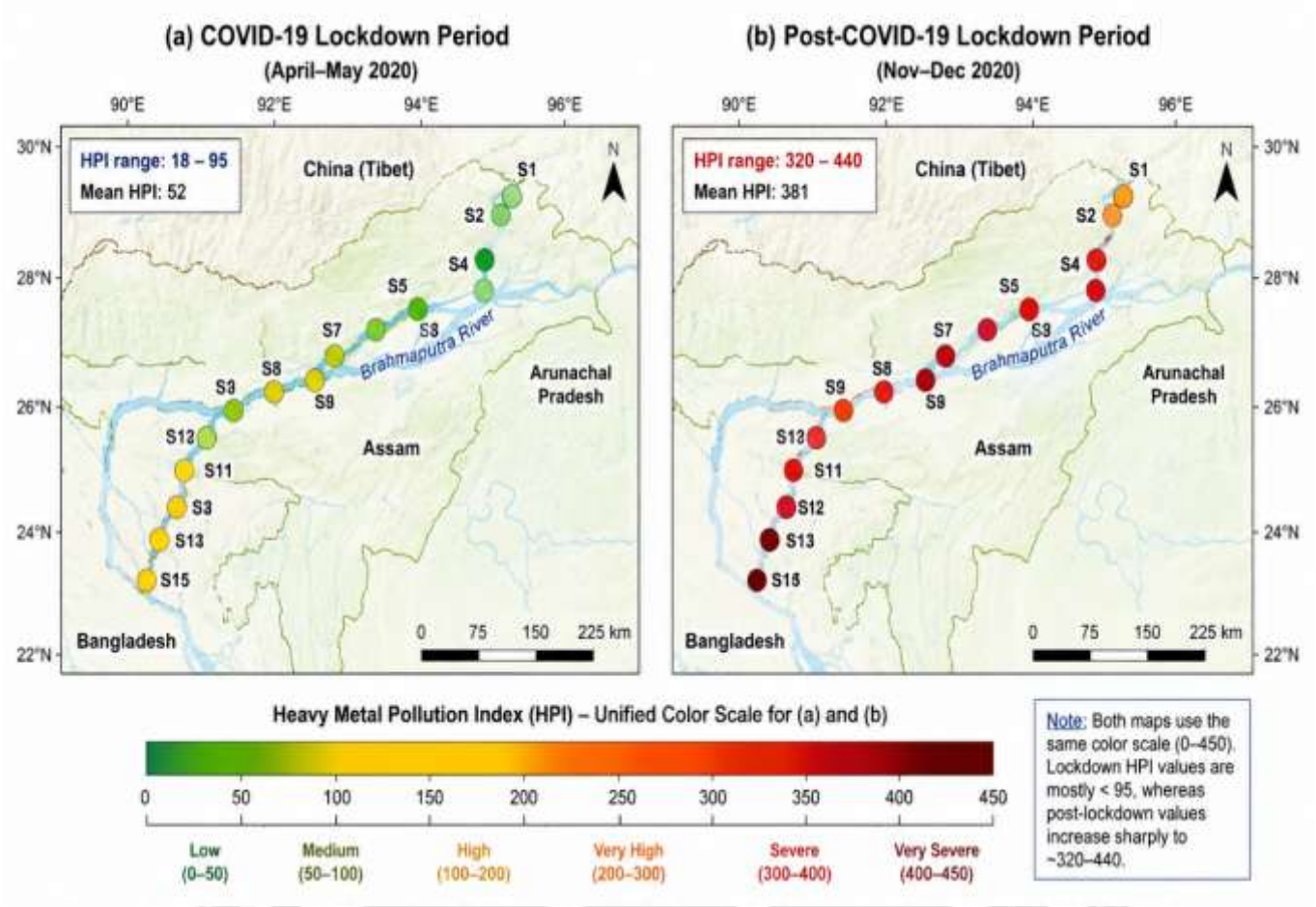

Fig.4.3. Spatial distribution of Heavy Metal Pollution Index (HPI) values in the Brahmaputra River during (a) COVID-19 lockdown and (b) post-COVID-19 lockdown period.

4.4.1.2 MI

MI readings in the Brahmaputra sampling stations ranged from 0.11 - 0.62 during the lockdown period and from 25.87 to 31.33 after the lockdown. According to Table 4.2, all the samples were classified as 'clean' except RB6 during lockdown. RB6 was classified as 'very clean'. All samples were categorized as "seriously affected" after the lockdown period. The HPI and MI readings for different sampling stations are shown in Table 4.5.

4.4.2 Cluster Analysis (CA)

Hierarchical cluster analysis (HCA) was performed to create a dendrogram (Fig. 4.4a and 4.4b) for the lockdown and post-lockdown periods, grouping the 9 HMs into clusters. A dendrogram is a graph with a tree-like structure used to display the results of a hierarchical clustering analysis. Depending on the selected distance measurement, the clustering result is either displayed as the distance between the clustered rows or columns or as their similarity [208,219]. Two heavy metal clusters were present at the time of the COVID-19 lockdown.

Table 4.5. Summary of Heavy Metal Pollution Index (HPI) and Metal Index (MI) of the water sample of the Brahmaputra River during and post-COVID-19 lockdown period

Sampling Stations	**During Covid-19 Lockdown**	**Post Covid-19 Lockdown**	**During Covid-19 Lockdown**	**Post Covid-19 Lockdown**
	HPI		**MI**	
RB1	94.63	320.17	0.55	25.87
RB2	94.61	380.75	0.41	27.07
RB3	94.58	436.67	0.42	27.87
RB4	94.63	320.22	0.53	26.02
RB5	94.61	439.00	0.40	28.07
RB6	94.47	378.42	0.11	26.87
RB7	94.61	378.45	0.40	26.94
RB8	94.61	320.18	0.53	31.33
RB9	94.59	320.24	0.49	25.96
RB10	94.63	320.22	0.55	26.00
RB11	94.66	320.17	0.62	25.87
Min.	94.47	320.17	0.11	25.87
Max.	94.66	439	0.62	31.33
Mean	94.60	357.68	0.45	27.08

Cluster 1 was formed by Zn, Cr and Hg, whereas Cluster 2 was formed by Cu, Fe and Ni. There were three clusters of heavy metals after the lockdown. Cluster 1 comprised As, Cr, Ni and Fe, whereas Cluster 2 comprised Pb and Hg. Cluster 3 included Cd, Cu and Zn.

4.4.3 Analysis of Heavy Metal Correlation

The Pearson correlation matrix is illustrated in Fig.4.5a and 4.5b. A strong negative correlation was found among Cd, Zn, Ni, Cr and Hg in the water samples collected during the lockdown. A significant positive correlation was also observed between Zn, Fe, and Ni. A weak positive correlation was found among Cd, Zn, Cr, Ni, Cu and Hg. Thus, there was no significant or weak relation between the heavy metals during the lockdown period, indicating low pollution. After the lockdown, a strong negative correlation was found among Cr, Cu, Ni, Zn, and Fe. A very strong positive correlation was found among Ni, As, and Cr, i.e., they have similar sources. A moderate positive correlation was also monitored among As, Fe, Hg, Cd, Pb, Cr and Ni.

4.4.4 Anticipated Risks to Human Health

This study employed a hazard index (HI) based on hazard quotients (HQ) from oral routes. This index highlighted the possible risks to human health from different heavy metals. Nine significant dangerous HMs, including As, Cd, Cr, Fe, Cu, Hg, Ni, Zn and Pb had their non-carcinogenic risk assessed. Table 4.6 presents the potential outcomes of health risk assessments for children, teenagers, and adults.

According to past discussions in this paper, HQ>1 denotes potentially detrimental non-carcinogenic effects, while HQ<1 denotes that non-carcinogenic effects are not expected to occur. The HQ value among children during the lockdown ranged from 0.000 to 0.007, 0.002–0.010, and 0.001–0.011 for Cu, Zn and Fe, respectively. It was found that the children's HQ values for the remaining six heavy metals were BDL for the lockdown period. The mean HQ values among children after the lockdown period for As, Cd, and Pb were 1.556, 1.867, and 1.333, respectively, indicating potential non-carcinogenic effects. The average HQ value for the remaining heavy metals was below 1.

The HQ value among teenagers for the lockdown period was below the detectable limit for As, Cd, Pb, Cr, Ni and Hg, ranging from 0.000-0.006, 0.001-0.009, and 0.001-0.009 for Cu, Zn and Fe, respectively, indicating under the tolerable limit. In the post-lockdown samples, the HQ values for teenagers were 1.333, 1.600, and 1.147 for As, Cd, and Zn, respectively, which exceeded the tolerable limit. The rest of the heavy metals had HQ values below the tolerable limit. The HQ values among adults for the lockdown period were BDL for As, Cd, Pd, Cr, Ni

and Hg while varied from 0.000-0.004, 0.001-0.006 and 0.001-0.007 for Cu, Zn and Fe, respectively,

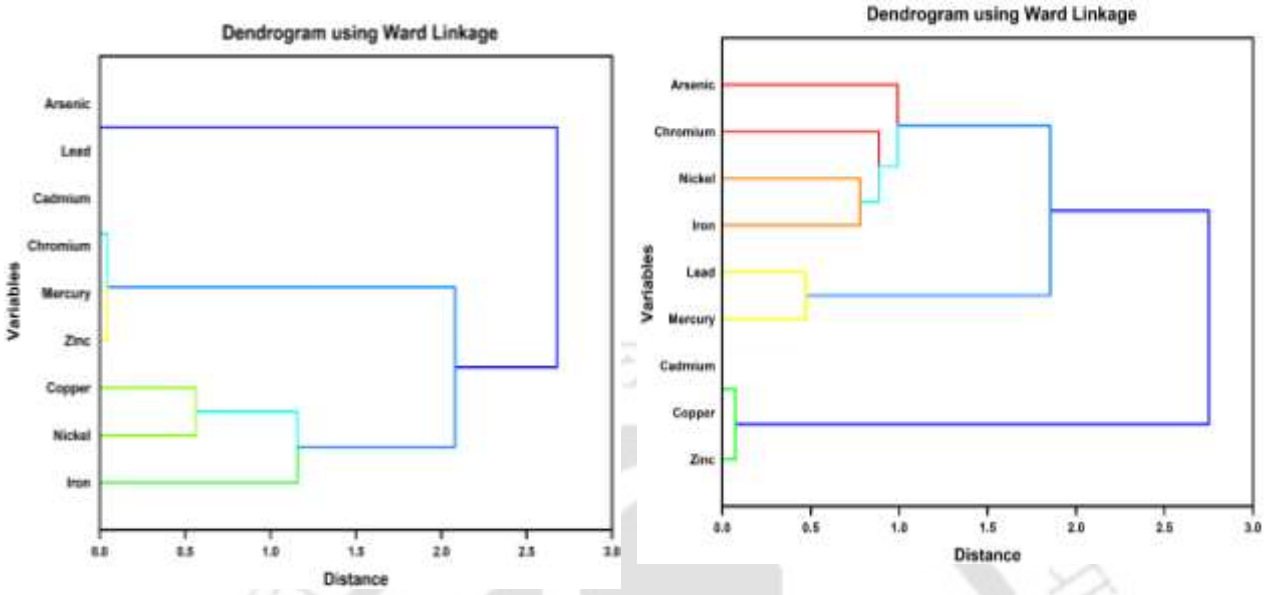

Fig. 4.4 Cluster analysis (CA) of heavy metals using ward linkage method (a)during COVID-19 lockdown (b) Post COVID-19 lockdown

indicating under the tolerable limit. The HQ values for the adults in the post-lockdown period ranged from 0.021 to 0.214, 0.816 to 0.833, 0.571 to 0.581, 0.581 to 0.029, 0.095 to 0.286, and 0.005 to 0.007 for Cu, Pd, Cr, Ni, Zn, Hg, and Fe, respectively. However, the minimum, maximum, and mean HQ values were the same for As, Cd and Ni, with values of 0.952, 1.143 and 0.143, respectively. The Cd exceeded its tolerable limit of HQ value.

The HI values calculated for the water samples varied from 0.000 to 0.086, 0.000–0.073, and 0.000–0.052 among children, teenagers, and adults, respectively, during the lockdown. For the samples examined after the lockdown, the HI value calculated ranged from 0.096-20.533, 0.082-17.600 and 0.059-12.571 among children, teenagers and adults, respectively. Table 4.5

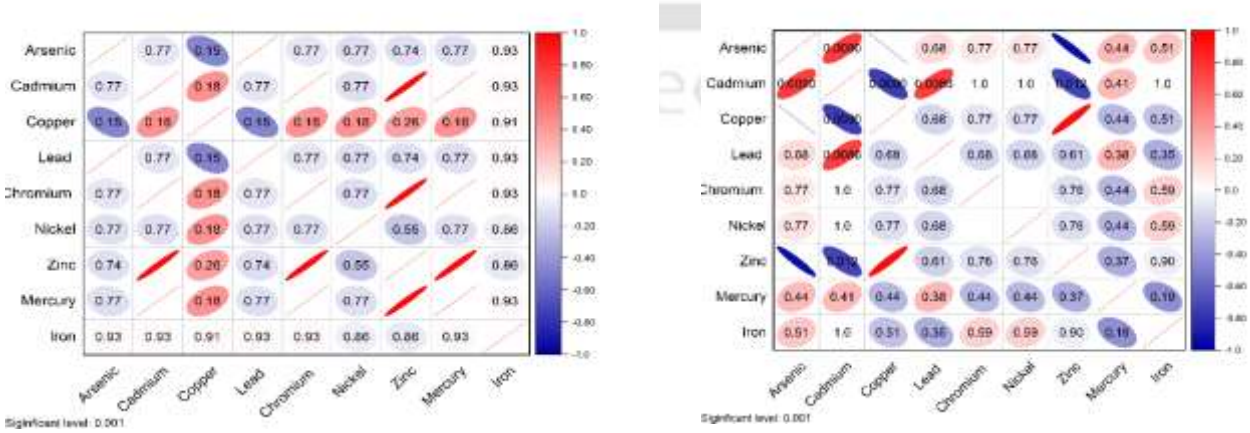

Fig. 4.5. Principal Correlation Matrix (PCM) of heavy metals (a)during COVID-19 lockdown (b) Post COVID-19 lockdown

shows that no children, teenagers, or adults were at risk during the lockdown, while 33% of children, 33% of teenagers, and 11% of adults were at risk during the post-lockdown period.

Table 4.6 Non-carcinogenic risk analysis for children, teens and adults due to heavy metals in the water sample of the Brahmaputra River during and post covid-19 lockdown period

Parameters	**During Lockdown**								
	Kids			**Teens**			**Adults**		
	Min	**Max**	**Mean**	**Min**	**Max**	**Mean**	**Min**	**Max**	**Mean**
As	BDL	BDL	BDL	BDL	BDL	BDL	BDL	BDL	BDL
Cd	BDL	BDL	BDL	BDL	BDL	BDL	BDL	BDL	BDL
Cu	BDL	0.007	0.004	BDL	0.006	0.003	BDL	0.004	0.002
Pb	BDL	BDL	BDL	BDL	BDL	BDL	BDL	BDL	BDL
Cr	BDL	BDL	BDL	BDL	BDL	BDL	BDL	BDL	BDL
Ni	BDL	BDL	BDL	BDL	BDL	BDL	BDL	BDL	BDL
Zn	0.002	0.010	0.003	0.001	0.009	0.003	0.001	0.006	0.002
Hg	BDL	BDL	BDL	BDL	BDL	BDL	BDL	BDL	BDL
Fe	0.001	0.011	0.008	0.001	0.009	0.007	0.001	0.007	0.005
HI	BDL	0.086	0.018	BDL	0.073	0.015	BDL	0.052	0.011
Samples under risk	**0%**			**0%**			**0%**		
	Post Lockdown								
	Kids			**Teens**			**Adults**		
	Min	**Max**	**Mean**	**Min**	**Max**	**Mean**	**Min**	**Max**	**Mean**
As	1.556	1.556	1.556	1.333	1.333	1.333	0.952	0.952	0.952
Cd	1.867	1.867	1.867	1.600	1.600	1.600	1.143	1.143	1.143
Cu	0.035	0.350	0.064	0.030	0.300	0.055	0.021	0.214	0.039
Pb	1.333	1.360	1.338	1.143	1.166	1.147	0.816	0.833	0.819
Cr	0.933	0.949	0.935	0.800	0.813	0.801	0.571	0.581	0.572
Ni	0.233	0.233	0.233	0.200	0.200	0.200	0.143	0.143	0.143
Zn	0.002	0.048	0.009	0.001	0.041	0.008	0.001	0.029	0.006
Hg	0.156	0.467	0.255	0.133	0.400	0.218	0.095	0.286	0.156
Fe	0.008	0.011	0.009	0.007	0.009	0.007	0.005	0.007	0.005
HI	0.096	20.533	7.657	0.082	17.600	6.563	0.059	12.571	4.688
Samples under risk	**33%**			**33%**			**11%**		

4.5 DISCUSSION

Excessive population growth, unscientific land use practices, and anthropogenic contamination are significant global challenges in the 21st century, with severe consequences for surface waters. Rapid industrialization is a primary cause of a significant increase in sewage generation and untreated effluent in surface waters. However, due to the COVID-19 lockdown, a temporary restriction of industrial sectors and economic operations provided an opportunity to improve river water quality.

Guwahati city, various industries, ports, bridges, refineries, power plants, agricultural lands, and dense settlements of people surround the study area of the Brahmaputra River. All the examined heavy metals, except Cu, Fe, and Pb, were below the detection limit during the lockdown. It might be mainly due to two reasons. First is the minimal discharge of effluents into the river due to the closure of industries and a decrease in agricultural activities. Secondly, the lockdown was imposed during the monsoon season, which caused a dilution effect due to the high discharge rate of the Brahmaputra River.

Cancers of the lungs, kidneys, bladder, and skin are significantly related to drinking water containing As. Interestingly, the presence of arsenic (As) was marginally high in the Brahmaputra River during 2017-2019 [199]. While arsenic in the Brahmaputra River is largely attributed to geogenic sources associated with Himalayan sediment transport, it is important to recognize that anthropogenic contributions cannot be entirely ruled out, particularly in localized regions influenced by industrial discharge, agricultural runoff, and urban activities, as discussed in Chapter 5. This combined geogenic–anthropogenic influence may contribute to the observed exposure levels and associated health risks. The closure of industries during the lockdown may have helped maintain the concentration of As within the desirable limits during and after the lockdown period. The mean value of Cd, Ni, Cr and Pb exceeded the acceptable limit post-lockdown. The source of Cd in river water could be the discharge of factories, waste disposal containing batteries made of nickel and cadmium, and the discharge of effluents into the river. Since all industries were shut down during the lockdown and agricultural activities were suspended, the concentration was below the detection limit. Cr concentration may increase due to industrial waste disposal in water, primarily from the chemical and cement industries [220]. Automobile emissions and agricultural waste disposal could cause the exceedance of the Pb limit during the post-lockdown period in water. Pb and Cr can cause several harmful effects on humans, causing damage to organs and retardation of growth. Due to the burning of fuels, increased municipal waste discharge, and industrial waste disposal, the Ni content might rise. The amount of Ni exceeding its permissible limit can harm the lungs,

liver and heart [221] Mercury is a poisonous metal and can cause death if consumed in an overdose [222]. The primary cause of mercury contamination at the RB3 and RB8 sampling stations after the lockdown period may be the discharge of industrial and medical waste containing mercury from mercury-containing equipment [223].

A significant reduction in microbiological contamination was observed during the lockdown period, indicating improved river water quality under reduced anthropogenic pressure. This decline is primarily attributed to decreased discharge of untreated domestic and commercial wastewater resulting from the closure of markets, institutions, and other urban activities. In contrast, the post-lockdown period showed a noticeable increase in bacterial counts, reflecting the resumption of sewage inflow and human activities. These findings highlight the strong dependence of microbial water quality on anthropogenic inputs and underscore the need for improved wastewater management and sanitation infrastructure to ensure long-term river health.

According to the HPI values, the water is medium-polluted during the lockdown and highly polluted after it; therefore, it is unsuitable for drinking. The correlation analysis depicted a correlation with the heavy metals during the post-lockdown period. The primary causes of metal contamination in this river are anthropogenic factors, including farming methods and industrial waste discharge. The hazard index (HI), based on hazard quotients (HQ), indicated that children, teenagers, and adults were not at risk during the lockdown. However, during the post-lockdown period, children and teenagers had a higher health risk than adults.

4.6 CONTROL MEASURES FOR HEAVY METAL POLLUTION

This study demonstrated that heavy metal levels in the Brahmaputra River water considerably decreased during the lockdown. After the lockdown was lifted, work resumed in all industries and agricultural operations, resulting in a rise in heavy metal levels. Among the nine metals examined, pollution with Cd, Pb, Ni and Cr was a problem for the study area. Iron, steel, and other chemical metallurgical industries could be the sources of this metal pollution. Electronic waste contamination of the water could be another source of pollution for Pb and Cr. Because of this, the administrators should closely adhere to pollution control policies to prevent harmful metals from contaminating surface water. Before being discharged into the river, the effluents from the industries need to be treated. It is essential to raise public knowledge of the dangers that heavy metal contamination poses to human health. The river water is not potable, and direct drinking of the water should be prohibited. Additionally, portable reverse osmosis water purifiers could be used in homes to obtain potable drinking water. The observed reduction in

heavy metal concentrations during the lockdown period is primarily attributed to the significant decline in anthropogenic activities, including industrial discharge and urban runoff. Since both sampling periods correspond to comparable non-monsoon conditions, the influence of seasonal hydrological variation is considered minimal. Therefore, the improvement in water quality can be directly linked to reduced pollutant input during the lockdown period. This highlights the dominant role of anthropogenic sources in controlling heavy metal contamination in the Brahmaputra River.

4.7 CONCLUSION

The results of the investigation unequivocally demonstrate that heavy metal contamination in the Brahmaputra River was under control during the lockdown. Heavy metal pollution was significantly observed after the lockdown. The HPI, MI, Pearson correlation analysis, and HCA were all evaluated in this study to determine the quality of river water. The microbiological indicators were also assessed, including fecal coliform bacteria, fecal streptococci, and total coliform bacteria. The hazard index assessed the possible risks to human health caused by various heavy metals. A substantial decrease in heavy metal concentrations validated the impact of the temporarily limited activities of various agricultural, industrial, and commercial operations. The increased levels of HPI values of water samples shortly after the unlocking demonstrated that anthropogenic intrusion was prevalent at all sampling sites. Based on MI values, the samples collected during the lockdown were found to be clean, but were seriously affected after the lockdown period.

All heavy metals were within the acceptable limit during the lockdown. The concentrations of Cd, Ni, Cr, and Pb exceeded the standard acceptable limits after the lockdown, respectively. The heavy metals can be arranged as Fe > Ni ≈ Pb > Cr ≈ Zn > Cu > Cd > As based on their mean concentration values in the post-lockdown. A minimal health risk existed for people throughout the lockdown. 33% of children, 33% of teenagers and 11% of adults were at health risk during the post-lockdown period. Monsoonal rainfall influences river water quality through two competing mechanisms: dilution of pollutants due to increased discharge, and enhanced surface runoff that introduces non-point source contaminants from the catchment. Despite this, the observed heavy metal concentrations during the lockdown period remained below detection limits (BDL). This indicates that runoff-driven non-point sources alone were insufficient to produce measurable contamination levels. Consequently, the results suggest that point sources, particularly industrial and urban discharges, play a more dominant role in

controlling heavy metal pollution in this stretch of the Brahmaputra River. Therefore, the lockdown had a positive impact on the decrease in heavy metal pollution. However, after the lockdown period ended, heavy metal pollution reached a startling peak. Therefore, the primary strategies for reducing the risk to human health from water pollution are stringent government regulations and increased public awareness.

Chapter 5

MAPPING POSSIBLE SOURCES OF HEAVY METALS IN THE BRAHMAPUTRA RIVER SAND BARS

5.1 INTRODUCTION

In the last few decades, the Brahmaputra basin in Assam has undergone rapid industrialization, particularly in the oil and gas, cement, paper and pulp, pharmaceutical, coal-based, and hazardous waste processing sectors. This has resulted in increasing concern regarding heavy metal pollution in riverine sediments. Heavy metals such as copper (Cu), zinc (Zn), nickel (Ni), and chromium (Cr) are persistent, non-biodegradable, and potentially toxic, making them suitable indicators for assessing anthropogenic impact on river systems. This chapter integrates sediment geochemistry, vertical profiling of sand bars, industrial inventory analysis, literature-based effluent signatures, and river hydrodynamics to systematically map the possible sources of heavy metals in Brahmaputra River sand bars. Particular emphasis is placed on understanding whether pollution generated upstream can realistically influence downstream sampling stations, using longitudinal dispersion analysis based on physical hydraulic modelling and advection–dispersion theory. Section 5.2 describes about the sand bars contaminated by heavy metals before exploring the metals exceed their toxicity reference values in section 5.3. section 5.8 presented the physical hydraulic modelling and dimensional analysis to assess the downstream transport potential of contaminants within the river system. Section 5.10 depicts linking of contaminated sand bars to potential upstream pollution sources before concluding in section 5.11.

5.2 SAND BARS AS INDICATORS OF HEAVY METAL CONTAMINATION

Sand bars in large alluvial rivers are formed through alternating phases of erosion, transport, and deposition during seasonal flow variations. Unlike floodplain soils, sand bars are frequently reworked, making them sensitive to both episodic and continuous pollutant inputs. Heavy metals entering the river system through industrial effluents, urban runoff, or atmospheric deposition tend to adsorb onto fine sediment fractions and organic coatings, which subsequently become incorporated into sand bars. Vertical stratification within sand bars provides valuable temporal information. In this study, sediments were analyzed at three depths: the upper layer (bed surface), middle layer (50 cm below surface), and lower layer (100 cm

below surface). Exceedance of Toxicity Reference Values (TRVs) in these layers allows discrimination between recent contamination (upper layer), sustained pollution (middle layer), and legacy contamination (lower layer).

5.3. HEAVY METAL CONCENTRATIONS EXCEEDING TOXICITY REFERENCE VALUE (TRV)

5.3.1 Copper (Cu)

Copper concentrations exceeded the TRV of 16 µg/g across multiple stations and all sediment layers. Upper-layer enrichment at stations such as S38 (24.95 µg/g) and S17 (18.22 µg/g) indicates ongoing Cu inputs. The middle layer showed even higher concentrations, notably at S35 (38.47 µg/g), reflecting sustained discharge over time. Lower-layer exceedances further confirm historical accumulation. The vertical persistence of Cu suggests continuous or recurring anthropogenic sources rather than isolated contamination events. Copper is widely reported in effluents from pharmaceutical manufacturing, cement plants, paper and pulp industries, refineries, and metal-processing units, all of which are prevalent along the Brahmaputra valley.

5.3.2 Zinc (Zn)

Zinc exhibited highly localized but extreme enrichment. The upper-layer concentration at station S8 (677.25 µg/g) far exceeded the TRV of 110 µg/g, while the middle layer showed moderate exceedance at S28 (125.4 µg/g). No exceedance was observed in the lower layer. This pattern indicates recent, point-source dominated Zn inputs with limited historical accumulation. Industries such as tyre pyrolysis oil units, galvanizing plants, oil refineries, and lead-acid battery manufacturing are well-known sources of Zn-rich effluents and are spatially associated with the observed hotspots.

5.3.4 Chromium (Cr)

Chromium concentrations exceeded the TRV of 26 µg/g in all sediment layers, with particularly alarming values in the upper layer at S34 (286.65 µg/g) and the middle layer at S32 (175.02 µg/g). Lower-layer enrichment across multiple stations indicates historical Cr loading. Cr is commonly discharged from cement manufacturing, paper and pulp processing, refineries, coal-based industries, and metal fabrication units. Its strong sediment-binding capacity explains its persistence at depth within sand bars.

5.4. VERTICAL DISTRIBUTION AND TEMPORAL INTERPRETATION

The combined vertical profiles of Cu, Zn, Ni, and Cr reveal distinct temporal trends:

- **Upper layer:** Reflects active and recent pollution, especially pronounced for Zn, Cu, and Cr at localized stations.
- **Middle layer:** Represents sustained pollution over intermediate time scales, showing peak enrichment for Cu, Ni, and Cr.
- **Lower layer:** Indicates legacy contamination, particularly for Ni and Cr, demonstrating long-term industrial impact.

The coexistence of exceedances across all layers confirms that sand bars function as long-term repositories of heavy metals rather than transient sinks.

5.5. INDUSTRIAL EFFLUENT SIGNATURES AND HEAVY METAL SOURCES

Extensive literature demonstrates that different industrial sectors release characteristic combinations of heavy metals are shown in Table 5.1. Pharmaceutical industries consistently discharge Cu, Zn, Ni, and Cr. Cement industries contribute Cu, Zn, Ni, Cr, and Cd through raw material processing and kiln emissions. Paper and pulp industries are significant sources of Cu, Zn, Ni, and Cr. Oil refineries and oil and gas extraction plants release Ni, Cr, Cu, and Zn via produced water, sludge, and accidental leaks. Coal tar distillation and coking processes are major contributors of Ni and Cr, while tyre pyrolysis oil units release Zn, Ni, and Cu. The heavy metal signatures observed in Brahmaputra sand bars closely match these documented effluent compositions, strongly implicating industrial activities as dominant sources.

5.6. SPATIAL DISTRIBUTION OF RED-CATEGORY INDUSTRIES

Assam hosts 448 red-category industrial units, of which 346 (77.23%) are categorized as Highly Polluting Industries (HCF) as tabulated in Table 5.2. These units are concentrated along the Brahmaputra valley, particularly in districts such as Kamrup Metropolitan, Kamrup, Nagaon, Dibrugarh, Jorhat, Sivasagar, and Tinsukia. Districts dominated by oil and gas extraction and refineries correspond spatially with widespread Ni and Cu enrichment. Areas with cement and paper-pulp clusters align with elevated Cr and Cu levels. Tyre pyrolysis oil, coal tar distillation, and lead-based industries coincide with localized Zn and Ni hotspots. This

spatial coherence strengthens the causal linkage between industrial clusters and sediment contamination.

Table 5.1. List of Industries dispersing type of heavy metals

Type of Unit	Heavy Metals from the Discharged Effluents													
	S NO.	Cu	Zn	Mn	Ni	Fe	Cr	Pb	Co	Cd	As	Hg	Ag	Reference
Pharmaceuticals	1	✓	✓	✓	✓		✓	✓	✓	✓				[224]
	2	✓	✓	✓	✓		✓	✓		✓	✓			[225]
	3	✓	✓		✓		✓	✓	✓	✓		✓		[226]
	4	✓	✓		✓		✓	✓		✓				[227]
	5	✓	✓		✓	✓		✓		✓				[228]
	6	✓	✓		✓			✓			✓	✓	✓	[229]
	7	✓					✓	✓	✓		✓			[230]
Cement	1	✓		✓	✓		✓		✓	✓		✓		[231]
	2	✓	✓				✓	✓		✓				[232]
	3	✓	✓		✓			✓		✓	✓	✓		[233]
	4	✓	✓	✓	✓		✓	✓		✓	✓			[234]
	5	✓			X (ND)		✓		X (ND)	✓				[235]
Paper and Pulp	1	✓	✓	✓	✓		✓	✓	✓	✓		✓		[236]
	2	✓	✓	✓	✓	✓	✓	✓		✓	✓	✓		[237]
	3	✓	✓	✓	✓	✓	✓	✓		✓	✓	✓		[238]
Lead Ingots	1	✓	✓					✓		✓				[239]
	2	✓	✓					✓		✓	✓	✓		[240]
	3							✓		✓				[241]
	4	✓	✓					✓		✓				[242]
	5	✓	✓		✓			✓		✓				[243]
Tyre Furnace Oil	1		✓			✓	✓	✓		✓				[244]
	2	✓		✓	✓		✓	✓	✓	✓	✓			[245]
Coking Process	1		✓	✓	✓				✓	✓	✓	✓		[246]
	2	✓	✓		✓	✓	✓	✓	✓	✓	✓			[247]
	3	✓	✓		✓		✓	✓		✓	✓	✓		[248]
	4	✓	✓		✓		✓	✓		✓	✓	✓		[249]
Refinery	1	✓			✓	✓	✓	✓		✓				[250]
	2		✓		✓		✓	✓						[251]
	3	✓	✓	✓	✓	✓	✓	✓		✓	✓	✓		[252]
	4	✓	✓	✓	✓	✓		✓		✓				[253]
	5	✓	✓	✓	✓		✓	✓		✓		✓		[254]

Table 5.2. Districts of Assam having red category Industrial unit

S No.	District (U/S to D/S)	Industry (No. of Units)	Total Unit
1	Tinsukia	HCF (25), Oil Refinery (1)	26
2	Dibrugarh	HCF (41), Oil and gas extraction Plant (2), Thermal Power Plant (1), Fertilizer (1), Petrochemicals Manufacturer (2)	47
3	Dhemaji	HCF (5)	5
4	Charaideo	Thermal Power Plant (1), C2+ RECOVERY PLANT FROM NATURAL GAS (1)	2
5	Sivasagar	HCF (14), Oil and gas extraction Plant (4)	18
6	Lakhimpur	HCF (12)	12
7	Jorhat	HCF (32), Oil and gas extraction Plant (1), Plywood (1), Lead Acid Manufacturer (1), Hazardous Waste Recycling Industry (1)	36
8	Golaghat	HCF (1), Oil Refinery (1)	2
9	Karbi Anglong	Extra Nutral Alcohol making unit (ENA) (1)	1
10	Biswanath	HCF (17)	17
11	Hojai	HCF (19), Cement (4), Railway Locomotive Workshop (1), Oil Pump Station Terminal (1)	25
12	Nagaon	HCF (45), Petrol Pump Station (1), Cement (1), Manufacturer of paints and Pigments (1)	48
13	Sonitpur	HCF (18), Paper & Pulp Industry (4)	22
14	West Karbi Anglong	HCF (1)	1
15	Morigaon	HCF (6), Cement (1), Milk dairy Products Industry (1)	8
16	Udalguri	HCF (2)	2
17	Darrang	HCF (8)	8
18	Kamrup Metropolitan	HCF (7), Cement (8), Coal Making-Liquefaction-Coal tar distillation (12), Bakery unit (2), Roofing Industry (2), Aluminium extrusion (1), Slaughter house (1), Steel Industry (1), Lead Ingot Manufacturer (2), Oil refinery (1), CBWTF (1), Sweets & biscuits Industry (1), Recycling industry (1), Industrial Carbon factory (1)	41
19	Kamrup	HCF (2), Tyre Pyrolysis oil (5), Dyeing Industry (4), Cement (3), Lead Ingot (3), Galvanizing (2), Milk & Dairy products (1), Aluminium Industry (1), Sodium silicate (1), Manufacturer of Lubricating oil & Grease (1), Paper & Pulp (1), Asbestos based industry (1), Grain distillery industry (1), Hume Pipe (1), Manufacturer of gravure printing cylinder (1)	28
20	Baksa	Cement (2)	2
21	Barpeta	HCF (16)	16
22	Goalpara	HCF (20), Steel Industry (1), Lead acid battery Manufacturer (1)	22
23	Bongaigaon	HCF (26), Coal Making-Liquefaction-Coal tar distillation (1)	27
24	Chirang	HCF (3), Coal Making-Liquefaction-Coal tar distillation (1), Oil Refinery (1)	5

Cont.			
25	Kokrajhar	HCF (6), Power generation plant (1)	7
26	Dhubri	HCF (20)	20
		Total industrial Unit (Red Category)	**448**

HCF – 346 **(77.23% of All Red Category Industries)**	Oil and gas extraction Plant – 7
Cement – 19	Paper & Pulp Industry – 5
Coal Making-Liquefaction-Coal tar distillation – 14	Tyre Pyrolysis oil – 5

5.7. NEED FOR HYDRODYNAMIC JUSTIFICATION IN SOURCE MAPPING

While spatial correlation between industries and contaminated sand bars is suggestive, a critical question remains: can pollution released upstream realistically reach downstream sampling stations? This is particularly important in the Brahmaputra, where the distance between consecutive sampling stations is approximately 15–20 km. To address this, longitudinal dispersion analysis based on physical hydraulic modelling was undertaken.

5.8. PHYSICAL HYDRAULIC MODELLING AND DIMENSIONAL ANALYSIS

Physical hydraulic models are commonly used to study pollutant transport under controlled conditions. However, such models operate at reduced geometric, kinematic, and dynamic scales. To extrapolate model results to the natural river (prototype), appropriate similarity laws must be applied. In this study, a distorted hydraulic model was used with different horizontal and vertical scaling ratios. Kinematic similarity was preserved using Froude similarity, which is appropriate for gravity-dominated free-surface flows. The measured model dispersion coefficient was $D_m = 0.081$ m²/s. The horizontal length scale was 1:500, the vertical scale was 1:67, and the velocity ratio was 1:8.18. Since longitudinal dispersion is governed primarily by horizontal mixing processes, the horizontal scale was applied for dispersion scaling. The dispersion coefficient has dimensions of L^2T^{-1}. The time scale ratio for kinematic similarity is given by the ratio of length scale to velocity scale, yielding a model-to-prototype time ratio of 0.01636 and a prototype-to-model ratio of 61.1. Applying dimensional analysis, the prototype dispersion coefficient was calculated as:

$$D_p = 331.42 \text{ m}^2/\text{s}$$

This value falls well within the range reported for large rivers worldwide, including the Mississippi (200–400 m²/s), Amazon (>300 m²/s), and previously reported estimates for the Brahmaputra (250–450 m²/s). This confirms that the scaled dispersion coefficient is physically realistic.

5.9 GOVERNING EQUATION FOR POLLUTANT TRANSPORT

Pollutant transport in the river channel is governed by the one-dimensional Advection–Dispersion Equation (ADE), which describes the combined effects of downstream transport by flow and spreading due to turbulence. The ADE does not directly provide concentration values unless solved with appropriate initial and boundary conditions. Analytical solutions of the ADE for instantaneous or continuous point sources provide concentration distributions as functions of space and time, accounting for advection, dispersion, decay, flow depth, and initial pollutant mass. These solutions are particularly useful for source–receptor analysis in river systems.

For practical interpretation, the downstream influence of a pollution source can be expressed as the total plume length, defined as the sum of advected length and dispersive spread as shown in equation 5.1.

$$L_{total}=L_{advection}+L_{dispersion}$$

$$L_{total}=Vt+4\sqrt{D_p t} \quad (5.1)$$

Using a mean flow velocity of 2 m/s and the estimated dispersion coefficient of 331.42 m²/s, the plume length after 1 hour of continuous discharge is approximately 11.57 km. After 2 hours, it increases to about 20.58 km, and after 5 hours, it reaches nearly 46 km.

5.10 IMPLICATIONS FOR INTER-STATION CONNECTIVITY AND SOURCE MAPPING FRAMEWORK

The plume length estimates demonstrate that within 1–2 hours, pollutants can travel distances comparable to the spacing between sampling stations along the Brahmaputra. Over longer durations, contamination can influence sand bars located several tens of kilometers downstream. This confirms that elevated heavy metal concentrations observed at downstream sand bars cannot be attributed solely to local sources. Instead, upstream industrial clusters are hydraulically capable of contributing to observed contamination patterns. By integrating

sediment geochemistry, vertical profiling, industrial inventories, effluent signatures, and longitudinal dispersion analysis, a robust framework for mapping heavy metal sources emerges. Nickel and chromium contamination is primarily linked to oil and gas extraction, refineries, cement plants, and coal-based industries. Copper originates from pharmaceuticals, cement, paper and pulp, and refineries, while zinc hotspots are associated with tyre pyrolysis oil units, galvanizing industries, and lead-based manufacturing. Sand bars downstream of major industrial clusters act as convergence zones where pollutants from multiple districts accumulate over time.

A conceptual diagram illustrating the Source–Pathway–Receptor (SPR) framework, highlighting the interaction between upstream industrial discharge plumes and downstream sand bar stratification has been shown in Fig 5.1 to enhance clarity and conceptual understanding of the pollutant transport mechanisms.

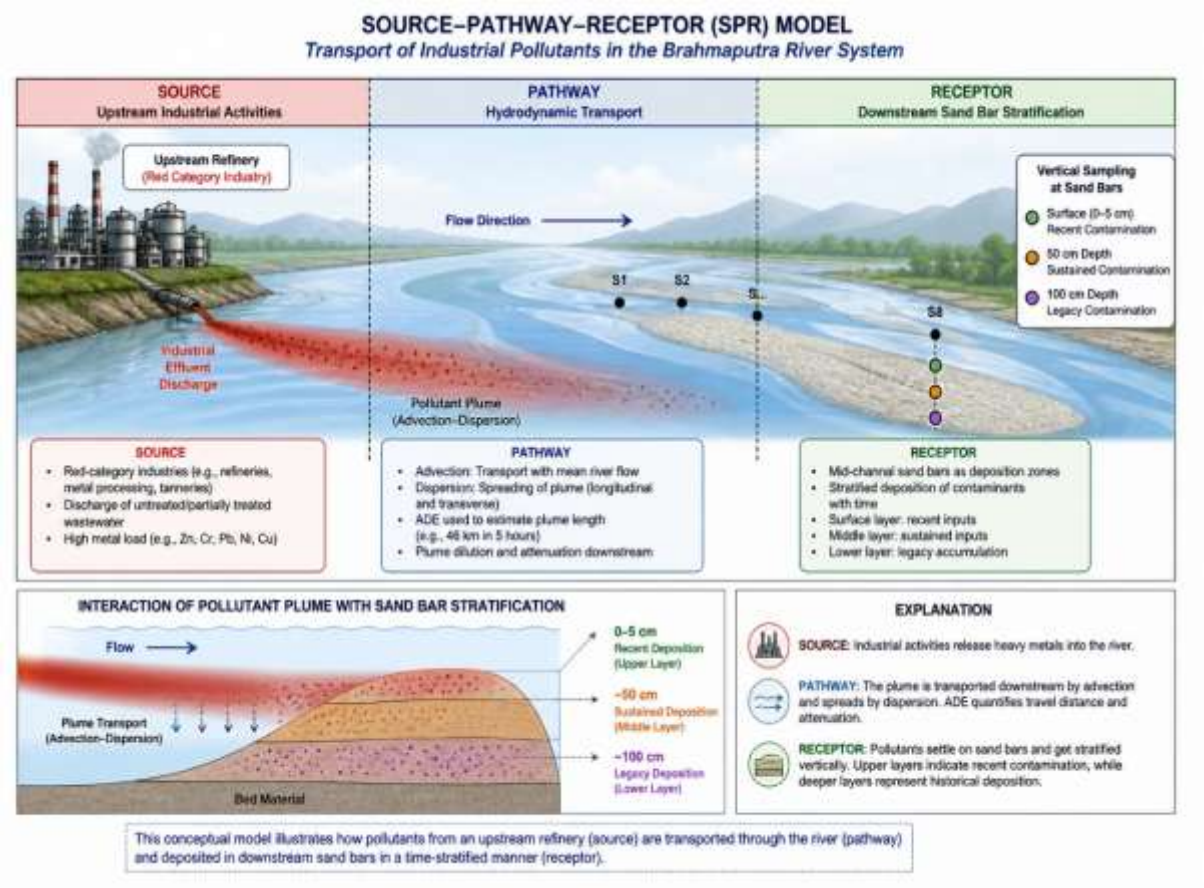

Fig 5.1: Typical Details of Source-Pathway-Receptor Model depicting the transport of pollutants

5.11 CONCLUSION

This chapter demonstrates that heavy metal contamination in Brahmaputra River sand bars is the cumulative outcome of sustained industrial activity across Assam, combined with the river's high dispersive capacity. The presence of Cu, Zn, Ni, and Cr exceedances across all sediment layers reflects both historical and ongoing pollution. Longitudinal dispersion analysis confirms that pollutants released upstream can realistically reach downstream sand bars over inter-station distances. Consequently, mapping potential sources of heavy metals based on industrial distribution, sediment contamination, and river hydrodynamics is scientifically justified and essential for effective river basin management.

भारतीय प्रौद्योगिकी संस्थान गुवाहाटी
Indian Institute of Technology Guwahati

Chapter 6

Pollutant Transport and Dispersion characteristics in the Brahmaputra River

6.1 INTRODUCTION

Understanding the movement and spreading of pollutants in river systems is a key element for forecasting the quality of water downstream, determining the potential hazards to the environment, and coming up with a plan for pollution control that works. In the case of large alluvial rivers, the transport of pollutants results from the complex interplay of various factors such as hydrodynamic conditions, changes in river channel shape, and exchanges between sediments and water. Longitudinal dispersion, out of the various mixing processes, is considered to be the chief one determining how the pollutants move downstream along the flow direction. In rivers with a braided pattern like the Brahmaputra, a variety of spatial factors such as the changes in channel width, depth, flow velocity, and bed roughness give rise to the pollutant transport mechanisms becoming even more complicated. Traditional empirical models that were developed based on straight or slightly meandering rivers are generally unable to depict the dispersion features in braided channels correctly. Herein, a physical hydraulic model experiment and tracer studies have been utilized to analyze longitudinal dispersion in the Brahmaputra River, along with the creation and testing of empirical formulas that fit braided river systems. Section 6.2.1 presented the materials and methodology adopted in this study for determination of longitudinal dispersion coefficient. Further 6.2.3 outlined the selected reach in the physical model of the Brahmaputra River for carrying out the experimental investigations at North Eastern Hydraulic and Allied Research Institute (NEHARI) in Guwahati. Theoretical estimation of longitudinal dispersion coefficient and its assessment criteria for comparing the accuracy of tested models is presented in the section 6.2.6 and 6.2.7. To assess how close the predicted values were to what actually occurred, three main measures were utilized: λ (the discrepancy ratio), AE (absolute error), and RE (relative error). These measures were determined by taking the difference between the measured value (obtained using a tracer test) and the projected values (obtained using empirical equations). Section 6.3 presented the results and discussed the model to river conversion of dispersion coefficient in section 6.4. Section 6.5 concludes the findings validation about the reliability of tracer-based methods for quantifying solute transport in open-channel flows.

6.2 METHODOLOGY

6.2.1 Materials and Methods Used

For carrying out the experimental study, an instrument was fabricated in laboratory made up of wooden material to collect the water sample at various depths. The instrument was fabricated in such a way that we can open its lid at desired depth and collect the water sample across the width and close it simultaneously. A scale was attached with it which enables the user to collect the water sample at particular location. In order to maximise the photographic survey, a coloured fluid was selected as the tracer [255]; specifically, methylene blue ($C_{16}H_{18}ClN_3S$) was chosen following a comparison of the chemicals available (reactive red, methyl blue, methyl red, Methyl violet and others). Methylene blue (MB) was used as a tracer dyestuff commonly used for tracer studies in water research to investigate performance of a process [256]. Specimen tubes for sample collection, measuring cylinder for injection of dye, distilled water bottle for rinsing and stopwatch for measuring the time were employed during the experimentation.

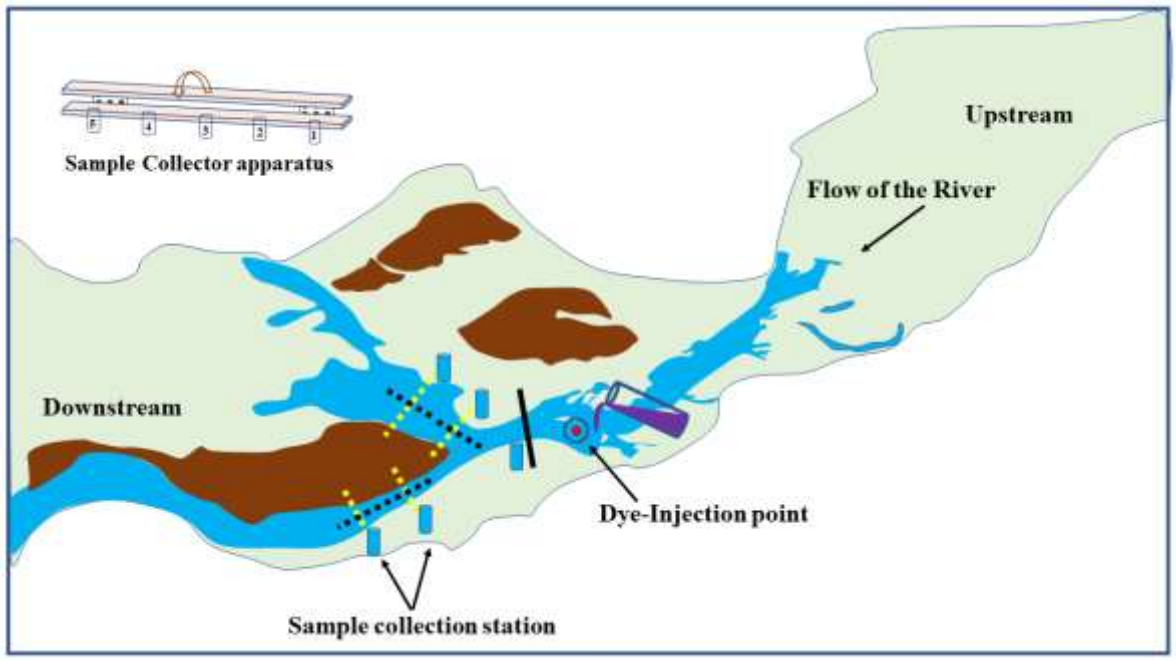

Fig 6.1 Schematic Diagram of the Tracer test conducting in an experimental model

Methylene blue (MB) was selected as a tracer for determination of the experimental dispersion coefficient of the channel. The tracer was injected in the upstream of the channel and sample collection was at a few meters downstream of the methylene blue injected location. The distance between the two samples collected from the channel was 20 cm which represents 100 m distance in the actual river as the scale of the model was 1:500 for horizontal direction. 15 samples were collected along the channel. Once the samples were collected from the channel, an analysis was

done in laboratory using UV-Spectrophotometry. A schematic diagram has been shown in Fig-6.1 representing the methodology.

6.2.2 Quality Control Analysis

Analytical grade chemicals and deionized water was used to prepare all standard samples for calibration of the Ultraviolet-Visible Spectrophotometry. A stock solution of 1000 ppm has been made by adding 1g of methylene blue in 1000 ml deionized water. Further the standard of 100, 50, 20 and 10 ppm were made using 1000 ppm solution. The standard samples were running after every 3 samples to check the accuracy of the instrument. The concentration of the standard and water samples was evaluated after note down the absorbance of UV-Spectrophotometry at wavelength 665 nm [257].

6.2.3 Experimental Setup

To carry out the present experimental work, a physical model of the river Brahmaputra was chosen.

Fig. 6.2 Plan of the Brahmaputra River near at Majuli Section

This physical model was fabricated by Brahmaputra board, a statutory body set up under the Ministry of Jal Shakti, Government of India. Reach of the Brahmaputra River modelled in this experimental setup was of 30 km. The selected model has a size of 80x45 m as L x B with a scale of 1:500 in horizontal direction, 1:67 in vertical direction. The kinematic similarity of the model

was 1: 8.18 for Velocity while 1: 274210 for discharge. Plan layout of the model has been shown in Fig 6.2.

6.2.4 Estimation of longitudinal dispersion coefficient

Measured longitudinal dispersion coefficient of the channel was done using the equation (6.1).

$$D_x = \delta \, V \, L \qquad (6.1)$$

Where, D_x = Longitudinal dispersion coefficient in m^2/s, V= Average velocity of the channel in m/s, L = Length of the reach of the channel in m, δ = dispersion number

Moment equation approach [258] was used for determination of the dispersion number (δ) and Normalised variance as shown in equation (6.2) and (6.3).

$$\delta = \frac{1}{8}\left[\sqrt{8\sigma^2 + 1} - 1\right] \qquad (6.2)$$

Where, σ^2 = Normalised variance

$$\sigma^2 = \frac{1}{\theta^2}\left[\frac{\sum_{i=1}^{n} C_i t_i^2}{\sum_{i=1}^{n} C_i} - \theta^2\right] \qquad (6.3)$$

The value of Θ has been determined as follows in equation (6.4);

$$\Theta = \left[\frac{\sum_{i=1}^{n} C_i t_i}{\sum_{i=1}^{n} C_i}\right] \qquad (6.4)$$

Where, C_i = Concentration of collected samples (mg/l), t_i = travel time (s), Θ = Average flow time (s).

6.2.5 Theoretical estimation of the longitudinal dispersion coefficient

Various empirical equations in dimensionless form, governed by the other researchers were used to estimate the longitudinal dispersion coefficient of the river. Further, the obtained results were transformed for channel with the help of dimensional analysis. Name of the model with their empirical equations were enlisted as shown in Table-6.1 [259]. Various hydraulic parameters such as channel width (W), Water depth (H), Flow velocity (U), Shear velocity (U*), Slope of the river (S), Discharge (Q), Hydraulic radius (R) and Froude No. (F_r) were used in the model empirical equations. Shear velocity U* was calculated using equation 6.5 as given below.

$$U* = \sqrt{gRS} \qquad (6.5)$$

6.2.6 Assessment criteria for comparing the accuracy of tested models

The longitudinal dispersion coefficient (Dx) of the channel was predicted by theoretical models governed by the various researchers listed in Table 6.1. The accuracy of the predicted values was evaluated using the discrepancy ratio (λ), absolute error (AE), and relative error (RE) as the main criteria. This was accomplished by using measured value (obtained by tracer test) and projected values (through empirical equations).

The criteria are presented as follows:

• **Discrepancy ratio (λ):** assesses the degree of accuracy of the prediction made by model. The tolerance limit for the assessment is ± 0.5. The equation describing the discrepancy ratio is presented in equation 6.6.

$$\lambda = \text{Log}\left(\frac{D_{xp}}{D_{xm}}\right) = \text{Log}\,(D_{XP}) - \text{Log}\,(D_{XM}) \qquad (6.6)$$

Where, λ = Discrepancy ratio, D_{XP} = predicted longitudinal dispersion coefficient in m^2/s and D_{XM} = measured longitudinal dispersion coefficient, m^2/s.

The following are the conditions of assessment:

i. If $\lambda = 0$, $D_{XP} = D_{XM}$ (predicted value equals measured value)

ii. If $\lambda > 0$, $D_{XP} > D_{XM}$ (over-prediction by model)

iii. If $\lambda < 0$, $D_{XP} < D_{XM}$ (under-prediction by model)

• **Absolute Error (AE):** measures the margin of error that is associated with the model predictions. In another word, it measures the difference between the actual value and the predicted value from the model. The equation for AE measurement is presented in equation 6.7.

$$AE = |D_{XM} - D_{XP}| \qquad (6.7)$$

• **Relative Error (RE)**: measures the margin of error relative to the actual value. In another word, it is the ratio of the absolute error to the actual value of the measurement. The RE is measured using equation 6.8.

$$RE = \left|\frac{(D_{XM} - D_{XP})}{D_{XM}}\right| \qquad (6.8)$$

Table 6.1 Name of the model with their empirical equations [5,6,9]

S No	Name of the Model	Empirical equations
1	Elder (1959)	$\frac{D_x}{HU^*} = 5.93$
2	Fischer (1975)	$\frac{D_x}{HU^*} = 0.011\left(\frac{U}{U^*}\right)^2\left(\frac{W}{H}\right)^2$
3	Liu (1977)	$\frac{D_x}{HU^*} = 0.18\left(\frac{U}{U^*}\right)^{0.5}\left(\frac{W}{H}\right)^2$
4	Iwasa and Aya (1991)	$\frac{D_x}{HU^*} = 2\left(\frac{W}{H}\right)^{1.5}$
5	Koussis and Rodriguez-Mirasol	$\frac{D_x}{HU^*} = 0.6\left(\frac{W}{H}\right)^2$
6	Seo and Cheong (1998)	$\frac{D_x}{HU^*} = 5.915\left(\frac{U}{U^*}\right)^{1.428}\left(\frac{W}{H}\right)^{0.62}$
7	Kashefipour and Falconer (2002)	$\frac{D_x}{HU^*} = \left[7.428 + 1.775\left(\frac{U}{U^*}\right)^{0.572}\left(\frac{W}{H}\right)^{0.62}\right]\left[\frac{U}{U^*}\right]^2 ; \frac{W}{H} \leq 50$
		$\frac{D_x}{HU^*} = \left[10.612\left(\frac{U}{U^*}\right)^2\right]; \frac{W}{H} \geq 50$
8	Sahay and Dutta (2009)	$\frac{D_x}{HU^*} = 2\left(\frac{U}{U^*}\right)^{1.25}\left(\frac{W}{H}\right)^{0.96}$
9	Etemad-Shahidi and Taghipour (2012)	$\frac{D_x}{HU^*} = 15.49\left(\frac{U}{U^*}\right)^{0.11}\left(\frac{W}{H}\right)^{0.78} ; \frac{W}{H} < 30.6$
		$\frac{D_x}{HU^*} = 14.12\left(\frac{U}{U^*}\right)^{0.85}\left(\frac{W}{H}\right)^{0.61} ; \frac{W}{H} > 30.6$
10	Li et al. (2013)	$\frac{D_x}{HU^*} = 2.282\left(\frac{U}{U^*}\right)^{1.4713}\left(\frac{W}{H}\right)^{0.7613}$
11	Zeng and Huai (2014)	$\frac{D_x}{HU^*} = 5.4\left(\frac{U}{U^*}\right)^{1.13}\left(\frac{W}{H}\right)^{0.7}$
12	Disley et al. (2015)	$\frac{D_x}{HU^*} = 3.563\left(\frac{U}{\sqrt{gH}}\right)^{-0.4117}\left(\frac{U}{U^*}\right)^{1.0132}\left(\frac{W}{H}\right)^{0.6776}$
13	Sattar and Gharabaghi (2015)	$\frac{D_x}{HU^*} = 8.45\left(\frac{U}{U^*}\right)^{1.65}\left(\frac{W}{H}\right)^{0.5-0.514Fr^{0.516}+\frac{U}{U*}0.42^{\frac{U}{U*}}}$
14	Wang and Huai (2016)	$\frac{D_x}{HU^*} = 17.648\left(\frac{U}{U^*}\right)^{1.16}\left(\frac{W}{H}\right)^{0.3619}$
15	Alizadeh et al (2017b)	$\frac{D_x}{HU^*} = 5.319\left(\frac{U}{U^*}\right)^{0.075}\left(\frac{W}{H}\right)^{1.206} ; \frac{W}{H} \leq 28$
		$\frac{D_x}{HU^*} = 9.931\left(\frac{U}{U^*}\right)^{1.802}\left(\frac{W}{H}\right)^{0.187} ; \frac{W}{H} \geq 28$

6.3 RESULT AND DISCUSSION

The results obtained from this work are presented in tables and figures, while the discussions are made subsequently:

Longitudinal dispersion coefficient of the river

Longitudinal dispersion coefficient of the channel has been enlisted in Table 6.2, corresponding to Q = 0.0365 m^3/s and 0.0729 m^3/s. A comparison between the dispersion coefficient predicted by the various models of the researchers and measured through tracer test has been formulated in Table 6.2.

For this study, the trend of the tracer response concentration-time curve (Fig 6.3) displayed a normal distribution, wherein the tracer concentration in the water sample grew from 0.5 mg/l to peak concentration of 2.78 mg/l at a sampling time of 2.06 s and thereafter drops to 0.85 concentration after 4.5 s. The normalized variance was also estimated from the tracer response concentration-time data (Table 6.3), and its value was actually dependent on the mean tracer time of travel, and not on the uniformity in time spacing.

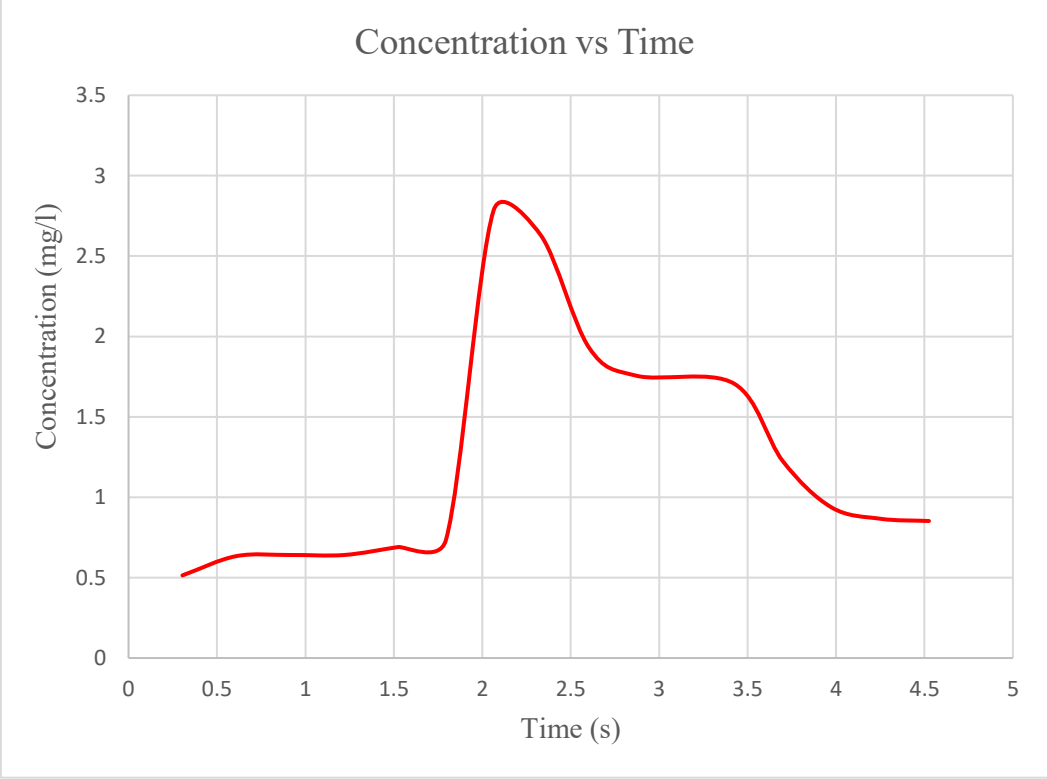

Fig 6.3. Plot of Tracer concentration with respect to time

Table 6.2 Dispersion coefficient predicted by the various models of the previous researchers and measured through tracer test

Q = 0.0365 m^3/s		Q = 0.0729 m^3/s	
Predicted	Measured	Predicted	Measured
0.000	0.081	0.000	0.101
10.175	0.081	30.972	0.101
2.370	0.081	6.984	0.101
0.356	0.081	0.806	0.101
2.281	0.081	6.245	0.101
0.229	0.081	0.430	0.101
0.075	0.081	0.103	0.101
0.345	0.081	0.746	0.101
0.104	0.081	0.183	0.101
0.229	0.081	0.460	0.101
0.144	0.081	0.273	0.101
0.160	0.081	0.292	0.101
0.073	0.081	0.112	0.101
0.071	0.081	0.115	0.101
0.102	0.081	0.155	0.101

Step wise calculation of measured longitudinal dispersion coefficient has been shown in Table 6.3. Normalised variance, dispersion number and average river flow time were estimated using the parameters given in following Table 6.3.

Table 6.3 Application of Leverspiel and Smith Model for D_{XM} measurement using experimental data from tracer technique

Sample No.	C_i (mg/l)	t_i (s)	t_i^2 (s^2)	$C_i t_i$ (mg-s/l)	$C_i t_i^2$ ($mg/s^2/l$)
1	0.514085	0.3048	0.092903	0.156693	0.04776
2	0.633803	0.6097	0.371734	0.38643	0.235606
3	0.640845	0.9145	0.83631	0.586053	0.535945
4	0.640845	1.2193	1.486692	0.781382	0.95274
5	0.690141	1.5241	2.322881	1.051844	1.603115
6	0.732394	1.794	3.218436	1.313915	2.357164
7	2.78389	2.0639	4.259683	5.745671	11.85849
8	2.624754	2.3338	5.446622	6.125652	14.29605
9	1.93007	2.6037	6.779254	5.025323	13.08443
10	1.755245	2.8736	8.257577	5.043871	14.49407
11	1.706294	3.4242	11.72515	5.842691	20.00654
12	1.223776	3.6995	13.6863	4.52736	16.74897
13	0.93662	3.9748	15.79904	3.722876	14.79769
14	0.866197	4.2501	18.06335	3.681425	15.64642
15	0.852113	4.5254	20.47925	3.856151	17.45062
SUM	18.53107	36.1154	112.8252	47.84734	144.1156

Where Θ = 2.582006 S, σ^2 = 0.16653, δ = 0.065896, L = 3m, U = 0.41 cm/s and Measured dispersion coefficient was estimated as D_{XM} = 0.081 m^2/s.

Discrepancy ratio, absolute error and relative error were the parameters to assess the accuracy of the model. It can be inferred from the Table-6.4 that discrepancy ratio obtained for Fischer, Liu, Koussis and Rodriguez-Mirasol possesses discrepancy ratio (λ >0) suggesting overestimation of the predicted longitudinal dispersion coefficient. Theoretical model of Kashefipour and Falconer is 0.035, Sattar and Gharabaghi is 0.043 while Wang and Huai are 0.056 are the close approximations to the experimentally obtained dispersion coefficient of the channel. Elder possesses discrepancy ratio less than 0 states underestimated value of dispersion coefficient. Absolute error and relative error of the Kashefipour and Falconer, Sattar and Gharabaghi and Wang and Huai are very close to zero suggests that these 3 models can be fitted for the proposed channel.

Table 6.4 Predicted Longitudinal dispersion coefficient by various models and their close approximations with the measured dispersion coefficient

Test Model	Predicted Longitudinal dispersion coefficient (D_{XP})	Discrepancy ratio (λ)	Absolute Error (AE)	Relative Erro (RE)
Elder (1959)	0.000	-2.727	0.081	0.998
Fischer (1975)	10.175	2.099	-10.094	-124.532
Liu (1977)	2.370	1.466	-2.289	-28.240
Iwasa and Aya (1991)	0.356	0.642	-0.274	-3.386
Koussis and Rodriguez-Mirasol	2.281	1.449	-2.199	-27.136
Seo and Cheong (1998)	0.229	0.451	-0.148	-1.826
Kashefipour and Falconer (2002)	0.075	-0.035	0.006	0.077
Sahay and Dutta (2009)	0.345	0.630	-0.264	-3.262
Etemad-Shahidi and Taghipour (2012)	0.104	0.108	-0.023	-0.283
Li et al. (2013)	0.229	0.452	-0.148	-1.828
Zeng and Huai (2014)	0.144	0.248	-0.062	-0.771
Disley et al. (2015)	0.160	0.297	-0.079	-0.979
Sattar and Gharabaghi (2015)	0.073	-0.043	0.008	0.095
Wang and Huai (2016)	0.071	-0.056	0.010	0.121
Alizadeh et al (2017b)	0.102	0.099	-0.021	-0.256
Measured Longitudinal dispersion coefficient (D_{XM}) = 0.081 m^2/s				

6.4 MODEL-TO-RIVER CONVERSION OF DISPERSION COEFFICIENT AND APPLICATION OF THE 1-D ADVECTION–DISPERSION EQUATION

Physical hydraulic models are often used to investigate pollutant transport processes in rivers; however, such models operate under reduced geometric, kinematic, and dynamic scales. To relate the model behaviour to the natural (prototype) river, appropriate scaling laws must be applied. In this study, a prototype river dispersion coefficient is estimated using the dispersion value measured in a distorted hydraulic model. The model incorporates different geometric scale ratios in the horizontal and vertical directions, and its kinematic similarity is preserved by applying Froude requirements. The pollutant transport calculations are then performed using the one-dimensional Advection–Dispersion Equation (ADE).

Given Data for the Physical Model

- **Model dispersion coefficient:** D_m=0.081 m^2/s
- **Scale ratios:**

  Horizontal length scale: L_r=1:500

  Vertical length scale: H_r=1:67

  Velocity ratio: V_r=1:8.18

  Discharge ratio: Q_r=1:274210

The scale applies to Dispersion Coefficient (D)?

The dispersion coefficient has dimensions:

$$D = \frac{L^2}{T}$$

For distorted models (different horizontal & vertical scales), **longitudinal dispersion is controlled by horizontal processes**, so **the horizontal scale** L_r must be used.

Time scale for kinematic similarity is:

$$T_r = \frac{L_r}{V_r} = \frac{1/500}{1/8.18} = 0.01636 = \frac{T_m}{T_p}$$

Thus prototype-to-model ratio is: $\frac{T_p}{T_m} = 61.1$

Now dispersion scale: $\frac{D_p}{D_m} = \frac{{L_r}^2}{T_r}$

Substituting: $D_p = D_m \frac{(1/500)^2}{0.01636}$ (model → prototype requires inverse)

$$D_p = 0.081x(500)^2 x \frac{1}{61.1}$$

$$\boldsymbol{D_p = 331.42 m^2/s}$$

This is **realistic**, because field studies in large rivers show:

- Mississippi River: 200–400 m²/s
- Amazon River: > 300 m²/s
- Brahmaputra (estimated in literature): 250–450 m²/s

So the scaling matches physical expectation.

1-D Advection–Dispersion Equation

The pollutant concentration in a river channel is governed by the one-dimensional Advection–Dispersion Equation 6.9.

$$\frac{\delta C}{\delta t} + U\frac{\delta C}{\delta x} = D\frac{\delta^2 C}{\delta x^2} \qquad (6.9)$$

This equation describes **how pollutant concentration changes in a river** due to **advection (transport by flow)** and **dispersion (spreading due to turbulence).**

- This is the **governing equation**.
- It tells you **how** a pollutant behaves (moves + spreads) in a river.
- It does **not give a concentration value** directly.
- It is like saying: "The pollutant moves downstream with velocity U and spreads with dispersion D."

This PDE expresses the combined effects of advection (transport by flow), dispersion (mixing and spreading), and decay. It does not directly yield numerical concentrations unless solved with appropriate initial and boundary conditions.

Governing Equation (1-D Advection–Dispersion)

$$C(x,y,t) = \frac{M_s}{4h\Pi t^* \sqrt{D_x D_y}} exp\left[-\frac{(x-x_s-v_x t^*)^2}{4D_X t^*} - \frac{(y-y_s-v_y t^*)^2}{4D_y t^*} - kt^*\right] \quad (6.10)$$

For an instantaneous point source with mass Ms, the solution is as follows in equation (6.11):

$$C(x,t) = \frac{M_s}{4h\Pi t^* \sqrt{D_x}} exp\left[-\frac{(x-x_s-v_x t^*)^2}{4D_X t^*} - kt^*\right] \quad (6.11)$$

This equation provides the concentration at any point in space and time while accounting for advection, turbulent dispersion, exponential decay, and flow depth h.

What it is:

- This is the **actual solution** to the advection–dispersion equation.
- It gives **real concentration at any point (x, y) and time t**.
- It includes:
  - advection (movement),
  - dispersion (spreading),
  - decay (k),
  - depth (h),
  - initial mass M_s

This tells you the actual pollutant concentration in the river at any time and location.

Total plume length after 1 hour of continuous discharge

Thus, the downstream travel distance is:

Plume length=(advected length)+(spread due to dispersion)

$$L_{total}=L_{advection}+L_{dispersion}$$

$$L_{total}=Vt+4\sqrt{D_p t}$$

For t=1hr= 3600s, V=2m/s,Dp= 331.42 m^2/s

$$L_{total}=7.2\ km+4.37\ km$$

$L_{total} \approx 11.57$ km

Similarly,

Time (hr)	L_{Total} (km)
1	11.57
2	20.58
3	29.17
4	37.54
5	45.77

6.5 CONCLUSION

This study experimentally determined the longitudinal dispersion coefficient of an open channel using methylene blue as a tracer to simulate solute transport processes in natural rivers. The tracer response exhibited a near-Gaussian distribution, with concentration increasing from 0.5 mg/L to a peak of 2.78 mg/L at 2.06 s, followed by a decline to 0.85 mg/L at 4.5 s. This pattern confirmed that longitudinal dispersion was the dominant mechanism governing solute mixing under steady flow conditions. The normalized variance analysis indicated that dispersion was mainly influenced by the mean travel time of the tracer rather than the temporal spacing of samples. A longitudinal dispersion coefficient (DLM) of 0.081 m^2/s was measured for the River Water using the tracer method. This indicates a moderate capacity for pollutant dispersion. Theoretical models from Kashefipour and Falconer and Sattar and Gharabaghi model respectively showed 0.073 m^2/s and 0.075 m^2/s as the closest approximations to the experimentally measured value of longitudinal dispersion coefficient of the River Water. The findings validate the reliability of tracer-based methods for quantifying solute transport in open-channel flows. Future research should extend this approach to variable flow regimes and sediment-laden conditions to improve the general applicability and precision of dispersion modelling in natural river environments.

भारतीय प्रौद्योगिकी संस्थान गुवाहाटी
Indian Institute of Technology Guwahati

Chapter 7

NANOCELLULOSE–BENTONITE COMPOSITE: A NOVEL MATERIAL FOR HEAVY METAL REMOVAL FROM AQUEOUS SOLUTIONS

7.1 INTRODUCTION

Accurately assessing and modelling the transport of contaminants is essential for successful mitigation of heavy metals pollution in water bodies. But these alone are not enough. We also need efficient and sustainable treatment technologies. Heavy metal removal by traditional methods, for example, chemical precipitation, membrane filtration, and ion exchange, usually, come with the problems of high operational costs, excessive energy requirements, and generation of secondary waste. Besides, adsorption, based methods are nowadays dominating the field due to their straightforwardness, high effectiveness, and the possibility of using cheap and environmentally friendly materials. The past several years have seen a growing focus on the utilization of agricultural waste for the production of environmentally friendly solutions. Materials derived from biomass, in addition to providing pollutant removal, also offer the advantage of waste diversion. The nanocellulose used in this study is derived from Bao Dhan rice husk and term as Rice Nanocellulose (RNC). The work reported in this chapter demonstrates the preparation, structural characterization, and efficiency testing of nanocellulose bentonite composite, which is a rice husk waste product, as an adsorbent for selective heavy metal removal from water. Nanocellulose is considered one of the leading adsorbent materials nowadays due to its various advantages of having a high surface area, plenty of hydroxyl functional groups, good mechanical strength, and being renewable. For instance, agricultural residues like rice husk can be a great and especially less utilized source of cellulose in the areas where rice cultivation dominates. It is a good idea to make use of rice husk waste for the production of nanocellulose, which is in line with the circular economy concept and at the same time, it gives us a green product that can be used for environmental purposes. Bentonite clay, on the other hand, is known for its high cation exchange capacity, the nature of its layered structure, and its strong attraction to metal ions. Still, there are instances when pure bentonite is not able to work perfectly as the particles tend to stick together and the adsorption efficiency can drop depending on the conditions. A hybrid composite material made from rice nanocellulose (RNC) and bentonite is Rice Nanocellulose-Bentonite (RNC-BENT), likely to

give a great adsorption capacity as it would combine the strengths of both the organic and inorganic parts. Section 7.2 presented the experimental methodology starting from materials used, surface area analysis and cation exchange capacity. Synthesis of composite material (RNC-BENT), its removal capacity and regeneration of adsorbent is described in section 7.3. A brief discussion on the results is elaborated in section 7.4 described adsorption capacity with RNC and RNC-BENT adsorbents. Section 7.5 briefed about the prevalent models used for adsorption studies and best fit of the model for the developed bio composite. Removal mechanism of the heavy metals and regeneration studies were explained in section 7.7 and 7.8 before concluding the chapter in section 7.8.

7.2 EXPERIMENTAL SECTION

7.2.1 Materials

The Bao Dhan husk obtained from the Bijoynagar area of Assam was used to conduct this research. Analytical grade chemicals and deionized water were used to prepare all standard samples for the calibration of atomic absorption spectroscopy (AAS). All the chemicals were obtained from Merck, India. Reagents such as sulphuric acid, hydrogen peroxide solution (30 vol.%), glacial acetic acid, ethanol, and sodium hydroxide were used in the study. The preparation of stock solutions of metals was done by dissolving the required quantities of potassium dichromate ($K_2Cr_2O_7$) and nickel chloride salt ($Ni(Cl)_2 \cdot 6H_2O$) in deionized water. The bentonite clay (BENT) obtained from the district of Barmer in Rajasthan, India, was used to form the composite material (RNC-BENT) with the Rice Nanocellulose (RNC).

7.2.2 BET Surface Area Analysis

The specific surface area (SSA) of the RNC-BENT composite was characterized using the Brunauer–Emmett–Teller (BET) method with a surface area analyzer (Quantachrome Instruments, Model: Autosorb-IQ MP). The nitrogen adsorption–desorption isotherms were recorded at 77 K, and the SSA was calculated from the adsorption data within the relative pressure range (P/P_0) recommended for BET analysis.

RNC and natural bentonite generally exhibit SSA values in the ranges of approximately 120–250 m^2/g and 50–150 m^2/g, respectively. The measured SSA of RNC-BENT was found to be 671.81 m^2/g, indicating a highly porous structure. The elevated surface area is expected to contribute significantly to the enhanced adsorption capacity by increasing the number of available active sites for ion-exchange and surface complexation processes.

7.2.3 Cation Exchange Capacity (CEC)

The cation exchange capacity (CEC) of bentonite was determined using the methylene blue (MB) adsorption method. In this procedure, a known mass of dry bentonite sample was dispersed in deionized water and titrated with standard methylene blue solution under continuous stirring. The endpoint was identified by the appearance of a permanent blue halo around the sample drop placed on filter paper, indicating saturation of exchangeable sites by methylene blue cations. The CEC was calculated using the volume of methylene blue solution consumed, its normality and the dry mass of bentonite according to given equation of CEC in equation 7.1. This method is widely employed for estimating the exchange capacity of clay minerals due to its simplicity and reliability.

$$CEC\ (meq/100g) = VB \times NBM \times 100/M_0 \qquad (7.1)$$

Where:

CEC = Cation Exchange Capacity (meq/100 g)

VB = Volume of MB adsorbed per gram of bentonite (mL/g)

NBM = Normality of MB solution (mol/L or eq/L)

M_0 = Mass of dry bentonite used (g)

A summarized table of bentonite clay properties highlighting the average particle size, surface area, and cation exchange capacity (CEC) has been summarized in Table-7.1.

Table 7.1: Various property and methodology adopted for RNC-BENT

Property	Value	Methodology
Average Particle Size	1.6 µm	Hydrometer Analysis (Sedimentation Method)
Specific Surface Area (SSA)	671.81 m^2/g	Determined by BET Surface area analyzer (Make: Quantachrome, Model: Autosorb-IQ MP)
Cation Exchange Capacity (CEC)	130.63 meq/100 g	Determined via methylene blue method

7.2.4 Characterization of RNC and RNC-BENT

The synthesized composite material (RNC-BENT) was characterized for a two-dimensional crystalline structure using powder X-ray diffraction (D8 Advance from the Netherlands) with

Cu Kα (λ=0.154nm) over the 2θ range (10–80). Fourier Transform Infra-red spectroscopy (FTIR) (IRAffinity-1 from Japan) analyzed the functional groups on the material's surface from 400 to 4000 cm^{-1}. SEM-EDAX (LEO-1430 from the UK) was used to establish the material's surface morphology and quantitative content.

7.3 SYNTHESIS OF RNC

The collected Bao Dhan rice husks were washed to remove soluble substances and dirt. It was put to dry under the sun for about two weeks and milled to get a powder form that could be used for further analysis. In the process, at first, an alkali treatment was performed to remove lignin and hemicellulose. In this process, 50g of powdered husk was weighed and treated with aqueous 5% NaOH under continuous vigorous stirring for 3 hours at 600 rpm using a magnetic stirrer at 60-80 °C. The sample obtained after the treatment may be alkaline, so it was washed with distilled water to reach neutrality (pH=7). After reaching neutrality, the sample was dried in the oven at 50 °C. The obtained alkali-treated sample was further bleached with 30% hydrogen peroxide for 3 hours at 80 °C by maintaining an acidic pH (drops of acetic acid to make it acidic if the solution is not acidic after adding hydrogen peroxide). The process was repeated three times. The obtained cellulose was then dried in an oven (40- 50 °C) and stored for the extraction of nanocellulose. The extracted cellulose was treated with 4M H_2SO_4 (50 mL) in a beaker under continuous stirring at a rate of 300 rpm. The hydrolysis time was found to be 50 min, which is optimal. The hydrolysis process was stopped by adding 100 mL of cold (ice) deionized water into the beaker. The suspension was washed at least 6 times, followed by centrifugation (1200 rpm for 10 mins), and the pH was again neutralized (pH 7) by using a titration method by the dropwise addition of 0.1 M NaOH or 0.1 M HCl under constant stirring until the target pH 7 was achieved. The product was further ultrasonicated for 10 minutes to obtain the nanocellulose (RNC). The yield of RNC was found to be 62.3%.

7.3.1 Synthesis of composite (RNC-BENT)

NaOH (6g) and thiourea (12g) were combined with RNC (3g) with magnetic stirring for 5 minutes at room temperature before being refrigerated for 18 hours. $CaCl_2$(0.1g) and NaH_2PO_4 (0.1g) were added to the solution, along with distilled water (50 mL) and the necessary amount of bentonite clay (3g), and vigorous stirring was performed for 15 minutes in a magnetic stirrer. The mixture was then placed into the oven for 7 hours at 80 °C. After being washed with DI and ethanol, the mixture was centrifuged, and the material was dried and named RNC-BENT (Fig. 7.1). The yield was found to be the RNC-BENT was used for the batch adsorption process for the metal ions.

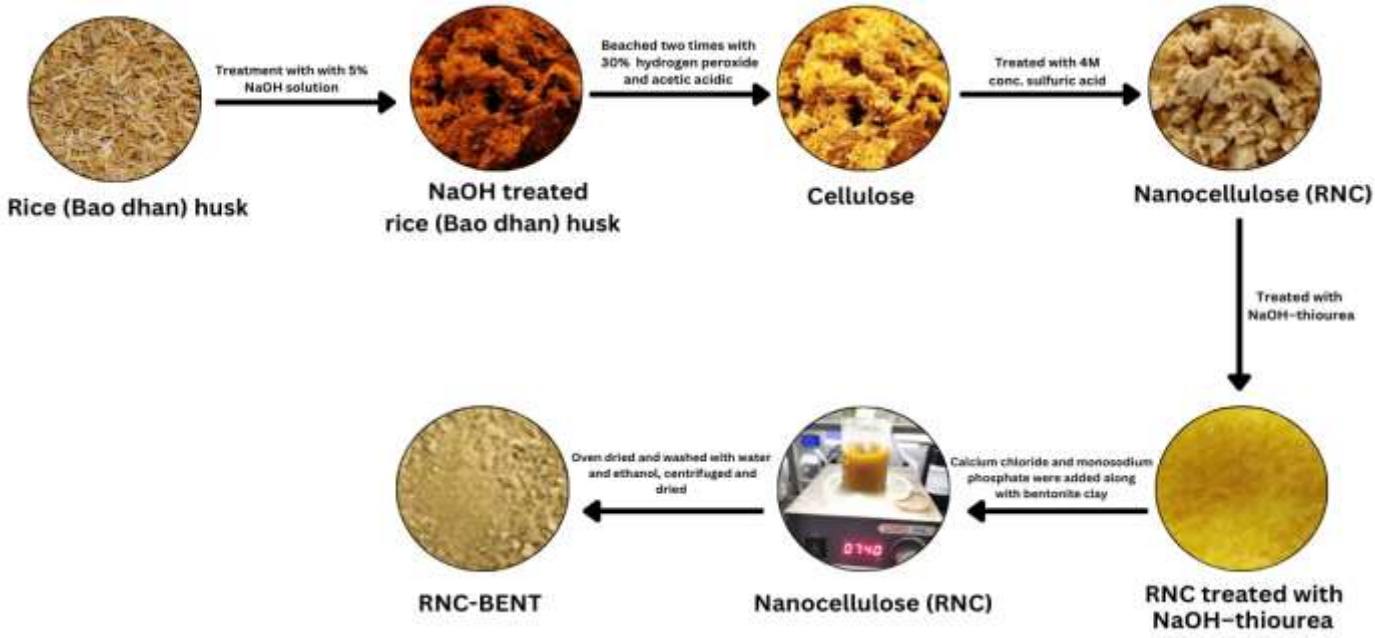

Fig 7.1. Schematic representation of the synthesis of RNC and RNC-BENT

7.3.2 Ni (II) and Cr (VI) removal from aqueous solution by RNC-BENT

The performance of RNC-BENT for removing Cr(VI) and Ni(II) was examined by optimizing several experimental parameters such as contact duration (0 to 120 minutes), adsorbent dose (0.02-0.1g), pH (3-11), and concentration (20-60 mg/L). The batch studies were carried out at a temperature of 27°C. To achieve the necessary pH, either 0.1 M NaOH or 0.1 M HCl were used. The samples were centrifuged to get a clear solution and then analyzed by AAS (atomic absorption spectrophotometry) (Spectra AA 220 FS from the Netherlands). To maintain equilibrium throughout the adsorption experiment, we used a rotary shaker (Bio Technics from

India) to shake the solutions continually. The removal effectiveness of Cr(VI) and Ni(II) in percentages was estimated using the following relation: (7.2)

$$\%\ Removal = \left[\frac{Co - Ct}{Co}\right] * 100 \qquad (7.2)$$

where C_0 and C_t have units ($molL^{-1}$), which represents the initial concentration and the concentration at any time after the reaction was conducted for time t(min) [260].

The removal mechanism of Cr(VI) by the RNC-BENT composite is more complex than that of cationic metal ions such as Ni(II), since Cr(VI) mainly exists as oxyanionic species including $HCrO_4^-$ and CrO_4^{2-} depending on the solution pH. Therefore, simple cation exchange cannot solely explain the adsorption behavior of Cr(VI). The adsorption of Cr(VI) may involve multiple mechanisms, including electrostatic attraction between negatively charged chromate species and positively charged surface sites, surface complexation with hydroxyl and oxygen-containing functional groups present in nanocellulose and bentonite, and possible partial reduction of Cr(VI) to Cr(III) under favorable conditions. These combined interactions likely contribute to the efficient removal of Cr(VI) by the RNC-BENT composite.

7.3.3 Regeneration of adsorbent

Rice husk contains cellulose, hemicellulose, lignin, and silica, with cellulose-derived hydroxyl groups playing a major role in metal binding through hydrogen bonding, surface complexation, and electrostatic interaction. Bentonite mainly consists of montmorillonite, an aluminosilicate clay mineral possessing layered structures, permanent negative surface charge and high cation exchange capacity. These characteristics facilitate ion exchange and adsorption of metal ions. The integration of nanocellulose with bentonite combines the abundant functional groups of cellulose with the ion exchange capability of bentonite, thereby enhancing the overall adsorption efficiency of the RNC-BENT composite. To assess the reusability of RNC-BENT, the regeneration of the spent adsorbents was also investigated. Initially, 0.1 g/L of the adsorbent was combined with 5 mL of 40 mg/L Cr(VI) and Ni (II) solutions, respectively, to load the adsorbent with the ions under study. 0.10 M HNO3 was used to elute the ions. The following formula 7.3 was used to determine the RNC-BENT adsorbent's regeneration efficiency (%RE):

$$(\%)RE = \frac{Q_r}{Q_o} * 100 \qquad (7.3)$$

Before regeneration, the adsorption capacity (mmol/g) is denoted by Q_0; following regeneration, it is denoted by Qr, The equilibrium adsorption capacity is denoted by Qe.[261].

7.4 RESULTS AND DISCUSSIONS

7.4.1 Characterization of RNC-BENT

The FTIR spectra of the RNC and RNC-BENT samples reveal key differences in their chemical composition and functional groups.

A broad peak observed around 3400 cm^{-1} (Fig 7.2) in both samples is attributed to O–H stretching vibrations, indicating the presence of hydroxyl groups, likely from water or alcohol functionalities. The RNC sample shows a peak near 2920 cm^{-1}, characteristic of C–H stretching in alkyl groups, suggesting the presence of organic content [262]. A peak around 1650 cm^{-1} appears in both samples and can be assigned to either C=O stretching or H–O–H bending, further confirming the presence of moisture or carbonyl-containing compounds [263].

A prominent peak near 1030 cm^{-1} in the RNC-BENT sample corresponds to Si–O stretching vibrations, typical of silicate structures, and is indicative of bentonite clay. Additionally, bands in the range of 800–500 cm^{-1} are associated with metal–oxygen bonds such as Al–O or Fe–O, further supporting the incorporation of bentonite in the RNC-BENT composite [264]. These spectral features collectively confirm successful modification of RNC with bentonite, highlighting changes in the material's structure and composition has been depicted in Table-7.2.

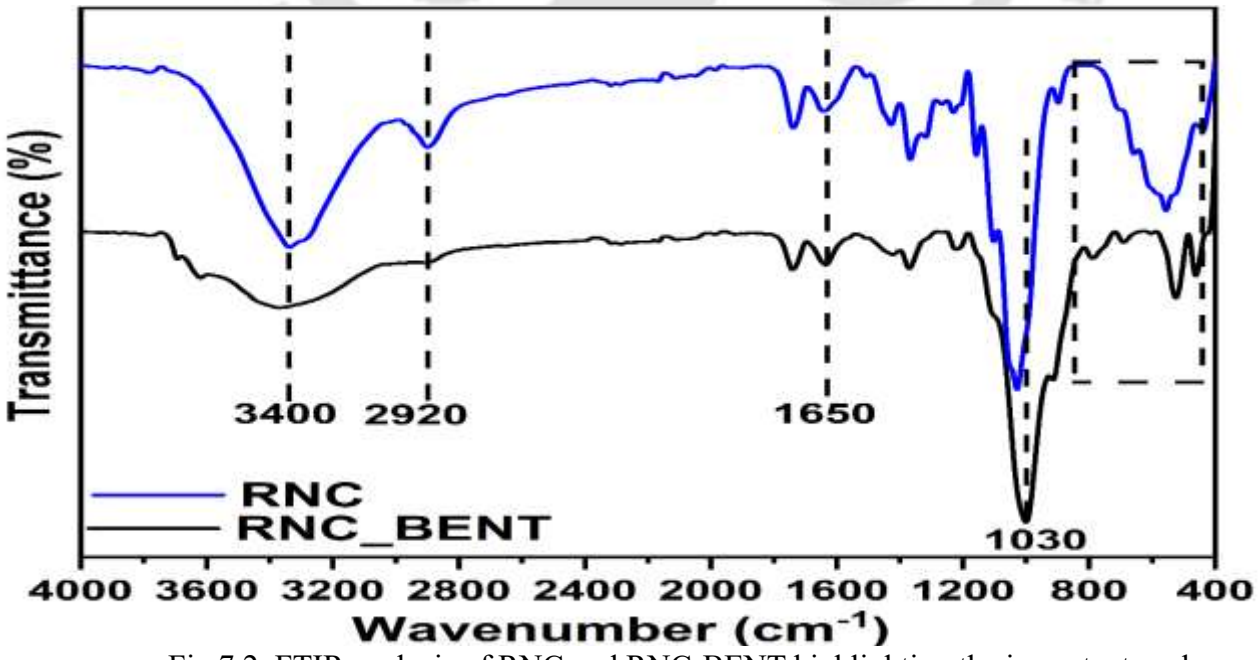

Fig 7.2. FTIR analysis of RNC and RNC-BENT highlighting the important peaks

Table 7.2: Wavenumber and their interpretation associated with functional groups

Wavenumber	Functional Group/Assignment	Sample	Interpretation/Notes
~3400	O–H stretching (hydroxyl group)	RNC, RNC-BENT	Broad peak, indicates –OH groups
~2920	C–H stretching (alkyl groups)	RNC	Possibly from organic content
~1650	C=O stretching / H–O–H bending	RNC, RNC-BENT	Water content or carbonyl groups
~1030	Si–O stretching (silicates)	RNC-BENT	Common in bentonite
~800–500	Metal–O (e.g., Al–O, Fe–O)	RNC-BENT	Indicates presence of clay minerals

"The X-ray diffraction (XRD) pattern of the RNC-BENT composite displays a combination of sharp and broad diffraction peaks, indicating a semi-crystalline structure (Fig 7.3). Distinct crystalline peaks observed in the 2θ range of approximately 20° to 35° correspond to the

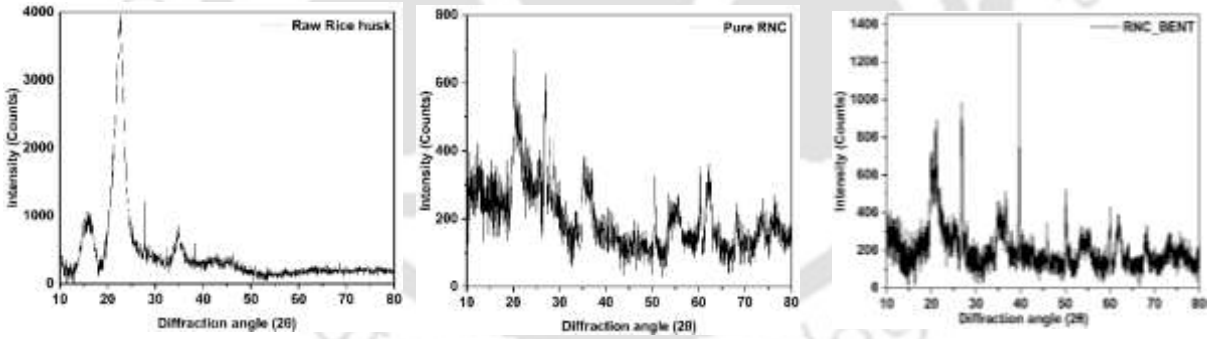

Fig 7.3. XRD analysis of Rice Husk, Pure RNC and RNC-BENT

layered silicate structure of bentonite, while the broader humps at lower angles are associated with the amorphous nature of the RNC component. The peak at 41.2° represents the presence of $Ca_5(PO_4)_3OH$ [265].

To quantify the degree of crystallinity, the Crystallinity Index (CI) was calculated using the Segal method. The intensity of the main crystalline peak at approximately 2θ ≈ 27° was measured to be 3300 a.u., and the minimum intensity of the amorphous region near 2θ ≈ 18° was around 2000 a.u. Based on these values, the estimated CI is:

$$CI=\frac{I_{cr}-I_{am}}{I_{cr}}x100=\frac{3300-2000}{3300}x100=39.4\%$$

This moderate crystallinity indicates a well-integrated composite structure, where the crystalline bentonite contributes mechanical stability and cation exchange capacity [264], while the amorphous cellulose component enhances surface area and accessibility of adsorption sites. This structural synergy is likely to enhance the material's performance in adsorption-based applications. To evaluate the structural evolution during synthesis, the crystallinity indices (CI) of raw rice husk, pure RNC and the RNC-BENT composite were compared. The CI values were calculated as 55.32%, 45.21% and 35.48%, respectively. The progressive decrease in crystallinity indicates partial disruption of the ordered cellulose structure during alkali treatment, acid hydrolysis and composite formation with bentonite. The increased amorphous nature of the RNC-BENT composite may enhance surface accessibility and facilitate improved adsorption performance toward heavy metal ions.

The RNC-BENT sample was placed on carbon tape for SEM analysis, and any extra particles were blown away using pressured air. The samples were covered with a 4 nm thick coating of Au-Pd alloy prior to analysis. The nanoparticles are adhered to one another in the SEM picture to create varying-sized aggregates (Fig 7.4).

The lack of visible cellulose fiber structure suggests that the bentonite clay completely enveloped the nanocellulose surface. A pore size distribution histogram (Fig 7.5) prepared from which, following interpretations can be inferred.

- Most of the pores are very small, with the majority of pore areas falling below 0.1 μm².
- A few pores reach up to ~0.7 μm², indicating some variability in the pore structure.
- The distribution is skewed towards smaller sizes, which is common in porous materials with compact, irregular morphology.

This analysis suggests that RNC-BENT adsorbent possesses a highly microporous structure, which could positively influence surface area and potential applications such as adsorption or catalysis.

The EDX study (Fig 7.4) supports the weight and atomic proportion percentages of the elements present on the surface of the RNC-BENT, The EDX analysis confirms the presence of sodium (2.1 wt%) and calcium (2.4 wt%) ions after adsorption, supporting the ion-exchange mechanism. These ions likely replaced hydrogen or native ions on the adsorbent surface. The high oxygen content (32.5 wt%) indicates the abundance of functional groups (-COOH, -OH)

facilitating ion-exchange. Minor elements like silicon and phosphorus suggest a silicate-based structure and phosphate groups aiding cation binding. FTIR analysis further supports this by showing shifts in -OH, C=O, and C–O bands, indicating the involvement of these groups in ion-exchange during adsorption.

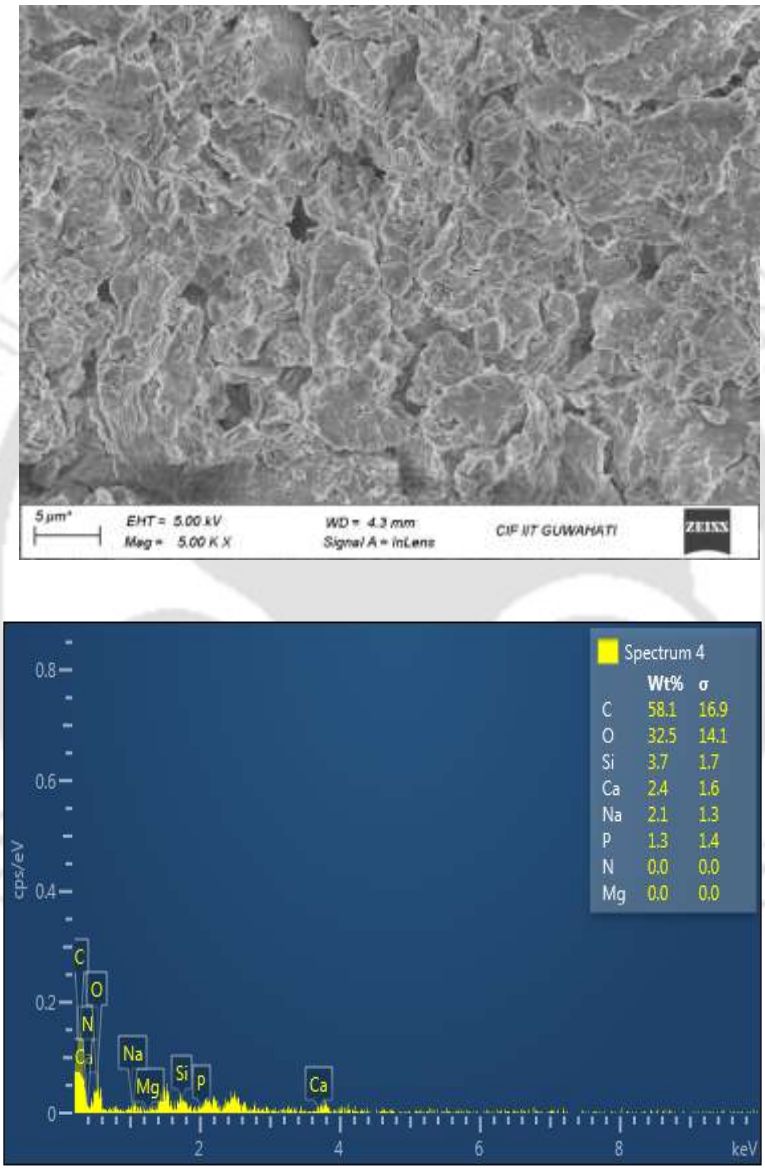

Fig 7.4. SEM and EDX data of the RNC-BENT composite material

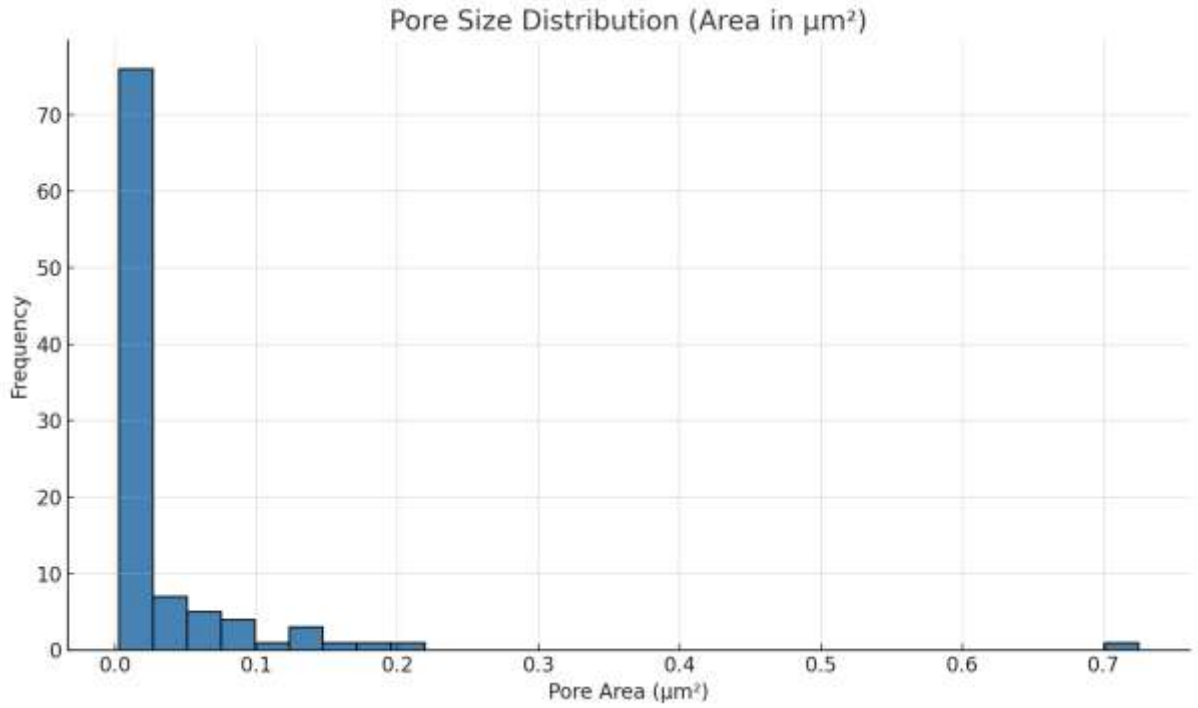

Fig 7.5. Histogram depicting pore size distribution

The presence of phosphorus detected in the EDX spectrum and the diffraction peak near 41.2° in the XRD pattern can be attributed to the incorporation of phosphate species originating from NaH_2PO_4 used during composite synthesis. In the presence of $CaCl_2$, phosphate ions facilitated the formation of calcium phosphate/hydroxyapatite-like phases within the RNC-BENT matrix. These phosphate-containing structures may enhance the adsorption performance by providing additional ion-interaction sites.

7.4.2 Adsorption investigations

7.4.2.1 Comparison of adsorption capacity with RNC and RNC-BENT adsorbents

50 mg adsorbent, RNC and RNC-BENT, were taken in 25 mL samples of 40ppm of Ni(II) and Cr (VI), respectively, with 2 hours of shaking at room temperature at neutral pH. Although the RNC worked as an adsorbent, the removal percentage increased more in the case of RNC-BENT usage for both, respectively (Fig 7.6). Thus, the produced composite showed superior adsorption ability for both the metal ions.

This could be because RNC-BENT is a calcium hydroxyapatite cellulose composite, and the ion exchange between the metal ions and Ca (II) ions is one possible removal process. Bentonite clay primarily comprises montmorillonite, a hydrated sodium calcium aluminium

magnesium silicate hydroxide. The ion exchange of Cr (VI) and Ni (II) ions for Ca (II) ions of bentonite clay is another possibility of removal efficiency.

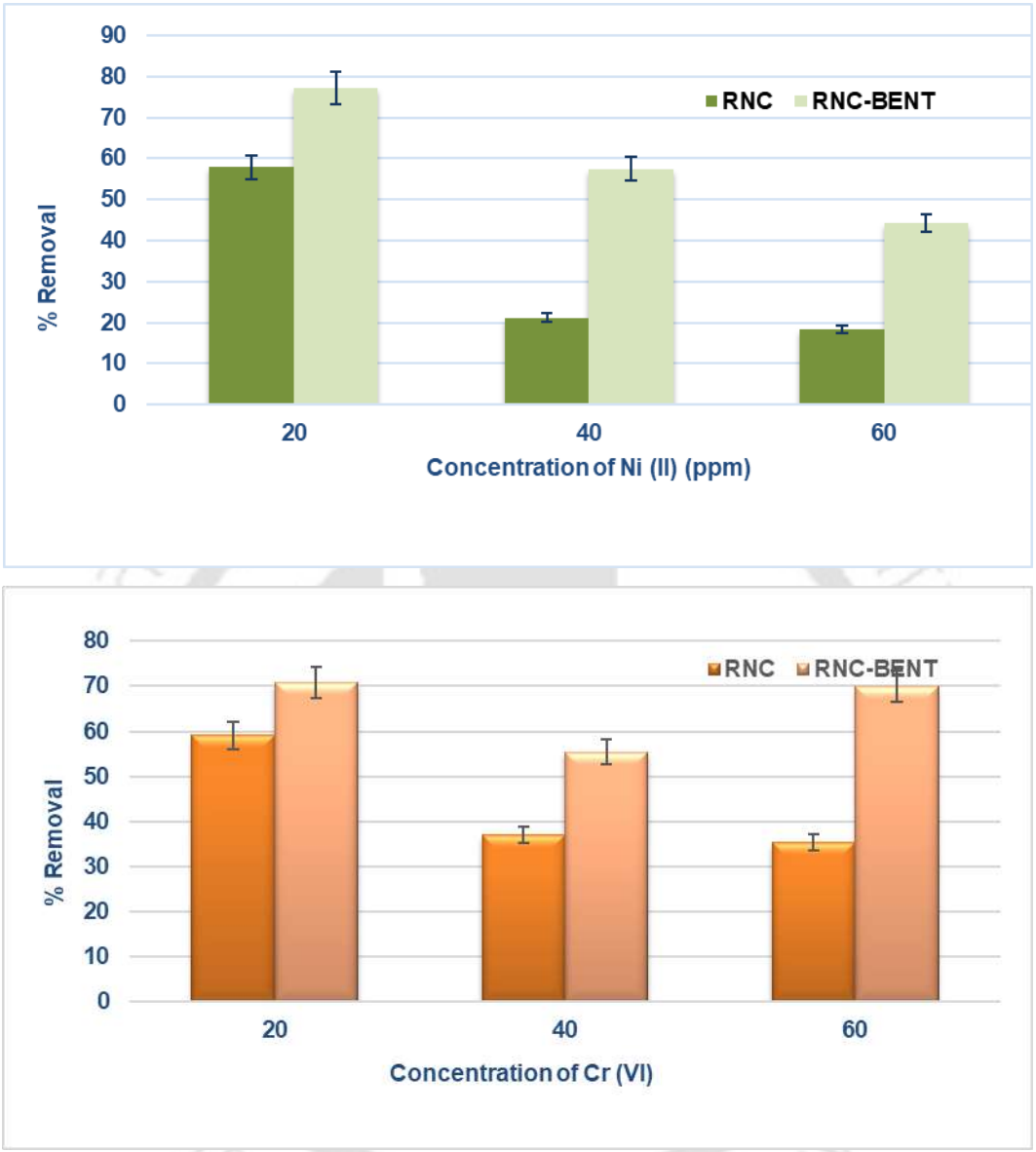

Fig 7.6. Removal percentage of Ni (II) and Cr (VI) at different concentrations

7.4.2.2 The pH effect

The effect of pH on Cr (VI) and Ni (II) adsorption was examined utilizing batch adsorption tests by taking 50 mg adsorbent in a 25 mL sample containing 40 ppm of the metal ions, respectively. The solutions were shaken for 2 hours at room temperature 27°C at pH varying from 3.0 to 11.0. (Fig 7.7). The pH range for adsorption studies was between 3-11. Alkaline pH was suitable for Cr (VI) and Ni (II) ions. The precipitation caused the adsorption capacity

to increase at higher pH values. However, the adsorption was suitable for only Cr (VI) ions in acidic and alkaline conditions.

7.4.2.3 Effect of Contact Time

Fig 7.8 illustrates how contact time affects the adsorption of the metal ions in aqueous solution. The duration of the adsorption experiments was 120 minutes. The adsorption capabilities increased rapidly as the contact duration increased, and the adsorption equilibrium of Ni (II) and Cr (VI) was attained within the first five minutes.

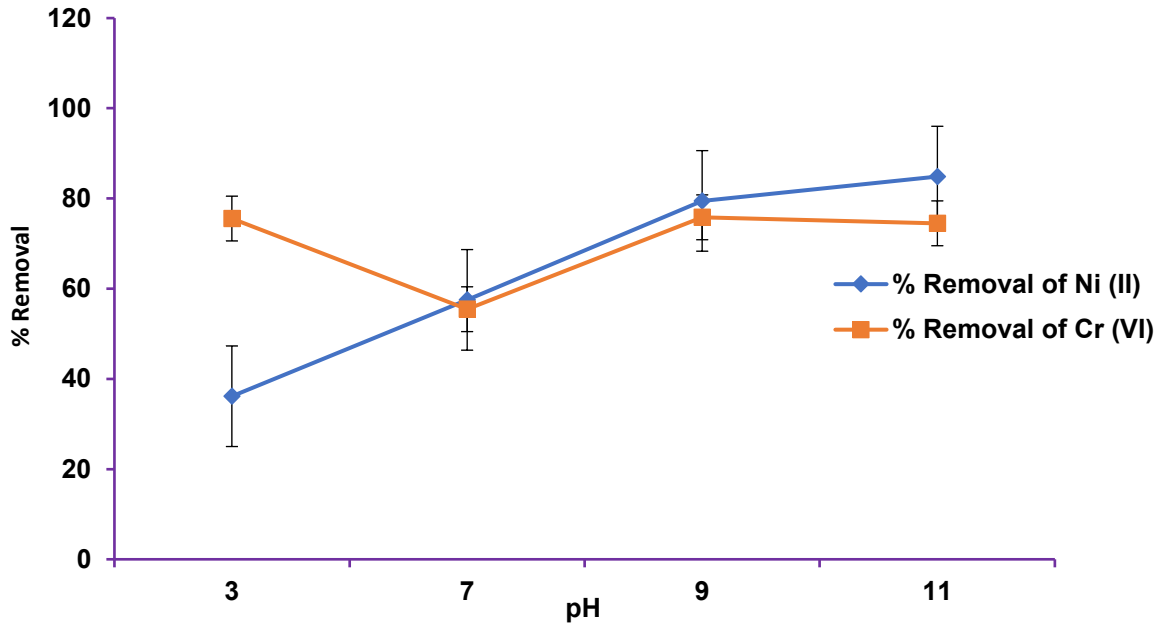

Fig 7.7. Removal percentage of Ni (II) and Cr (VI) at different pH values

Adsorption kinetic modeling was tested using pseudo first order (Pfo) and pseudo second order (Pso) models. The following equation 7.4, is an expression for the non-linear Pfo model:

$$q_t = q_e(1 - e^{-k_1 t}) \qquad (7.4)$$

The rate-determining step in Pso is represented by equation 7.5

$$q_t = \frac{k_2 q_e^2 t}{1 + k_2 q_e t} \qquad (7.5)$$

q_t (mmol/g) is the quantity of adsorbed Ni(II) and Cr(VI) at a duration of t (min), and q_e(mmol/g) is the quantity of adsorbates at equilibrium. The k_1 (min^{-1}) and k_2 ($gmmol^{-1}min^{-1}$) are the rate constants of the Pfo and Pso models, respectively [266]. The adsorption process

Pso kinetic model, with R-values of 0.84 and 0.88 for Ni (II) and Cr (VI), reveals that the process involves chemisorption (Table-7.3).

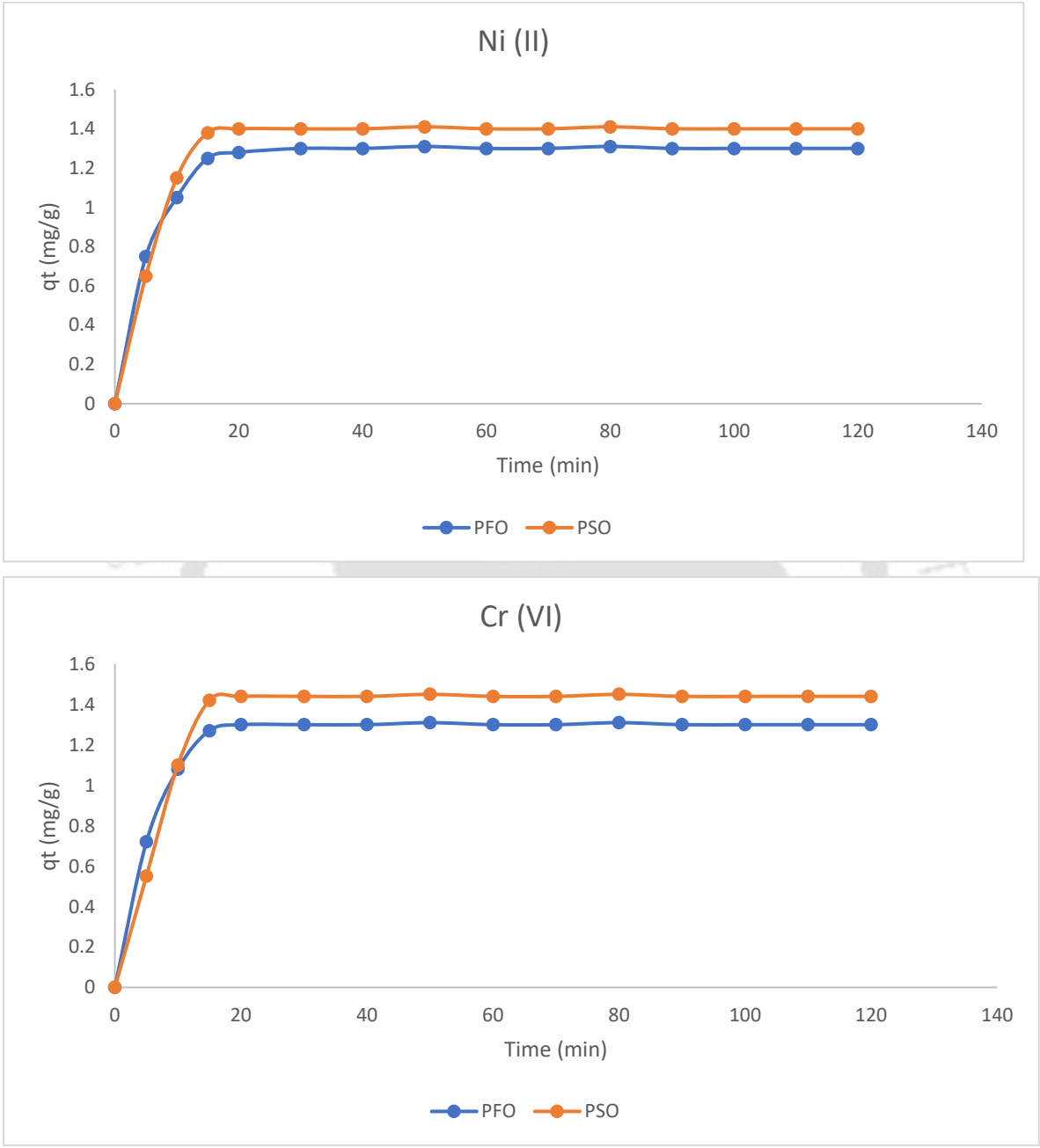

Fig. 7.8 The contact time effect on the adsorption of Ni (II) and Cr (VI) on RNC-BENT.

Table 7.3 Kinetic study of Ni (II) and Cr (VI) adsorption on RNC-BENT, respectively

	Pfo				Pso		
Adsorbate	q_e (mmolg^{-1})	q_t (mmolg^{-1})	k_1 (min^{-1})	R^2	q_t (mmolg^{-1})	k_2 (g/mg*min)	R^2
Ni (II)	1.253	0.944	2.639	0.478	1.270	1.421	0.84
Cr (VI)	1.229	1.252	1.571	0.707	1.262	1.573	0.88

7.4.2.4 Effect of adsorbent dosage

0.02g, 0.05g and 0.1g adsorbent (RNC-BENT) amounts were taken respectively in 25 mL sample solution for the two metal ions with 2 hours of shaking at room temperature at neutral pH (Fig 7.9). The adsorption capacity of Cr (VI) and Ni (II) was observed to increase with an increase in the amount of adsorbent.

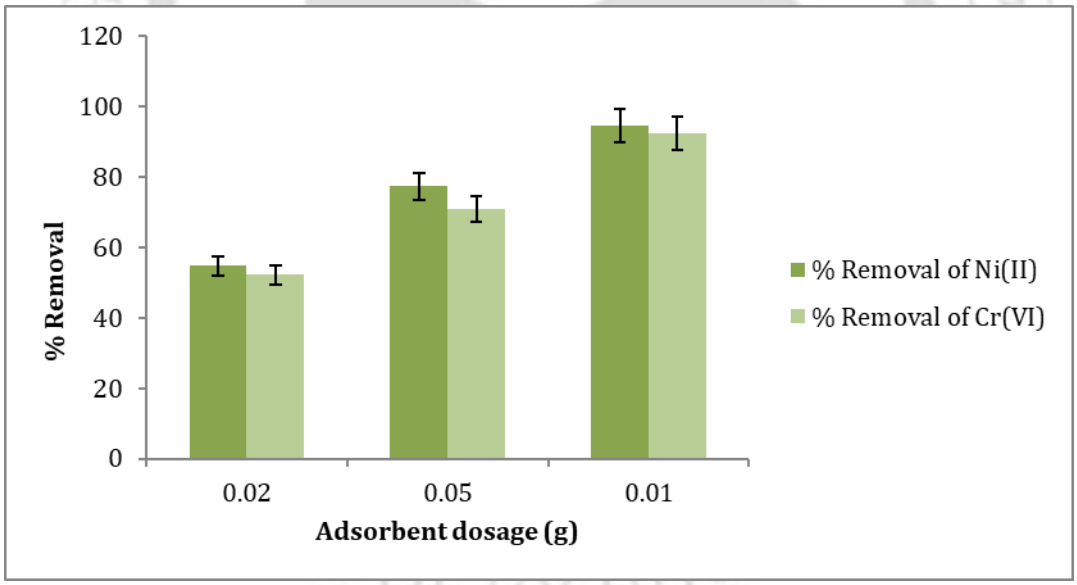

Fig. 7.9 Removal percentage of Ni (II) and Cr (VI) at different adsorbent dosage

It was found that with a very small amount of 0.02g adsorbent, the removal percentage reached over 50%. For both Cr (VI) and Ni (II), the removal percentage exceeded 90% when 0.1g of adsorbent was used compared to other amounts. Therefore, it implies that the prepared adsorbent is required in a minimal amount to carry out the adsorption process, making the adsorbent more sustainable and economical. A Comparative analysis of present study with similar other adsorbents and their adsorption capacity is represented in Table-7.4.

Table 7.4 Comparison of RNC-BENT with several other adsorbents

Adsorbent	Target Metal Ion(s)	Maximum Adsorption Capacity (mg/g)	Reference
RNC-BENT	Ni(II), Cr(VI)	Ni(II):77.25%, Cr(VI): 70.8%	Present Study
Chemically modified rice husk	Pb(II), Cd(II), Zn(II)	Pb: 99.8%, Cd: 95%, Zn: 97% removal	[267]
Rice husk-derived adsorbents (charcoal, silica, etc.)	Pb(II), Cr(VI), Ni(II)	Enhanced adsorption after HCl activation; specific capacities not specified	[268]
Rice husk activated carbon (RHAC) and PVP composite	Heavy metals (unspecified)	Significant removal; exact capacities not specified	[269]
RHA–aluminium oxide composite	U(VI)	85 mg/g	[270]
MgO–rice husk biochar composite	Cd(II)	Enhanced adsorption; specific capacity not specified	[271]
Acid modified rice husk charcoal (AMRHC)	Methyl Orange (MO) dye	11.53 mg/g	[272]
Xanthate-modified rice husk	Cd(II)	138.85 mg/g	[273]
Rice husk-based nanocellulose (CNFs)	Pb(II), La(III)	Pb: 193.2 mg/g, La: 100.7 mg/g	[274]
Iron-oxide/rice husk composite	Pb(II), Cu(II)	Higher than pristine carbonized RH; specific capacities not specified	[275]
RHA-based zeolite Faujasite	Cr(VI), Pb(II)	Cr(VI): 95% removal, Pb(II): 99% removal	[276]

7.5 ADSORPTION ISOTHERMS

The Langmuir and Freundlich and adsorption isotherms are the most prevalent models used for adsorption studies [264]. The Langmuir isotherm model assumes that intermolecular interactions rapidly diminish with distance from the sorption surface and that adsorption occurs at specific adsorption sites that are uniformly distributed inside the biosorbent. The reversible adsorption process is described by the Freundlich isotherm, which can be applied to multilayer adsorption by a heterogeneous surface affinity. This isotherm illustrates surface heterogeneity and the adsorption energy and active site distribution exponentially [277].

Mathematically, Langmuir can be expressed in equation 7.6 [278],

$$q_e = \frac{q_{max} K_L C_e}{1 + K_L C_e} \tag{7.6}$$

The equilibrium adsorption capacity is represented by q_e, and the maximum amount of the ions adsorbed per unit weight of the adsorbent is represented by q_{max}. Both q_e and q_{max} have the units as $mmolg^{-1}$. K_L (L/mmol) is the binding site affinity.

A dimensionless equilibrium parameter may be used to evaluate the fundamental property of the Langmuir isotherm in nature given in equation 7.7 [278].

$$R_L = \frac{1}{1 + K_L C_o} \tag{7.7}$$

R_L is dimensionless; Co ($mmolL^{-1}$) is the initial adsorbate solution concentration, if $R_L>1$, the adsorption process is unfavourable. If $R_L<1$, the adsorption process is favourable. If $0<R_L<1$, the adsorption process is unfavourable. If R_L is 1, the adsorption is represented as linear, and if it is 0, the adsorption process is considered irreversible.

The Freundlich model can be represented as in equation 7.8 [278]

$$q_e = K_f C_e^{1/n_f} \tag{7.8}$$

q_e denotes the amount of solute adsorbed; K_f denotes the relative indicator of adsorption capacity; $1/n_f$ denotes the intensity of the reaction; $n_f > 1$ indicates that the adsorption conditions are favourable.

A substantial R^2 value (Table-7.5) further supported the adsorption for both ions, and the Freundlich isotherm represented a better fit for the experimental data than the Langmuir (Fig. 7.10a and 10b). The complex structure of the adsorbent surface and the dissimilarity of the active sites are shown by the very low correlation coefficients of the Langmuir model. Therefore, it is reasonable to suppose that a heterogeneous surface was the site of the adsorption process. These findings are also consistent with characterization investigations that showed several functional groups on the RNC-BENT surface that may serve as adsorption sites for the ions under investigation.

Table 7.5 Isotherm parameters of Ni (II) and Cr (VI) adsorption on RNC-BENT, respectively

	Langmuir				Freundlich		
Adsorbate	$q_{m,exp}$ (mmolg^{-1})	q_m(mmolg^{-1})	K_L	R^2	n_f	K	R^2
Ni (II)	22.46	25.65	2.43	0.91	2.24	22.47	0.99
Cr (VI)	19.71	20.74	1.94	0.90	2.02	24.12	0.97

An ideal adsorption condition is indicated when the Freundlich constant (nf) exceeds 1. For Ni (II) and Cr (VI), The highest adsorption capacity (qm,exp) can be as high as 22.46 mmolg^{-1} and 19.71 mmolg^{-1}, respectively. The discharge of substantial amounts of heavy metals into aquatic systems poses serious environmental and health risks, while also driving up the costs associated with wastewater treatment[279].

The RNC-BENT composite demonstrated exceptionally high maximum adsorption capacities of 22.46 mmol/g for Ni(II) and 19.71 mmol/g for Cr(VI), significantly exceeding the concentrations typically

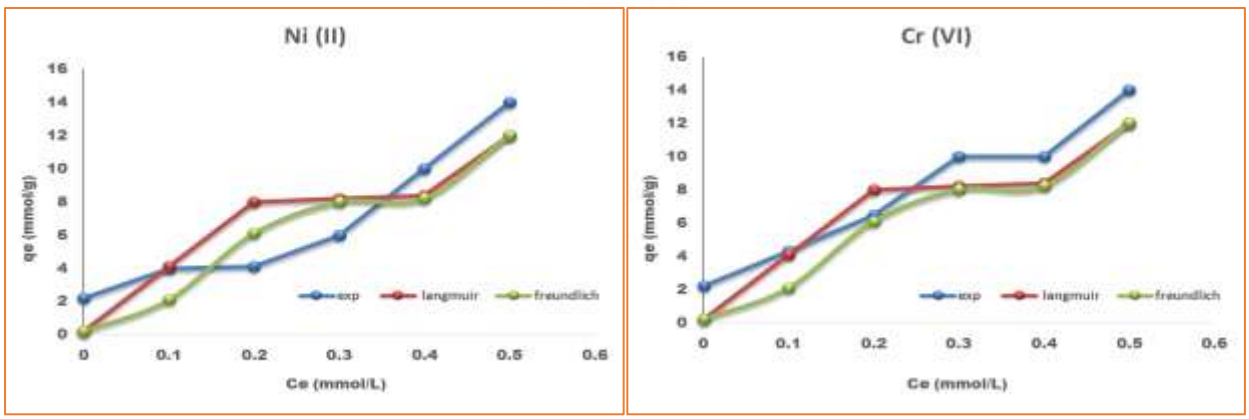

Fig. 7.10 Adsorption isotherm of Ni (II) and Cr (VI) respectively

found in contaminated water sources. These capacities are particularly noteworthy when compared to the WHO permissible limits for Ni(II) (0.07 mg/L) and Cr(VI) (0.05 mg/L) in drinking water, indicating that the composite has a strong potential for effectively reducing heavy metal concentrations to safe levels [280].

7.6 REMOVAL MECHANISM

There are several potential pathways via which RNC-BENT might adsorb metal ions. Adsorbent properties (such as concentration, ionic size, ionic charge, and molecular structure), binding site characteristics (such as structure, functional groups and surface properties), and solution chemistry (such as pH and ionic strength) can all have an impact on the absorption process. One possible elimination mechanism for Ni (II) is ion exchange between the bivalent ion and calcium. Montmorillonite, which is hydrated sodium calcium aluminium magnesium silicate hydroxide, is the primary component of bentonite clay. The bentonite clay making a composite with the nanocellulose could use metal ions in the ion exchange of Ni (II) for Ca (II) and Mg (II) ions more effectively.

7.7 REGENERATION STUDIES

An essential feature of an adsorbent from an economic and environmental perspective is its renewability. In addition, efficient eluents are needed for the quantitative recovery of heavy metal ions. After the first reaction, filtration was used to separate the adsorbent. 0.1 M HNO_3 was used in the Soxhlet method to extract the solid mass. The recovered solid was dried using a vacuum desiccator overnight and used as an adsorbent for further adsorption of the metal ions. Four catalytic runs were successfully finished with the same adsorbent (0.01g) without any noticeable performance decrease (Fig 7.11). After four cycles, the adsorption capacity of RNC-BENT decreased from 94.53% to 86.21% for Cr (VI) and from 92.32% to 84.54% for Ni(II), respectively.

A gradual decline in adsorption capacity was observed after four regeneration cycles. This reduction may be attributed to structural degradation of the RNC-BENT composite, partial loss or deformation of active sites, and potential fouling due to the accumulation of residual metal ions on the adsorbent surface. Additionally, repeated chemical treatments during desorption might have contributed to weakening the adsorption efficiency. These findings align with

previous studies, where repeated adsorption–desorption cycles led to reduced performance due to surface fouling and active site blockage [281].

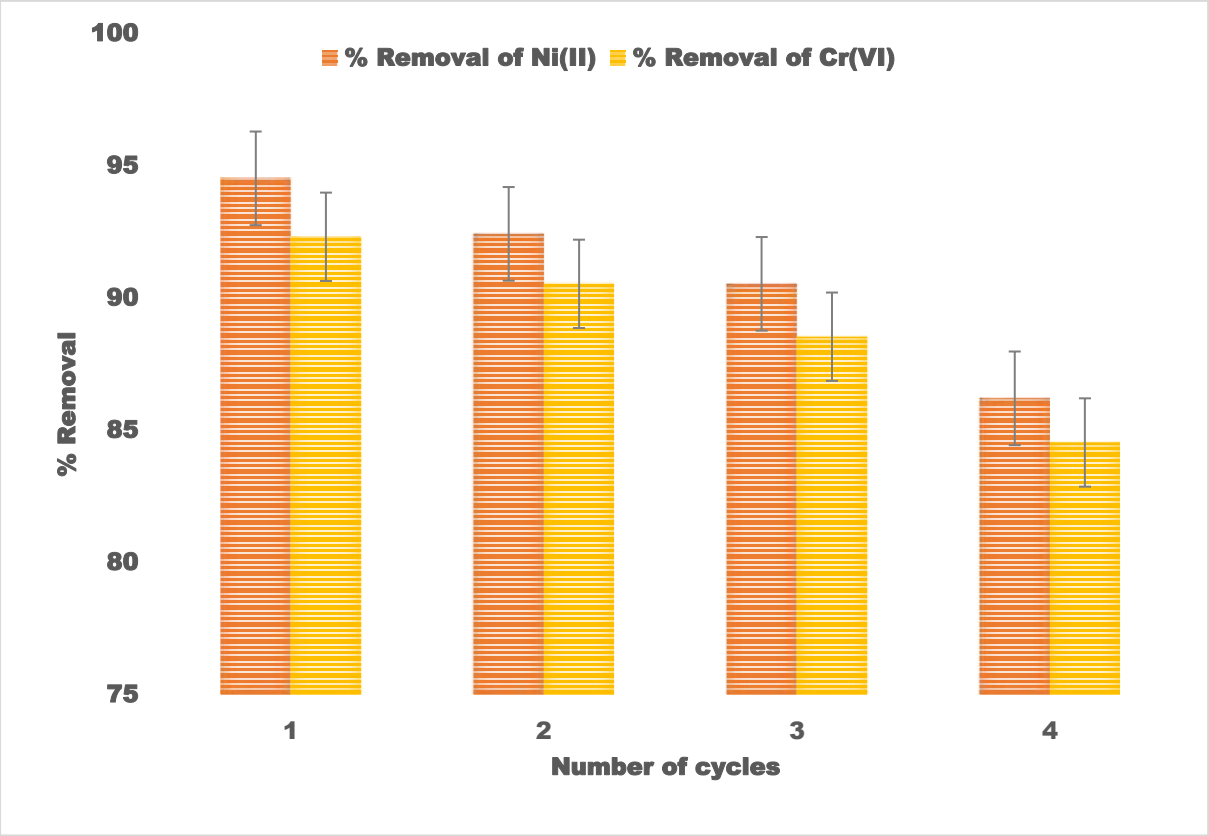

Fig 7.11. Regeneration studies using RNC-BENT

Further optimization of the regeneration protocol is necessary to improve the long-term stability and reusability of the composite material [282].

7.8 CONCLUSION

RNC-BENT was used as an adsorbent in this study to study the adsorption of Ni(II) and Cr(VI) from an aqueous solution. While the synthesis process shows promising potential for scale-up, certain challenges, such as maintaining uniform RNC dispersion, ensuring consistent nanocellulose–bentonite interaction, and managing energy-intensive steps like ultrasonication and drying, may arise. However, process optimization and appropriate engineering interventions can effectively address these drawbacks, enabling the composite's viable transition to large-scale production. The synthesized adsorbent proved highly efficient, with maximal adsorption capacities of 22.46 mmol/g for Ni(II) and 19.71 mmol/g for Cr(VI). The pH of the solution was found to affect the adsorption, and an alkaline pH was shown to be

optimal. The experimental adsorption isotherm data fit well with the Freundlich isotherm model for the examined ions in the isotherm investigations. The adsorption/desorption cycle results showed that the adsorbent was regenerable for up to four cycles. Using Bao Dhan rice husk, an agricultural byproduct, and naturally abundant bentonite clay reduces environmental waste and adds value to underutilized resources through their transformation into functional adsorbents. This approach minimizes the dependency on synthetic materials and supports eco-friendly remediation strategies. Moreover, the synthesis and application of the RNC-BENT composite underscore the potential of green materials to replace conventional adsorbents in wastewater treatment, ultimately leading to resource conservation and reduced ecological footprint.

Chapter 8

CONCLUSIONS

8.1 CHAPTERWISE SYNOPTIC CONCLUSIONS FROM THE PRESENT WORK

The present research comprehensively investigated the interlinked issues of sediment quality, water quality, pollutant transport, and remediation potential in the Brahmaputra River system with a focus on navigation feasibility, environmental safety, and human health protection. The study uniquely integrates field-scale sediment and water quality assessment, experimental dispersion analysis, and sustainable remediation strategies to support informed river management. The assessment of mid-sand bars revealed that rapid urbanization and unregulated anthropogenic discharges have imposed significant stress on sediment quality, particularly in the river stretch influenced by Guwahati city. The speciation analysis of heavy metals (Cu, Zn, Fe, Mn, Ni, Pb, Co, Cd, and Cr) in vertically profiled sediment cores demonstrated enrichment in the order Fe > Mn > Zn > Ni > Cr > Cu, while Co, Cd, and Pb remained below detection limits. Notably, the mean concentration of Ni in all sediment layers exceeded both the toxic reference value and USEPA standards, indicating localized contamination hotspots. Enrichment factor analysis showed moderate enrichment of Cu and Ni and severe enrichment of Mn and Ni, with Zn exhibiting extremely high enrichment in the surface and subsurface layers of Reach-2. In contrast, Reach-1 largely exhibited low enrichment and negligible contamination, highlighting strong spatial variability governed by anthropogenic influence. Multivariate statistical analyses (CM, CA, and PCA) consistently indicated a common origin of heavy metals, predominantly linked to industrial effluents, municipal discharges, and urban runoff. Based on integrated sediment quality indices, the study concludes that dredging of mid-sand bars is environmentally feasible in Reach-1 and in carefully selected locations within Reach-2, provided that strict monitoring and mitigation measures are implemented. Strategically planned dredging can contribute to improved navigability, channel deepening, and flood mitigation, particularly in the Guwahati stretch, which experiences recurrent monsoonal flooding due to its narrow channel geometry. The investigation further demonstrated that water quality exhibited a strong temporal dependence on anthropogenic activity. During the COVID-19 lockdown, heavy metal concentrations and microbiological indicators were largely within permissible limits, reflecting reduced industrial, agricultural, and commercial operations. Post-lockdown conditions, however, showed a sharp

deterioration in water quality, with Cd, Ni, Cr, and Pb exceeding acceptable limits. Heavy metal pollution indices (HPI and MI) confirmed a transition from clean to seriously affected water quality after the lockdown. Health risk assessment revealed minimal non-carcinogenic risk during lockdown conditions, whereas post-lockdown analysis indicated elevated risk levels, particularly for children and teenagers. These findings clearly demonstrate the dominant role of human activity in governing river water quality and associated health risks. To understand pollutant transport and downstream impact, the study experimentally quantified the longitudinal dispersion coefficient of river water using a tracer-based approach. The observed near-Gaussian tracer response confirmed longitudinal dispersion as the dominant mixing mechanism, with an experimentally determined dispersion coefficient of 0.081 m^2/s. This value closely matched established theoretical models, validating the reliability of tracer techniques for simulating solute transport. The findings emphasize the importance of dispersion coefficient estimation for identifying pollutant travel distances and mapping contamination spread along river reaches. Recognizing the persistence of heavy metal pollution, the study also explored an eco-friendly remediation strategy using a rice-husk-derived nanocellulose–bentonite (RNC-BENT) bio composite. The synthesized adsorbent exhibited high adsorption capacities for Ni(II) and Cr(VI), optimal performance under alkaline conditions, good conformity with the Freundlich isotherm model, and effective regeneration over multiple cycles. The utilization of agricultural waste and naturally abundant clay highlights the potential of sustainable, low-cost alternatives to conventional treatment methods.

Overall, the study establishes a holistic framework linking sediment contamination, water quality degradation, pollutant transport dynamics, and green remediation solutions. The findings underscore the need for stringent regulatory enforcement, improved public awareness, and integrated river basin management to safeguard the Brahmaputra River. This work provides a scientifically robust foundation for sustainable navigation development, pollution control, and long-term environmental resilience of large river systems.

The major outcomes of this research work are encapsulated below:

1. The assessment of mid-channel sandbar sediments for heavy metal contamination indicates that the degree of contamination varies significantly along the Brahmaputra River. The upstream portions of the river appear to have low levels of contamination, while the downstream sections, affected by urbanisation and industry, have moderate to high levels of contamination for some metals. By applying multiple sediment quality indices, it

appears that dredging for navigational purposes could be environmentally hasty at many rivers reaches, although certain areas of concern should be managed carefully or remediated. This demonstrates that sediment quality assessment should be part of dredging and navigational planning efforts. The essential takeaways are:

• The heavy metals Cu, Zn, Ni, Cr, Mn, and Fe were found in all 42 sampling stations, which means that a long approx. 600 km stretch of the river is contaminated with these toxic agents.

• The FESEM, XRD, and particle-size analyses showed that the sand-bar sediments are mostly made up of fine sand and silty materials, and the angular morphology of the particles suggests short-distance fluvial transport and recent geological weathering.

• Ni and Zn were regularly detected at several locations, particularly in downstream industrial areas, at concentrations exceeding Toxicity Reference Values (TRVs), thus indicating the strong anthropogenic impact.

• The vertical profiles showed that the middle layers (50cm) often had higher levels of Mn and Fe, pointing to accumulation from the past in the subsurface layers.

• The geochemical indices (Igeo, EF, CF, PERI, PLI) revealed that contamination local hotspots notwithstanding, most of the sand-bar sediments are classified as low to moderately contaminated.

• Multivariate statistical analysis suggested that Cu, Ni, Zn, and Fe have common anthropogenic sources, while Mn and Cr had mixed geogenic and human-derived sources.

This research represents the first spatial–vertical systematic survey of heavy metals in sand bars of the Brahmaputra, thus it is an indispensable tool for environmental monitoring and dredging feasibility assessment.

2. The COVID-19 lockdowns gave a one-of-a-kind chance to see how the Brahmaputra River reacts to lesser human pressures. Findings revealed a significant enhancement of water quality during lockdown as evidenced by the reduction in levels of heavy metals and microbial contaminants. Furthermore, the post lockdown condition of the river showed a very fast return of pollution levels which highlighted the major impact of human activities on the water quality of the river. Quantitative health risk assessment based on the level of contamination in the river water during and after the lockdown period indicated minimal

risk during the lockdown and an increased risk, with children and teenagers being the most vulnerable, in the post, lockdown phase. A comparative study of heavy-metal concentrations and microbiological indicators in river water during and after the COVID-19 lockdown has led to the following conclusions:

• The improvement in water quality was very clear during the lockdown period when the industrial, commercial, and transportation activities were largely shut down.

• The Pb, Cr, Ni, Cd, and bacterial contamination post-lockdown sampling were so substantial that they pointed to the immediate impact of anthropogenic activities.

• Fecal coliform and total coliform levels were found to be above the allowed limits at some locations downstream after the lockdown, which is indicative of the entry of sewage and bad waste-management practices.

• The hazard quotient (HQ) and hazard index (HI) showed that children are the most vulnerable group, especially to Pb and Cr contamination.

• Lifetime cancer risk (LCR) values for Ni and Cr were higher than USEPA thresholds at several sites after lockdown.

The study cites that human activities have an instant and direct effect on the water quality of the Brahmaputra River and thus, the need for strict effluent monitoring is imperative.

3. A comprehensive source-apportionment framework was put together to figure out the industrial sources of heavy-metal contamination in the environment. Some of the major points uncovered by the study are:

• Data on industries from CPCB highlighted that along the basin, petroleum refineries, cement factories, pharmaceuticals, metal-processing units, and hazardous waste recyclers have been the leading contributors of toxic metals.

• The use of TRV for the screening exposed that Zn, Ni, and Cu are metals that cause higher ecological risks than other metals.

• The statistical techniques (correlation, PCA, CA) helped in segregating the metals into separate groups indicating:

Human sources → Zn, Ni, Fe

Mixed sources → Cu, Mn

Natural sources → Cr (in the certain upstream areas)

• The GIS-based mapping has revealed that Guwahati, Nagaon, Tezpur, and Bongaigaon industrial corridors are the regions where pollution is extremely high.

The source-mapping framework is a decision support tool for environmental regulators and policymakers.

4. Tracer studies have been carried out on the physical hydraulics models to provide an accurate estimate of the longitudinal dispersivity of braided rivers. The studies showed an exceptionally high degree of spatial variability in the dispersive characteristics; this variability was influenced by channel morphology, flow regime and hydraulic conditions. The comparison of the findings with the available empirical models, indicated that the classical empirical equations are inadequate for braided river systems. The development of the new empirical relationships has provided improved predictive capability for modelling water quality within large alluvial rivers. A large-scale physical model was employed to judge the river dispersion behaviour. The findings are:

• The Longitudinal dispersion coefficient (DL) values were getting higher with increased discharge, larger channel cross-sections and higher width-to-depth ratios.

• Flow splitting around sand bars induced secondary circulation zones, thus, significantly increasing pollutant mixing.

• Existing classical models (e.g. Fischer) demonstrated only partial agreement, and the differences pointed to the unique hydrodynamics of the braided river system.

• A set of new empirical relationships was formulated to calculate dispersion coefficients just for the Brahmaputra River.

Such outcomes represent the essential parameters for pollution prediction, spill handling, and environmental-flow modelling.

5. The research team successfully fabricated a nanocellulose bentonite composite from agricultural waste and tested it for heavy metal removal from water. The composite possessed excellent adsorption capacity, fast kinetics, and maintained its functionality after several reuse cycles. Utilizing rice husk waste as the raw material offers a promising way to combine waste valorisation with environmental remediation. The results indicate that the developed composite can serve as a green and economically viable solution for treating water polluted with heavy metals. A new hybrid adsorbent was made with nanocellulose from rice husk (Bao Dhan) and bentonite clay. The main points are:

• Various techniques like FTIR, XRD, SEM–EDAX, and BET were used to analyze the material and all the analyses confirmed the successful formation of a porous, high-surface-area composite (671.81 m^2/g).

• The composite turned out to be very good in adsorption: 22.46 mmol/g for Ni(II), 19.71 mmol/g for Cr(VI)

• Adsorption obeyed the Freundlich isotherm and pseudo-second-order kinetics, which suggests that multilayer chemisorption took place.

• The regeneration experiments demonstrated that the composite was able to maintain most of its adsorption performance over several cycles, thus, it is economically feasible.

This hybrid material constitutes an ecologically safe, inexpensive, and area-specific method of heavy metal removal in Assam.

8.2 CONTRIBUTIONS OF THE THESIS

The present doctoral research makes original and significant contributions toward understanding sediment quality, water contamination, pollutant transport, and sustainable remediation strategies in large alluvial river systems, with specific emphasis on the Brahmaputra River. The major contributions of the thesis are summarized as follows:

1. The Present work employed the characterization of heavy metal distribution in riverine sediments. Vertical profiling of mid-sand bar sediments (surface, 50 cm, and 100 cm depths) was performed for multiple heavy metals, providing new insights into sediment stratification, historical contamination trends, and pollutant accumulation behaviour in braided river environments, which are largely unexplored in Indian river systems.

2. A systematic study established the spatial variability of sediment contamination across river reaches and identified zones suitable and unsuitable for dredging operations based on enrichment factor, contamination indices, and ecological risk assessment.

3. Multivariate statistical techniques, including Pearson's correlation analysis, cluster analysis, and principal component analysis, were employed to distinguish natural and anthropogenic sources of heavy metals. The study established strong links between industrial effluents, urban runoff, and localized contamination hotspots along the Brahmaputra River.

4. The research critically examined the potential environmental risks associated with dredging contaminated sediments, including resuspension of toxic metals. Practical mitigation and sediment management strategies were proposed to support sustainable navigation development while minimizing ecological impacts.

5. The study quantified changes in heavy metal concentrations and microbiological indicators in Brahmaputra River water during and post COVID-19 lockdown periods. The findings demonstrated a clear improvement in water quality during lockdown and deterioration afterward, highlighting the impact of anthropogenic activities on river health.

6. A detailed non-carcinogenic health risk assessment was performed for adults, teenagers, and children using chronic daily intake, hazard quotient, and hazard index approaches. The results identified vulnerable population groups and provided a scientific basis for public health risk management related to river water usage.

7. Tracer experiments using a physical hydraulic model of the Brahmaputra River were conducted to estimate longitudinal dispersion coefficients. New empirical relationships were developed using dimensional analysis and regression techniques, accounting for braided river morphology, discharge, depth, and flow velocity.

8. The newly proposed dispersion equations demonstrated improved prediction accuracy compared to existing models, contributing to better understanding of solute transport, pollution spreading mechanisms, and hydrodynamic behaviour in large alluvial braided river systems.

9. A sustainable nanocellulose–bentonite composite was synthesized from agricultural waste (Bao dhan rice husk) and natural clay. The material was successfully characterized and demonstrated high adsorption efficiency for Ni(II) and Cr(VI), offering an eco-friendly solution for water treatment applications.

10. The thesis uniquely integrates field investigations, laboratory experiments, physical modelling, statistical analysis, and material development to provide a holistic framework for river water quality management, pollutant transport assessment, and sustainable remediation strategies. The outcomes of this research provide scientifically validated inputs for policymakers, river

basin managers, and navigation authorities to support environmentally responsible dredging, pollution control, and water resource management in the Brahmaputra River basin and similar large river systems.

8.3 FUTURE SCOPE OF WORK

This work lays a foundation for future studies in different areas:

1. Expansion of Field Studies

- ✓ Extend sampling to cover monsoon and pre-monsoon seasons to be able to understand seasonal fluctuations in metal mobility.
- ✓ Initiate repeated seasonal sampling over several years to comprehend long-term contamination trends.

2. Engineering-Scale Applications of the Composite Adsorbent

- ✓ Design pilot-scale adsorption units (fixed-bed or fluidized-bed reactors) employing RNC–BENT.
- ✓ Real industrial wastewater can be used to test the composite performance under variable conditions.

3. Alternative Sustainable Adsorbents

- ✓ Develop nanocomposites using local biomass materials like water hyacinth, bamboo particles, banana fibers, etc.
- ✓ Test hybrid materials comprising biochar, zeolites, and layered double hydroxides.

4. Community-Level Implementation

- ✓ Production of adsorbent composites made from local materials for rural water purification can be encouraged.
- ✓ Local communities and industries can be trained on the implementation of low-cost remediation technologies by organizing workshops and seminars.

Bibliography

[1] Allan, J.D. & Castillo, M.M. (2007). Stream Ecology: Structure and Function of Running Waters. Dordrecht: Springer.

[2] Goswami, D.C. (1985). Brahmaputra River system. Geomorphology, 1, pp.13–28.

[3] Milliman, J.D. & Meade, R.H. (1983). World-wide delivery of river sediment to the oceans. Journal of Geology, 91, pp.1–21.

[4] Baruah, D.C., Sarma, J.N. & Phukan, M.K. (2012). Socio-economic significance of the Brahmaputra River. Water Policy, 14, pp.1024–1040.

[5] Das, S. & Sarma, J.N. (2015). Urbanisation and river pollution in Guwahati. Environmental Earth Sciences, 74, pp.7019–7033.

[6] Bhuyan, M.S., Bakar, M.A. & Sharif, A.S.M. (2019). Assessment of river pollution. Environmental Monitoring and Assessment, 191, pp.1–14.

[7] Förstner, U. & Wittmann, G.T.W. (1983). Metal Pollution in the Aquatic Environment. Berlin: Springer.

[8] Nriagu, J.O. & Pacyna, J.M. (1988). Quantitative assessment of global metal pollution. Nature, 333, pp.134–139.

[9] Salomons, W. & Förstner, U. (1984). Metals in the Hydrocycle. Berlin: Springer.

[10] Calmano, W., Hong, J. & Förstner, U. (1993). Mobilization of heavy metals in contaminated sediments. Marine Chemistry, 43, pp.175–186.

[11] Jaishankar, M., Tseten, T., Anbalagan, N., Mathew, B.B. & Beeregowda, K.N. (2014). Toxicity of heavy metals. Interdisciplinary Toxicology, 7(2), pp.60–72.

[12] Chapman, D. et al. (2016). Water quality management. Water Research, 93, pp.182–192.

[13] Sarma, J.N. (2005). Fluvial processes and morphology of the Brahmaputra River. Geomorphology, 70, pp.226–256.

[14] Fischer, H.B., List, E.J., Koh, R.C.Y., Imberger, J. & Brooks, N.H. (1979). Mixing in Inland and Coastal Waters. New York: Academic Press.

[15] Mohanty, A.K., Vivekanandhan, S., Pin, J.M. & Misra, M. (2018). Sustainable composites for environmental applications. Science, 362, pp.536–542.

[16] Chapman, D., Bradley, C., Gettel, G.M. et al. (2016). Developments in water quality monitoring and management. Water Research, 93, pp.182–192.

[17] Müller, G. (1981). The heavy metal pollution of sediments. Geojournal, 5, pp.247–255.

[18] Burton, G.A. (2002). Sediment quality criteria in use around the world. Limnology, 3, pp.65–75.

[19] Singh, M., Müller, G. & Singh, I.B. (2005). Source identification of heavy metals in sediments. Environmental Geology, 48, pp.60–68.

[20] Dutta, V., Dubey, D. & Kumar, S. (2020). Impact of COVID-19 lockdown on river water quality. Journal of Environmental Management, 276, 111347.

[21] Kumar, P., Hama, S., Omidvarborna, H. et al. (2021). Temporary reduction in pollution during COVID-19 lockdown. Environmental Research, 197, 111016.

[22] Jaishankar, M., Tseten, T., Anbalagan, N. et al. (2014). Toxicity and health impacts of heavy metals. Interdisciplinary Toxicology, 7(2), pp.60–72.

[23] Fischer, H.B., List, E.J., Koh, R.C.Y., Imberger, J. & Brooks, N.H. (1979). Mixing in Inland and Coastal Waters. New York: Academic Press.

[24] Rutherford, J.C. (1994). River Mixing. Chichester: Wiley.

[25] Wang, J. & Chen, C. (2009). Biosorbents for heavy metals removal. Biotechnology Advances, 27, pp.195–226.

[26] Mohanty, A.K., Vivekanandhan, S., Pin, J.M. & Misra, M. (2018). Sustainable materials for environmental remediation. Science, 362, pp.536–542.

[27] Knighton, D. (1998). Fluvial Forms and Processes: A New Perspective. London: Arnold.

[28] Bridge, J.S. (2003). Rivers and Floodplains: Forms, Processes, and Sedimentary Record. Oxford: Blackwell Publishing.

[29] Walling, D.E. (2006). Human impact on land–ocean sediment transfer. Geomorphology, 79, pp.192–216.

[30] Salomons, W. & Förstner, U. (1984). Metals in the Hydrocycle. Berlin: Springer.

[31] Julien, P.Y. (2010). Erosion and Sedimentation. 2nd ed. Cambridge: Cambridge University Press.

[32] Leopold, L.B., Wolman, M.G. & Miller, J.P. (1964). Fluvial Processes in Geomorphology. San Francisco: Freeman.

[33] Goswami, D.C. (1985). Brahmaputra River system. Geomorphology, 1, pp.13–28.

[34] Förstner, U. & Salomons, W. (2010). Sediment research and management of river basins. Journal of Soils and Sediments, 10, pp.1440–1452.

[35] Chapman, D. (1996). Water Quality Assessments: A Guide to the Use of Biota, Sediments and Water in Environmental Monitoring. 2nd ed. London: Chapman & Hall.

[36] WHO (2017). Guidelines on Sanitation and Health. World Health Organization, Geneva.

[37] Alloway, B.J. (2013). Heavy Metals in Soils. 3rd ed. Dordrecht: Springer.

[38] Förstner, U. & Wittmann, G.T.W. (1983). Metal Pollution in the Aquatic Environment. Berlin: Springer.

[39] Nriagu, J.O. & Pacyna, J.M. (1988). Quantitative assessment of worldwide contamination of air, water and soils by trace metals. Nature, 333, pp.134–139.

[40] Salomons, W. & Förstner, U. (1984). Metals in the Hydrocycle. Berlin: Springer.

[41] Alloway, B.J. (2013). Heavy Metals in Soils. Springer, Dordrecht.

[42] Nriagu, J.O. & Pacyna, J.M. (1988). Quantitative assessment of global metal pollution. Nature, 333, pp.134–139.

[43] Salomons, W. & Förstner, U. (1984). Metals in the Hydrocycle. Springer, Berlin.

[44] Tchounwou, P.B., Yedjou, C.G., Patlolla, A.K. & Sutton, D.J. (2012). Heavy metal toxicity. EXS, 101, pp.133–164.

[45] WHO (2001). Zinc in Drinking-water. World Health Organization, Geneva.

[46] Sutherland, R.A. (2000). Bed sediment-associated heavy metals. Environmental Geology, 39, pp.611–627.

[47] Förstner, U. & Wittmann, G.T.W. (1983). Metal Pollution in the Aquatic Environment. Springer, Berlin.

[48] ATSDR (2005). Toxicological Profile for Zinc. U.S. DHHS.

[49] Drever, J.I. (1997). The Geochemistry of Natural Waters. Prentice Hall.

[50] Singh, M., Müller, G. & Singh, I.B. (2005). Heavy metals in sediments. Environmental Geology, 48, pp.60–68.

[51] WHO (2004). Iron in Drinking-water. World Health Organization.

[52] Eggleton, J. & Thomas, K.V. (2004). Bioavailability of metals. Environment International, 30, pp.973–983.

[53] Kabata-Pendias, A. (2011). Trace Elements in Soils and Plants. CRC Press.

[54] Calmano, W., Hong, J. & Förstner, U. (1993). Metal mobilization in sediments. Marine Chemistry, 43, pp.175–186.

[55] ATSDR (2012). Toxicological Profile for Manganese. U.S. DHHS.

[56] Förstner, U. (1995). Land contamination by metals. Science of the Total Environment, 165, pp.113–123.

[57] UNEP (2010). Nickel and the Environment. United Nations Environment Programme.

[58] Alloway, B.J. & Ayres, D.C. (1997). Chemical Principles of Environmental Pollution. Blackie Academic.

[59] IARC (2012). Nickel and Nickel Compounds. International Agency for Research on Cancer.

[60] Eisler, R. (1998). Nickel Hazards to Fish. U.S. Geological Survey.

[61] Kabata-Pendias, A. & Pendias, H. (2001). Trace Elements in Soils and Plants. CRC Press.

[62] Förstner, U. & Salomons, W. (2010). Sediment management. Journal of Soils and Sediments, 10, pp.1440–1452.

[63] ATSDR (2004). Toxicological Profile for Cobalt. U.S. DHHS.

[64] Costa, M. (2003). Toxicity and carcinogenicity of chromium. Critical Reviews in Toxicology, 33, pp.1–33.

[65] Vidu, R., Matei, E., Predescu, A.M., Alhalaili, B., Pantilimon, C., Tarcea, C. and Predescu, C., 2020. Removal of heavy metals from wastewaters: A challenge from current treatment methods to nanotechnology applications. Toxics, 8(4), p.101.

[66] Azimi, A., Azari, A., Rezakazemi, M. and Ansarpour, M., 2017. Removal of heavy metals from industrial wastewaters: a review. ChemBioEng Reviews, 4(1), pp.37-59.

[67] Patterson, J.W. and Minear, R., 2013. Physical-chemical methods of heavy metals removal. Heavy metals in the aquatic environment, pp.261-276.

[68] Khulbe, K.C. and Matsuura, T., 2018. Removal of heavy metals and pollutants by membrane adsorption techniques. Applied water science, 8(1), p.19.

[69] Manap, N. and Voulvoulis, N., 2015. Environmental management for dredging sediments–The requirement of developing nations. Journal of environmental management, 147, pp.338-348.

[70] Kurniawan, T.A., Chan, G.Y., Lo, W.H. and Babel, S., 2006. Physico–chemical treatment techniques for wastewater laden with heavy metals. Chemical engineering journal, 118(1-2), pp.83-98.

[71] Charerntanyarak, L., 1999. Heavy metals removal by chemical coagulation and precipitation. Water Science and Technology, 39(10-11), pp.135-138.

[72] Malik, L.A., Bashir, A., Qureashi, A. and Pandith, A.H., 2019. Detection and removal of heavy metal ions: a review. Environmental Chemistry Letters, 17(4), pp.1495-1521.

[73] Gunatilake, S.K., 2015. Methods of removing heavy metals from industrial wastewater. Methods, 1(1), p.14.

[74] Luptakova, A., Ubaldini, S., Macingova, E., Fornari, P. and Giuliano, V., 2012. Application of physical–chemical and biological–chemical methods for heavy metals removal from acid mine drainage. Process Biochemistry, 47(11), pp.1633-1639.

[75] Czikkely, M., Neubauer, E., Fekete, I., Ymeri, P. and Fogarassy, C., 2018. Review of heavy metal adsorption processes by several organic matters from wastewaters. Water, 10(10), p.1377.

[76] Iyer, S., Deshmukh, S.M. and Tapre, R.W., 2025. Review on removal of heavy metals from industrial effluents by adsorption. Reviews in Inorganic Chemistry, 45(3), pp.479-496.

[77] Ugwu, E.I., Othmani, A. and Nnaji, C.C., 2022. A review on zeolites as cost-effective adsorbents for removal of heavy metals from aqueous environment. International Journal of Environmental Science and Technology, 19(8), pp.8061-8084.

[78] Förstner, U., & Wittmann, G. T. W. (1981). Metal Pollution in the Aquatic Environment. Springer-Verlag, Berlin.

[79] Salomons, W., & Förstner, U. (1984). Metals in the Hydrocycle. Springer-Verlag, Berlin.

[80] Singh, M., Müller, G., & Singh, I. B. (2005). Heavy metals in freshly deposited sediments of the Ganga River: A case study from the middle Ganga plain. Environmental Geology, 48, 117–128.

[81] Zhang, J., Liu, C. L., & Xu, J. (2017). Source identification and ecological risk assessment of heavy metals in river sediments. Science of the Total Environment, 581–582, 160–169.

[82] Horowitz, A. J. (1991). A Primer on Sediment–Trace Element Chemistry (2nd ed.). U.S. Geological Survey, Water-Supply Paper 2277.

[83] Calmano, W., Hong, J., & Förstner, U. (1993). Binding and mobilization of heavy metals in contaminated sediments affected by pH and redox potential. Water Science and Technology, 28(8–9), 223–235.

[84] Muller, G. (1969). Index of geoaccumulation in sediments of the Rhine River. Geojournal, 2(3), 108–118.

[85] Varol, M., & Şen, B. (2012). Assessment of surface water and sediment contamination by trace metals in the upper Tigris River, Turkey. Catena, 92, 1–10.

[86] Bing, H., Wu, Y., Zhou, J., & Sun, H. (2016). Historical trends of heavy metal contamination in river sediments: A case study. Journal of Hydrology, 541, 973–985.

[87] Ayman, A., El-Sayed, S., & Abdel-Monem, M. (2019). Distribution and risk assessment of heavy metals in river sediments under different depositional environments. Environmental Earth Sciences, 78, 1–15.

[88] Sundaray, S. K., Nayak, B. B., Lin, S., & Bhatta, D. (2011). Geochemical speciation and risk assessment of heavy metals in river estuarine sediments. Environmental Earth Sciences, 62, 177–190.

[89] Islam, M. S., Ahmed, M. K., Raknuzzaman, M., Habibullah-Al-Mamun, M., & Islam, M. K. (2015). Heavy metal pollution in surface water and sediment: A preliminary assessment. Environmental Science and Pollution Research, 22, 764–775.

[90] Hakanson, L. (1980). An ecological risk index for aquatic pollution control: A sedimentological approach. Water Research, 14(8), 975–1001.

[91] Sutherland, R. A. (2000). Bed sediment-associated trace metals in an urban stream, Oahu, Hawaii. Environmental Geology, 39, 611–627.

[92] Reimann, C., Filzmoser, P., & Garrett, R. G. (2008). Statistical Data Analysis Explained: Applied Environmental Statistics with R. Wiley, Chichester.

[93] Varol, M. (2011). Assessment of heavy metal contamination in sediments of the Tigris River (Turkey) using pollution indices and multivariate statistical techniques. Journal of Hazardous Materials, 195, 355–364.

[94] Eggleton, J., & Thomas, K. V. (2004). A review of factors affecting the bioavailability of contaminants during sediment disturbance events. Environment International, 30, 973–980.

[95] Nikora, V., Habersack, H., Huber, T., & McEwan, I. (2010). Drag forces in gravel-bed rivers: The role of roughness, sediment transport, and channel morphology. Journal of Hydraulic Engineering, 136(8), 500–510.

[96] Förstner, U., & Wittmann, G. T. W. (1981). Metal Pollution in the Aquatic Environment. Springer-Verlag.

[97] Singh, M., Müller, G., & Singh, I. B. (2005). Heavy metals in river water and sediments. Environmental Geology, 48, 117–128.

[98] Varol, M. (2011). Temporal variation of heavy metals in river water. Journal of Hazardous Materials, 195, 355–364.

[99] Islam, M. S., Ahmed, M. K., Raknuzzaman, M., et al. (2015). Heavy metal pollution in surface water. Environmental Science and Pollution Research, 22, 764–775.

[100] Zhang, J., Liu, C. L., & Xu, J. (2017). Seasonal variability of heavy metals in rivers. Science of the Total Environment, 581–582, 160–169.

[101] Zambrano-Monserrate, M. A., Ruano, M. A., & Sanchez-Alcalde, L. (2020). Indirect effects of COVID-19 on the environment. Science of the Total Environment, 728, 138813.

[102] Yunus, A. P., Masago, Y., & Hijioka, Y. (2020). COVID-19 and surface water quality. Water, 12, 1640.

[103] USEPA (2011). Exposure Factors Handbook. United States Environmental Protection Agency.

[104] Fischer, H. B., List, E. J., Koh, R. C. Y., Imberger, J., & Brooks, N. H. (1979). Mixing in Inland and Coastal Waters. Academic Press.

[105] Seo, I. W., & Cheong, T. S. (1998). Predicting longitudinal dispersion coefficient in natural streams. Journal of Hydraulic Engineering, 124(1), 25–32.

[106] Kashefipour, S. M., & Falconer, R. A. (2002). Longitudinal dispersion coefficients in natural channels. Water Research, 36, 1596–1608.

[107] Rutherford, J. C. (1994). River Mixing. Wiley.

[108] Reimann, C., Filzmoser, P., & Garrett, R. G. (2008). Statistical Data Analysis Explained. Wiley.

[109] Varol, M. (2011). Assessment of heavy metal contamination using multivariate statistics. Journal of Hazardous Materials, 195, 355–364.

[110] Singh, M., Müller, G., & Singh, I. B. (2005). Heavy metals in river sediments. Environmental Geology, 48, 117–128.

[111] Varol, M., & Şen, B. (2012). Trace metal contamination in river sediments. Catena, 92, 1–10.

[112] Zhang, J., Liu, C. L., & Xu, J. (2017). Source identification of heavy metals in river systems. Science of the Total Environment, 581–582, 160–169.

[113] Central Pollution Control Board (CPCB) (2018). Industrial Categorization and Pollution Load Assessment in India. Government of India.

[114] Sundaray, S. K., Nayak, B. B., Lin, S., & Bhatta, D. (2011). Geochemical speciation and source identification of heavy metals. Environmental Earth Sciences, 62, 177–190.

[115] Nikora, V., Habersack, H., Huber, T., & McEwan, I. (2010). Hydrodynamics and sediment transport in rivers. Journal of Hydraulic Engineering, 136, 500–510.

[116] Fu, F., & Wang, Q. (2011). Removal of heavy metal ions from wastewater. Journal of Environmental Management, 92, 407–418.

[117] Barakat, M. A. (2011). New trends in removing heavy metals from industrial wastewater. Arabian Journal of Chemistry, 4, 361–377.

[118] Babel, S., & Kurniawan, T. A. (2003). Low-cost adsorbents for heavy metals uptake. Journal of Hazardous Materials, 97, 219–243.

[119] Wang, J., & Chen, C. (2009). Biosorption of heavy metals by biomass. Biotechnology Advances, 27, 195–226.

[120] Crini, G., & Lichtfouse, E. (2019). Advantages and disadvantages of adsorption. Environmental Chemistry Letters, 17, 145–155.

[121] Bhattacharyya, K. G., & Gupta, S. S. (2008). Adsorption of heavy metals on bentonite. Advances in Colloid and Interface Science, 140, 114–131.

[122] Wang, S., et al. (2018). Bentonite-based composites for metal adsorption. Applied Clay Science, 160, 1–9.

[123] Klemm, D., et al. (2011). Nanocelluloses: A new family of nature-based materials. Angewandte Chemie International Edition, 50, 5438–5466.

[124] Trache, D., et al. (2017). Nanocellulose as a green material. Carbohydrate Polymers, 164, 74–85.

[125] Zhang, Y., et al. (2016). Hybrid adsorbents for wastewater treatment. Chemical Engineering Journal, 284, 174–188.

[126] Crini, G., et al. (2019). Recent advances in adsorption-based wastewater treatment. Environmental Chemistry Letters, 17, 195–213.

[127] Gupta, V. K., et al. (2020). Nanocomposites as adsorbents for heavy metal removal. Journal of Molecular Liquids, 297, 111935.

[128] Islam, M. S., Shammi, R. S., Jannat, R., Kabir, M. H., & Islam, M. S. (2023). Spatial distribution and ecological risk of heavy metal in surface sediment of Old Brahmaputra River, Bangladesh. Chemistry and Ecology, 39(2), 173-201.

[129] Sarhat, A. R., & Al-Obaidi, B. S. (2023). Assessment of heavy metal pollution in Sirwan river by heavy metal pollution index (HPI) and metal index (MI). Water Conservation Science and Engineering, 8(1), 12.

[130] Nouri, M. (2016). Assessment of metals contamination and ecological risk in ait Ammar abandoned iron mine soil, Morocco. Ekológia, 35(1), 32.

[131] Tenebe, I. T., Ogbiye, A. S., Omole, D. O., & Emenike, P. C. (2016). Estimation of longitudinal dispersion co-efficient: A review. Cogent Engineering, 3(1), 1216244.

[132] Chowdhury, S., & Saha, P. (2011). Adsorption kinetic modeling of safranin onto rice husk biomatrix using pseudo-first-and pseudo-second-order kinetic models: Comparison of linear and non-linear methods. CLEAN–Soil, Air, Water, 39(3), 274-282.

[133] Panigrahi, S. S., & Pattnaik, B. (2019). Water quality assessment of rivers in India: A review. Environmental Monitoring and Assessment, 191, 705.

[134] Hazarika, A., & Kalita, H. (2020). Assessment of water pollution in the Brahmaputra River. SN Applied Sciences, 2, 1248.

[135] Biswas, A., & Pathak, A. (2022). Spatio-temporal assessment of heavy metal pollution in Brahmaputra River. Environmental Research, 209, 112879.

[136] Pradhan, N.S. et al. (2021) Sustainable river management; Sustainability, 13, 1087.

[137] Hazarika, A.K. & Kalita, U. (2020) Heavy metals in Brahmaputra; Environ. Sci. Pollut. Res., 27, 31595–31614.

[138] Action Plan for Brahmaputra River Priority – iv – Pollution Report, Pollution Control Board of Assam government; http://www.pcbassam.org/RRC%20Action%20Plan%20Final/R%20Action%20Plan/Action%20plan_Brahmaputra.pdf

[139] USEPA (2007) Method 7000B: Flame AAS.

[140] APHA–AWWA–WEF (1992) Standard Methods for the Examination of Water and Waste Water.

[141] Datta, D.K. & Subramanian, V. (1998) Heavy metals in Ganga–Brahmaputra sediments; Environ. Geol., 36, 93–101.

[142] Loring, D.H. & Rantala, R.T. (1992) Marine sediment analysis; Earth Sci. Rev., 32, 235–283.

[143] Mahanta, C. & Subramanian, V. (2004) Sediment biogeochemistry; Springer.

[144] Dalman, Ö. et al. (2006) Heavy metals in sediments and fish; Food Chemistry, 95(1), 157–162.

[145] Ranjan, R.K. et al. (2008) Tsunami sediments; Environ. Monit. Assess., 147, 389–411.

[146] Bhuyan, M. et al. (2019) Heavy metal contamination in the Old Brahmaputra River; Appl. Water Sci., 9(5).

[147] Bensharada, M. et al. (2022) Organic matter determination in sediments; J. Paleolimnol., 67, 191–197.

[148] Ramasamy, V. et al. (2011) Radionuclides in sediments; Appl. Radiat. Isot., 69, 184–195.

[149] Chaturvedi, E. et al. (2021) Mineralogical characterization of sediments; Adv. Powder Technol., 32(4), 1247–1263.

[150] Khan, M.H.R. et al. (2020) Anthropogenic heavy metals; Environ. Sci. Pollut. Res., 27, 19688–19702.

[151] El-Sorogy, A.S. et al. (2016) Toxic metals in coastal sediments; Environ. Earth Sci., 75(5).

[152] Hossain, M.B. et al. (2021) Vertical distribution of heavy metals; Environ. Geochem. Health, 43, 4235–4249.

[153] Subramanian, V. et al. (1987) Metals in Ganga–Brahmaputra sediments; Environ. Geol., 9, 93–103.

[154] Turekian, K.K. & Wedepohl, K.H. (1961) Crustal element distribution; GSA Bulletin, 72, 175–192.

[155] Hakanson, L. (1980) Ecological risk index; Water Res., 14, 975–1001.

[156] Ahdy HH and Khaled A (2009) Heavy metals contamination in sediments of the western part of Egyptian Mediterranean Sea; Aust. J. Basic & Appl. Sci., 3(4), 3330–3336.

[157] Tomlinson, D.L. et al. (1980) Pollution index formation; Helgoländer Meeresuntersuchungen, 33, 566–575.

[158] Mohiuddin, K.M. et al. (2010) Trace metals in urban rivers; Int. J. Sci. Environ. Technol., 7, 17–28.

[159] Muller, G. (1969) Geoaccumulation index; Geojournal, 2, 108–118.

[160] Amin, B. et al. (2009) Anthropogenic impacts on heavy metal concentrations; Environ. Monit. Assess., 148, 291–305.

[161] Taylor, S.R. (1964) Crustal element abundance; Geochim. Cosmochim. Acta, 28, 1273–1285.

[162] Varol, M. & Sen, B. (2012) Heavy metals in Tigris River; Catena, 92, 1–10.

[163] Blasius, J. & Greenacre, M. (1998). Visualization of categorical data. Academic Press.

[164] Kaufman, L. & Rousseeuw, P.J. (2009). Cluster Analysis. Wiley.

[165] Ivosev, G. et al. (2008) PCA visualization; Analytical Chemistry, 80, 4933–4944.

[166] Dekov, V.M. et al. (1998) Chemical composition of Brahmaputra sediments; Sci. Total Environ., 212, 89–105.

[167] Martin, J.M. & Meybeck, M. (1979) Elemental balance in rivers; Marine Chemistry, 7, 173–206.

[168] Hoque, R.R. et al. (2011) Speciation of heavy metals; Environ. Monit. Assess., 177, 457–466.

[169] Jain, C.K. (2004) Metal fractionation in Yamuna sediments; Water Res., 38, 569–578.

[170] Nazneen, S. et al. (2019) Heavy metal fractionation; Quat. Int., 507, 370–388.

[171] Singh, H. et al. (2013) River Ganga sediments; PNAS India, 83, 371–384.

[172] Saha, P.K. & Hossain, M.D. (2011) Buriganga River sediment quality.

[173] Hassan & Md Shareful (2015) River bank erosion in Bangladesh; J. Geosci. Environ. Prot., 4(1).

[174] Salah, E.A.M. et al. (2012) Euphrates River sediments; J. Water Resour. Prot., 4.

[175] Li, F. et al. (2009) Heavy metal contamination in soils; Environmental Earth Sciences, 57, 1815–1823.

[176] Wang, Y. et al. (2011) Yangtze River sediments; Environ. Monit. Assess., 172, 407–417.

[177] Suresh, G. et al. (2015) Heavy metals in beach sediments; Mar. Pollut. Bull., 91, 389–400.

[178] Kukrer, S. et al. (2014) Ecological risk assessment; Environ. Monit. Assess., 186, 3847–3857.

[179] Malvandi & Hassan (2017) Heavy metal contamination in Iran; Mar. Pollut. Bull., 117, 547–553.

[180] Duan, K. et al. (2021) Toxic metals in agricultural soil; J. Environ. Qual., 50(1), 122–133.

[181] Varol, M. et al. (2013) Dissolved metals in Tigris River; Environ. Sci. Pollut. Res., 20, 6096–6108.

[182] Tsering, T. et al. (2020) Metal fractionation in Brahmaputra sediments; Int. J. Environ. Res. Public Health, 17.

[183] Chou, J.S. & Chiu, Y.C. (2021) Risk factors in river dredging projects; J. Flood Risk Manage., 14(1).

[184] Yan, J. & Li, F. (2023) Effects of sediment dredging; Environ. Sci. Pollut. Res., 30, 119612–119626.

[185] Hanley & Russell (2011) Environmental monitoring of dredging; APPEA Journal, 51(1), 273–294.

[186] Zainal, A.J.M. et al. (1993) Marine ecological monitoring; Photogramm. Eng. Remote Sens., 59(3).

[187] Walker, D.I. and McComb, A.J., 1992. Seagrass degradation in Australian coastal waters. Marine Pollution Bulletin, 25(5-8), pp.191-195.

[188] Larkum, A.W.D. and West, R.J., 1990. Long-term changes of seagrass meadows in Botany Bay, Australia. Aquatic botany, 37(1), pp.55-70.

[189] Lee, S.Y. (1997) Seagrass biomass cycles; Marine Biology, 129, 183–193.

[190] Fong, T.C. (2000) Seagrass conservation; Asian Mar. Biol., 16, 109–121.

[191] Pringle & Waddon (1989) Dredging impacts in Queensland.

[192] Long B G, D M Dennis, T D Skewes and I R Poiner (1996) Detecting an environmental impact of dredging on seagrass beds with a BACIR sampling design; Aquat. Bot., 53(3-4), pp.235-243. https://doi.org/10.1016/0304-3770(95)01006-8.

[193] Roelofs, A. et al. (2001) Seagrass monitoring; Ports Corporation of Queensland.

[194] Amado Filho, G.M. et al. (2004) Metal accumulation by Halodule wrightii populations; Aquat. Bot., 80(4), 241–251.

[195] Penn, N. (1983) Coral sand dredging impacts; Bull. Mar. Sci.

[196] De Falco, Giovanni, Maura Baroli, Ester Murru, Giuseppe Piergallini, and Gianluigi Cancemi (2000) Photo-aerial image processing and sediment analysis as indicators of environmental impact on Posidonia oceanica in the Mediterranean Sea; Biol. Mar. Mediterr., 7(2), pp.349-352.

[197] Erftemeijer, P.L.A. (2002) Evaluation of dredging impacts; Delft Hydraulics Report.

[198] Erftemeijer, P.L.A. & Wijsman, J. (2004) Monitoring dredging impacts; Delft Hydraulics Report.

[199] Hazarika A K, Kalita U. (2020). Incidence of heavy metals and river restoration assessment of a major South Asian transboundary river. Environmental Science and Pollution Research, 27(25), 31595–31614. https://doi.org/10.1007/s11356-020-09328-5

[200] APHA (2005) Standard methods for the examination of water and wastewater. 21st edn. Washington, DC: American Public Health Association.

[201] Salati, S. and Moore, F. (2010) 'Assessment of heavy metal concentration in river water and sediment', Environmental Monitoring and Assessment, 164, pp. 677–689. https://doi.org/10.1007/s10661-009-0920-y

[202] Karuppannan, S. and Serre Kawo, N. (2020) 'Groundwater quality assessment using geospatial techniques and WQI', Hydrospatial Analysis, 3(1), pp. 22–36. https://doi.org/10.21523/gcj3.19030103

[203] Rezaei, A., Hassani, H. and Jabbari, N. (2019) 'Evaluation of groundwater quality and assessment of pollution indices', Sustainable Water Resources Management, 5(2), pp. 491–512. https://doi.org/10.1007/s40899-017-0209-1

[204] Edet, A.E. and Offiong, O.E. (2002) 'Evaluation of water quality pollution indices for heavy metal contamination monitoring', GeoJournal, 57, pp. 295–304.

[205] Tamasi, G. and Cini, R. (2004) 'Heavy metals in drinking waters from Mount Amiata, Italy', Science of the Total Environment, 327(1–3), pp. 41–51. https://doi.org/10.1016/j.scitotenv.2003.10.011

[206] Milivojević, J., Krstić, D., Šmit, B. et al. (2016) 'Assessment of heavy metal contamination and calculation of its pollution index', Bulletin of Environmental Contamination and Toxicology, 97, pp. 737–742. https://doi.org/10.1007/s00128-016-1918-0

[207] Arora, G., Sharma, T., Taijas, K.K., Pant, P., Gupta, C. and Sharma, R.K. (2022) 'Rejuvenation and restoration of surface water quality amid COVID-19 lockdown: a comprehensive review in Indian context', Environmental Engineering Research, 28(3), pp. 220144. https://doi.org/10.4491/eer.2022.144

[208] Yerima Kwaya M, Hamidu H, Ibrahim Mohammed A, Nura Abdulmumini Y, Habib Adamu I, Muhammed Grema H. (2019). Heavy Metals Pollution Indices and Multivariate Statistical Evaluation of Groundwater Quality of Maru town and environs. J. Mater. Environ. Sci, 10(1), 32–44. http://www.jmaterenvironsci.com.

[209] Onyele, O.G. and Anyanwu, E.D. (2018) 'Human health risk assessment of some heavy metals in a rural spring', African Journal of Environment and Natural Science Research, 1, pp. 1–10.

[210] Boateng, T.K., Opoku, F. and Akoto, O. (2019) 'Heavy metal contamination assessment of groundwater quality: a case study of Oti landfill site, Kumasi', Applied Water Science, 9(2), pp. 1–9. https://doi.org/10.1007/s13201-019-0915-y

[211] USEPA IRIS (2011) Integrated Risk Information System. Washington, DC: US EPA. Available at: http://www.epa.gov/iris/

[212] Ricolfi, L., Barbieri, M., Muteto, P.V., Nigro, A., Sappa, G. and Vitale, S. (2020) 'Potential toxic elements in groundwater and their health risk assessment', Environmental Geochemistry and Health, 42(9), pp. 2733–2745. https://doi.org/10.1007/s10653-019-00507-z

[213] World Health Organization (WHO) (2011) Guidelines for drinking-water quality. 4th edn. Geneva: WHO.

[214] Adimalla, N. (2020b) 'Heavy metals pollution assessment and its associated human health risk evaluation of urban soils from Indian cities: a review', Environmental Geochemistry and Health, 42(1), pp. 173–190. https://doi.org/10.1007/s10653-019-00324-4

[215] Karunanidhi D, Aravinthasamy P, Subramani T, Setia R. (2021). Effects of COVID-19 pandemic lockdown on microbial and metals contaminations in a part of Thirumanimuthar River, South India: A comparative health hazard perspective. Journal of Hazardous Materials, 416. https://doi.org/10.1016/j.jhazmat.2021.125909

[216] Anyanwu, E. and Adetunji, O. (2018) 'Human health risk assessment of some heavy metals in a rural spring, Southeastern Nigeria', African Journal of Environment and Natural Science Research, 1, pp. 15–23.

[217] United States Environmental Protection Agency (1983) Water quality standards handbook. Washington, DC: US EPA.

[218] Bureau of Indian Standards (BIS) (2012) Indian standard drinking water specification (IS 10500:2012). New Delhi: BIS.

[219] Fatoba, J.O., Sanuade, O.A., Hammed, O.S. and Igboama, W.W. (2017) 'Multivariate statistical analysis of groundwater hydrochemistry', Arabian Journal of Geosciences, 10(15), pp. 1–15. https://doi.org/10.1007/s12517-017-3125-7

[220] Gavhane, S.K., Sapkale, J.B., Susware, N.K. and Sapkale, S.J. (2021) 'Impact of heavy metals in riverine and estuarine environment: a review', Research Journal of Chemistry and Environment, 25(5), pp. 226–233.

[221] Cempel, M. and Nikel, G. (2006) 'Nickel: a review of its sources and environmental toxicology', Polish Journal of Environmental Studies, 15(3), pp. 375–382.

[222] Rahman Z, Singh V P. (2019). The relative impact of toxic heavy metals (THMs) (arsenic (As), cadmium (Cd), chromium (Cr)(VI), mercury (Hg), and lead (Pb)) on the total environment: an overview. Environmental Monitoring and Assessment. Springer International Publishing. https://doi.org/10.1007/s10661-019-7528-7

[223] Obiri S, Dodoo D K, Armah F A, Essumang D K, Cobbina S J. (2010). Evaluation of lead and mercury neurotoxic health risk by resident children in the Obuasi municipality, Ghana. Environmental Toxicology and Pharmacology, 29(3), 209–212. https://doi.org/10.1016/j.etap.2010.01.001

[224] Akin, B.S. (2016) 'Treatment of pharmaceutical wastewater containing heavy metals', Journal of Environmental Chemical Engineering, 4(1), pp. 114–121.

[225] Begum, A. and Huq, S.M.I. (2016) 'Heavy metal pollution in industrial effluents and their environmental impact', Journal of Environmental Science and Health, Part A, 51(9), pp. 734–742.

[226] Laffite, A., Kilunga, P.I. and Devarajan, N. (2016) 'Hospital effluents as a source of heavy metals', Science of the Total Environment, 548–549, pp. 203–212.

[227] Hsu, L.-C. (2016) 'Occurrence of heavy metals in pharmaceutical wastewater', Environmental Monitoring and Assessment, 188, pp. 1–12.

[228] Oliveira, H., Lopes, T. and Almeida, C.M.R. (2017) 'Pharmaceutical industry effluents as sources of metal pollution', Environmental Science and Pollution Research, 24(1), pp. 132–142.

[229] Nadeem, M., Shafiq, M. and Anwar, S. (2020) 'Heavy metals in pharmaceutical industrial wastewater', Environmental Technology, 41(15), pp. 1943–1952.

[230] Ammar, T., Bouabidi, Z.B. and Abdelkader, B. (2022) 'Assessment of pharmaceutical effluents and associated heavy metal pollution', Environmental Science and Pollution Research, 29(14), pp. 20745–20758.

[231] Cipurković, A., Trumić, M. and Selimbašić, V. (2014) 'Heavy metals in cement industry effluents', Chemical Industry & Chemical Engineering Quarterly, 20(2), pp. 233–240.

[232] Ogunkunle, C.O. and Fatoba, P.O. (2014) 'Pollution loads and heavy metals from cement industries', Environmental Monitoring and Assessment, 186, pp. 765–777.

[233] Dong, Z., Liu, J. and Wang, X. (2015) 'Heavy metal contamination from cement plants', Environmental Earth Sciences, 73(4), pp. 1741–1748.

[234] Begum, A. and Huq, S.M.I. (2016) 'Heavy metal pollution in industrial effluents and their environmental impact', Journal of Environmental Science and Health, Part A, 51(9), pp. 734–742.

[235] Akpambang, V.O.E., Ewa, E.E. and Okorie, A. (2022) 'Heavy metal contamination associated with cement production activities', Environmental Monitoring and Assessment, 194, pp. 1–15.

[236] Labunska, I., Brigden, K. and Santillo, D. (2001) 'Heavy metals in paper and pulp mill discharges', Environmental Pollution, 114(3), pp. 337–345.

[237] Sharma, B.M., Nizzetto, L. and Larssen, T. (2020) 'Heavy metals in pulp and paper mill effluents', Environmental Pollution, 263, pp. 114–121.

[238] Sharma, B.M., Bharat, G.K. and Tayal, S. (2022) 'Metal contamination from paper industries', Journal of Hazardous Materials, 423, pp. 127–135.

[239] Cartwright, B.G., Merry, R.H. and Tiller, K.G. (1976) 'Heavy metal contamination of soils around lead smelters', Environmental Pollution, 11(1), pp. 1–12.

[240] Samanta, G., Sharma, R. and Roychowdhury, T. (1995) 'Environmental impact of lead industries', Environmental Geochemistry and Health, 17(4), pp. 185–191.

[241] Kachenko, A.G. and Singh, B. (2005) 'Heavy metals contamination in soils near lead industries', Environmental Geology, 47(4), pp. 550–558.

[242] Zhang, J., Liu, C. and Li, F. (2012) 'Heavy metal pollution from lead smelting activities', Environmental Earth Sciences, 66(4), pp. 1101–1109.

[243] Jamal, A., Khan, A. and Ahmad, I. (2019) 'Environmental impacts of lead smelting industries', Environmental Pollution, 252, pp. 124–133.

[244] Shakya, P.R. and Shrestha, P. (2006) 'Heavy metal pollution from tyre recycling plants', Environmental Monitoring and Assessment, 122, pp. 43–54.

[245] Czajczyńska, D., Anguilano, L., Ghazal, H. et al. (2020) 'Potential of pyrolysis processes in the waste tyre management sector', Waste Management, 107, pp. 112–130.

[246] Konieczyński, J., Zajusz-Zubek, E. and Jabłońska, M. (2011) 'The release of trace elements from coking processes', Fuel, 90(6), pp. 2161–2168.

[247] Peng, B., Wu, D. and Xu, S. (2012) 'Heavy metals released from coke production', Fuel Processing Technology, 104, pp. 138–145.

[248] Gu, Y., Wu, Y. and Zhang, H. (2021) 'Heavy metal emissions from coking industries', Science of the Total Environment, 781, pp. 146–156. (NA)

[249] Wan, D., Liu, X. and Zhang, Y. (2022) 'Heavy metal emission characteristics of coking plants', Environmental Science and Pollution Research, 29(3), pp. 4212–4224.

[250] Owamah, H.I. (2013) 'Heavy metals determination in petroleum refinery effluents', Journal of Applied Sciences and Environmental Management, 17(3), pp. 473–479.

[251] Apeti, D.A. and Hartwell, S.I. (2015) 'Heavy metal concentrations in refinery effluents', Marine Pollution Bulletin, 91(1), pp. 190–196.

[252] Mustafa, S., Niaz, A. and Riaz, M. (2015) 'Assessment of refinery wastewater contamination', Journal of Environmental Management, 156, pp. 58–66.

[253] Sose, M.T., Isaac, J. and Bassey, E. (2017) 'Refinery effluent discharge and metal contamination', Environmental Monitoring and Assessment, 189, pp. 1–13.

[254] Xu, S., Wang, T. and Liu, Y. (2018) 'Trace metals in refinery wastewater and associated risks', Chemosphere, 210, pp. 45–53.

[255] Citarella, D., Cupola, F., Tanda, M.G., Zanini, A. Evaluation of dispersivity coefficients by means of a laboratory image analysis. J. Contam. Hydrol. 172, 10–23 (2015). https://doi.org/10.1016/j.jconhyd.2014.11.001

[256] Landel, J.R., Thomas, A.L., McEvoy, H., Dalziel, S.B. Convective mass transfer from a submerged drop in a thin falling film. J. Fluid Mech. 789, 630–668 (2016). https://doi.org/10.1017/jfm.2015.742

[257] Dariani, R.S., Esmaeili, A., Mortezaali, A., Dehghanpour, S. Photocatalytic reaction and degradation of methylene blue on TiO_2 nano-sized particles. Optik 127(18), 7143–7154 (2016). https://doi.org/10.1016/j.ijleo.2016.04.026

[258] Levenspiel, O., Smith, W.K. Notes on the diffusion-type model for the longitudinal mixing of fluids in flow. Chem. Eng. Sci. 6(4–5), 227–235 (1957). https://doi.org/10.1016/0009-2509(57)85021-0

[259] Uyigue, L. and Abah, M.A. (2020) 'Evaluation of the longitudinal dispersion coefficient for Dor-Nwezor-Bodo River using tracer experiment and theoretical measurement', Research & Reviews: Journal of Engineering and Technology, 9(1), pp. 6–13, March. e-ISSN 2319-9873; p-ISSN 2347-2324.

[260] M. Kaur and J. Pal, "Evaluation of efficiency of Wheat straw nanocellulose as nano adsorbent for the removal of divalent copper, lead and zinc from aqueous solution,"

Carbohydrate Polymer Technologies and Applications, vol. 6, Dec. 2023, doi: 10.1016/j.carpta.2023.100350

[261] A. K. El-Sawaf, A. A. Nassar, A. A. El Aziz Elfiky, and M. F. Mubarak, "Advanced microcrystalline nanocellulose-based nanofiltration membranes for the efficient treatment of wastewater contaminated with cationic dyes," Polymer Bulletin, vol. 81, no. 14, pp. 12451–12476, Sep. 2024, doi: 10.1007/s00289-024-05279-w.

[262] S. Sen Gupta and K. G. Bhattacharyya, "Adsorption of Metal Ions by Clays and Inorganic Solids." [Online]. Available: www.rsc.org/advances

[263] A. K. Dhar, H. A. Himu, M. Bhattacharjee, M. G. Mostufa, and F. Parvin, "Insights on applications of bentonite clays for the removal of dyes and heavy metals from wastewater: a review," Jan. 01, 2023, Springer Science and Business Media Deutschland GmbH. doi: 10.1007/s11356-022-24277-x.

[264] O. P. Prastuti, E. L. Septiani, Y. Kurniati, Widiyastuti, and H. Setyawan, "Banana peel activated carbon in removal of dyes and metals ion in textile industrial waste," in Materials Science Forum, Trans Tech Publications Ltd, 2019, pp. 204–209. doi: 10.4028/www.scientific.net/MSF.966.204.

[265] A. K. Dhar, H. A. Himu, M. Bhattacharjee, M. G. Mostufa, and F. Parvin, "Insights on applications of bentonite clays for the removal of dyes and heavy metals from wastewater: a review," Jan. 01, 2023, Springer Science and Business Media Deutschland GmbH. doi: 10.1007/s11356-022-24277-x.

[266] S. Hokkanen, A. Bhatnagar, V. Srivastava, V. Suorsa, and M. Sillanpää, "Removal of Cd2+, Ni2+ and PO43− from aqueous solution by hydroxyapatite-bentonite clay-nanocellulose composite," Int J Biol Macromol, vol. 118, pp. 903–912, Oct. 2018, doi: 10.1016/j.ijbiomac.2018.06.095.

[267] El-Shafey, E.I. (2010) 'Removal of heavy metals from aqueous solutions using chemically modified rice husk', Water, Air, & Soil Pollution, 209(1–4), pp. 319–334.

[268] Ahmed, M.J. and Theydan, S.K. (2013) 'Adsorption of heavy metals onto rice husk-derived materials: Effect of chemical activation', Journal of Analytical and Applied Pyrolysis, 100, pp. 75–82.

[269] Boussad, A. and Hajjaji, M. (2018) 'Synthesis and characterization of rice husk activated carbon–PVP composites for heavy metal removal', Journal of Environmental Chemical Engineering, 6(1), pp. 987–995.

[270] Saleh, T.A. and Gupta, V.K. (2017) 'Synthesis and characterization of alumina-based adsorbents derived from rice husk ash for uranium(VI) removal', Journal of Environmental Management, 198, pp. 99–108.

[271] Zheng, Y., Wang, A., Deng, Z., Luo, Y. and Liu, X. (2018) 'Enhanced adsorption of cadmium by MgO-modified rice husk biochar', Journal of Environmental Chemical Engineering, 6(2), pp. 2304–2313.

[272] Nguyen, T.T., Le, H.N., Nguyen, T.D. and Nguyen, T.V. (2022) 'Removal of methyl orange from aqueous solution using acid-modified rice husk charcoal', Environmental Technology & Innovation, 25, p. 102135.

[273] Shukla, S., Srivastava, V., Tang, X. and Jaiswal, A. (2023) 'Xanthate-modified rice husk as an efficient biosorbent for cadmium(II) removal from water', Chemical Engineering Journal, 451, p. 138695.

[274] Chai, W., Ma, Z. and Wang, Y. (2020) 'Rice husk-based nanocellulose for efficient adsorption of Pb(II) and La(III) from aqueous solutions', International Journal of Biological Macromolecules, 165, pp. 1674–1685.

[275] Ahmed, S.F., Zhou, J.L., Ngo, H.H., Guo, W. and Chen, M. (2024) 'Iron oxide–rice husk composite as an efficient adsorbent for heavy metal removal from water', Journal of Hazardous Materials, 461, p. 132567.

[276] Mohammed, A.A. and Ali, M.A. (2022) 'Synthesis of rice husk ash-based Faujasite zeolite for removal of chromium(VI) and lead(II) from aqueous solutions', Environmental Science and Pollution Research, 29(18), pp. 26945–26958.

[277] T. Shahnaz, V. Sharma, S. Subbiah, and S. Narayanasamy, "Multivariate optimisation of Cr (VI), Co (III) and Cu (II) adsorption onto nanobentonite incorporated nanocellulose/chitosan aerogel using response surface methodology," Journal of Water Process Engineering, vol. 36, Aug. 2020, doi: 10.1016/j.jwpe.2020.101283.

[278] X. Sun, X. Lv, C. Han, L. Bai, T. Wang, and Y. Sun, "Fabrication of Polyethyleneimine-Modified Nanocellulose/Magnetic Bentonite Composite as a Functional Biosorbent for Efficient Removal of Cu(II)," Water (Switzerland), vol. 14, no. 17, Sep. 2022, doi: 10.3390/w14172656.

[279] A. A. E. A. Elfiky, M. F. Mubarak, M. Keshawy, I. E. T. El Sayed, and T. A. Moghny, "Novel nanofiltration membrane modified by metal oxide nanocomposite for dyes removal from wastewater," Environ Dev Sustain, vol. 26, no. 8, pp. 19935–19957, Aug. 2024, doi: 10.1007/s10668-023-03444-1.

[280] Guidelines for Drinking-water Quality THIRD EDITION INCORPORATING THE FIRST AND SECOND ADDENDA Volume 1 Recommendations Geneva 2008 WHO Library Cataloguing-in-Publication Data. 2008.

[281] Bhaumik, M., Choi, H.J., McCrindle, R.I. and Maity, A., 2014. Composite nanofibers prepared from metallic iron nanoparticles and polyaniline: high performance for water treatment applications. Journal of colloid and interface science, 425, pp.75-82.

[282] Choudhury, R., Saikia, L, Barua, A., Nath, B., Mukherjee, A., Bhattacharya, P., 2026. A dedication to Chandan Mahanta (1962- 2023): A rare gem and pioneer in environmental hydrology. Journal of Environmental Science, Health & Sustainability, 2(1), 1–2.

List of Publications from the Thesis

List of Publications in International Journals

1. **Meena, V.**, Sarma, A.K. Dredging for navigation: a cogitative study on Brahmaputra River. Arab J Geosci 17, 261 (2024). https://doi.org/10.1007/s12517-024-12059-3

2. **Meena, V.**, Paul, S. & Sarma, A.K. Nanocellulose/bentonite composite: a novel material for heavy metal removal from aqueous solutions. Polym. Bull. 82, 7101–7121 (2025). https://doi.org/10.1007/s00289-025-05825-0